Adam Mickiewicz University
Poznań

Faculty of Mathematics and Computer Science

A doctoral dissertation
Natural sciences
Computer and information sciences

Multi-scale mathematical modeling of vegetation, soil and weather

Miłosz Makowski

Uniwersytet im. Adama Mickiewicza w Poznaniu
Wydział Matematyki i Informatyki

Rozprawa doktorska
Dziedzina nauk ścisłych i przyrodniczych
Dyscyplina informatyka

Wielopoziomowe matematyczne modelowanie roślinności, gleby i pogody

Thesis supervisor (Promotor):
prof. dr hab. Maciej Wygralak

Thesis assistant supervisor (Promotor pomocniczy):
dr Wojciech Pałubicki

Poznań, 2023

Abstract

Modeling realistic ecosystems of vegetation under variable climatic conditions is an open and a very complex problem, demanding an approach able to capture the enormous amount of detail and various interactions between the vegetation, soil and weather. Previous methods process trees and other plants by coarse geometrical approximations to reduce the computational complexity at the cost of decreased accuracy. On the other hand, there exist methods which are able to model the vegetation at a very detailed level. These, however, are unsuitable for large ecosystem simulations without an enormous computational power. Furthermore, the interplay between plants and weather has received increased attention recently, because of the observation that vegetation contributes substantially to local climatic variations.

In this dissertation, we introduce a multi-scale representation of plant ecosystems, which allows for realistic modeling of individual plants, capturing biological features such as growth, seeding, tropism and competition for resources. Our method leverages self-similarities of branching structures to efficiently handle the complexity of modeling and rendering. We also model the feedback between vegetation, soil and weather, including local variations of climate. In particular, we aim at simulating hydrological cycle. For this purpose, we develop a cloud dynamics model, which handles evaporation of plants and soil, cloud formation and precipitation. We also model water propagation in the soil based on soil properties and gravity.

Our approach provides the means to run interactive simulations of hundreds of thousands of plants, with a great amount of detail, and capture interactions with local variations of climate at the same time. Our results adhere to biological priors known in forestry, botany and ecology research.

Consequently, our method advances the state-of-the-art of generating highly realistic outdoor landscapes of vegetation and weather. Furthermore, it may potentially serve as the means for validation of biological hypotheses.

Abstrakt

Modelowanie realistycznych ekosystemów roślin w zmiennych warunkach klimatycznych jest otwartym i bardzo złożonym zagadnieniem. Wymaga ono podejścia, które jest w stanie uchwycić ogromną ilość szczegółów i różnorodnych zależności pomiędzy roślinnością, glebą i pogodą. Poprzednie metody przetwarzają drzewa i inne rośliny za pomocą zgrubnych geometrycznych przybliżeń, aby zredukować złożoność obliczeniową kosztem zmniejszonej dokładności. Z drugiej strony istnieją metody, które są w stanie modelować roślinność na bardzo dokładnym poziomie - te jednakże nie są odpowiednie do symulacji dużych ekosystemów bez dysponowania ogromną mocą obliczeniową. Ponadto badanie zależności pomiędzy roślinami i pogodą zyskuje w ostatnim czasie rosnące zainteresowanie, ze względu na obserwację, że roślinność wpływa znacząco na lokalne zróżnicowanie klimatu.

W niniejszej rozprawie wprowadzamy wielopoziomową reprezentację ekosystemów roślin, która pozwala na realistyczne modelowanie poszczególnych roślin, a także biologicznych zjawisk takich jak wzrost, rozsiewanie, tropizm oraz współzawodnictwo o zasoby. Nasza metoda wykorzystuje samopodobieństwo struktur drzewiastych, aby wydajnie radzić sobie ze złożonością modelowania i renderowania. Modelujemy również sprzężenie zwrotne pomiędzy roślinnością, glebą i pogodą, wraz z lokalnym zróżnicowaniem klimatu. W szczególności naszą motywacją jest symulacja cyklu hydrologicznego. W tym celu rozwijamy model dynamiki chmur, który obsługuje parowanie roślin i gleby, formację chmur i opady atmosferyczne. Modelujemy również transport wody w glebie na podstawie właściwości gleby oraz grawitacji.

Nasze podejście dostarcza środków do przeprowadzania interaktywnych symulacji setek tysięcy roślin, z dużą szczegółowością, z jednoczesnym uwzględnieniem interakcji na poziomie lokalnego zróżnicowania klimatu. Nasze wyniki są zgodne z biologicznymi modelami znanymi w leśnictwie, botanice i ekologii.

W rezultacie nasza metoda udoskonala najnowocześniejsze sposoby generowania wysoce realistycznych terenów z roślinnością i pogodą. Ponadto służyć może ona potencjalnie jako narzędzie do weryfikacji hipotez biologicznych.

Acknowledgements

I would like to express my sincere gratitude to my thesis supervisor, Professor Dr. Maciej Wygralak, for his invaluable guidance and support throughout my higher education. His expertise has been integral to the completion of this work, and I am deeply grateful for his mentorship.

I would also like to thank my co-supervisor, Doctor Wojciech Pałubicki, for his essential help, patience and support. His insights and expertise in modeling of natural phenomena cannot be overstated. I am truly obliged for all his tutoring and sharing with me his extensive knowledge.

Moreover, I would like to thank Prof. Dr. Dominik L. Michels, Prof. Dr. Daniel T. Banuti, Dr. Sören Pirk, Dr. Torsten Hädrich, Weronika Gajda and Jan Scheffczyk for the successful collaboration on our SIGGRAPH publications.

Finally, I would like to express my appreciation to my beloved wife Sonja, who has supported me throughout this journey with her unwavering love and encouragement. I am forever grateful for all that she has done to help me achieve this milestone.

Contents

1 Introduction **7**

2 Synthetic Silviculture: Multi-scale Modeling of Plant Ecosystems **9**
2.1 Introduction . . . 9
2.2 Related Work . . . 10
2.3 Overview . . . 11
2.4 Multiscale Modeling of Growth . . . 12
2.4.1 Single Plant Growth . . . 13
2.4.2 Plant Population Growth . . . 13
2.5 Self-Similar Plant Models . . . 14
2.5.1 Plant Architecture . . . 15
2.5.1.1 Light and Vigor Distribution . . . 15
2.5.1.2 Orienting Modules . . . 16
2.5.2 Branch Module Prototypes . . . 17
2.5.2.1 Selecting Modules . . . 17
2.5.3 Module Development . . . 18
2.5.3.1 Module Adaptation . . . 19
2.6 Ecosystem Simulation . . . 19
2.6.1 Plant Types and Biomes . . . 19
2.6.2 Global Shadowing . . . 20
2.6.3 Flowering and Seeding . . . 21
2.6.4 Climatic Adaptation . . . 22
2.6.5 Interactive Design of Ecosystems . . . 24
2.7 Implementation and Results . . . 24
2.7.1 Results . . . 25
2.8 Evaluation, Discussion, and Limitations . . . 29
2.8.1 Discussion and Limitations . . . 31
2.9 Conclusion . . . 32
2.10 References . . . 32

3 Towards Modeling Complex Interactions between Weather and Vegetation **37**
3.1 Introduction . . . 37
3.2 Cloud Model . . . 37
3.2.1 Atmosphere . . . 38
3.2.1.1 Atmospheric Pressure . . . 38
3.2.1.2 Temperature Profile . . . 38
3.2.2 Thermodynamics . . . 38
3.2.2.1 Generalities . . . 38
3.2.2.2 Temperature in the Rising Thermal . . . 39
3.2.2.3 Buoyancy and Acceleration of the Thermal . . . 39
3.2.2.4 Condensation and Cloud Formation . . . 40
3.2.2.5 Heat Release from Condensation . . . 40
3.2.2.6 Prediction of Cloud Boundaries . . . 40
3.2.3 Fluid Dynamics . . . 41
3.2.3.1 Transport Equations . . . 41
3.2.3.2 Mass . . . 43

3.2.3.3 Momentum . . . 43
3.2.3.4 Energy . . . 43
3.2.3.5 Water Continuity . . . 43
3.3 Conclusion . . . 44
3.4 References . . . 44

4 Ecoclimates: Climate-response Modeling of Vegetation 45
4.1 Introduction . . . 45
4.2 Related Work . . . 46
4.3 Overview . . . 48
4.4 Ecoclimates . . . 49
4.5 Model . . . 50
4.5.1 Spaces . . . 50
4.5.2 Input and Output . . . 51
4.5.3 Hypotheses . . . 52
4.5.4 Time Scales and Model Integration . . . 52
4.5.5 Vegetation Model . . . 53
4.5.5.1 Calculating Vapor Maps . . . 54
4.5.6 Soil Model . . . 55
4.5.7 Atmosphere Model . . . 56
4.5.7.1 Fluid dynamics . . . 56
4.5.7.2 Calculating Precipitation Maps . . . 57
4.6 Implementation Details . . . 57
4.7 Results and Evaluation . . . 59
4.7.1 Ecoclimate Dynamics . . . 59
4.7.1.1 Atmosphere . . . 59
4.7.1.2 Atmosphere-Vegetation . . . 59
4.7.1.3 Vegetation-Atmosphere . . . 62
4.7.2 Microclimate . . . 62
4.7.2.1 Geomorphic Effects and Plant Cooperation . . . 62
4.7.2.2 Edge Effects . . . 63
4.7.2.3 Deforestation Effects . . . 63
4.7.2.4 Foehn Effects . . . 63
4.7.3 Comparative Analysis . . . 66
4.8 Discussion and Limitations . . . 68
4.9 Conclusion . . . 70
4.10 References . . . 70

5 Future work 77

6 Publications by Miłosz Makowski 79

1 Introduction

Multifariousness of natural phenomena has been fascinating researches since ever. One the one hand, biologists try to describe the laws of fauna and flora, exploring the various processes down to a great detail. Recently, astounding computational resources opened great possibilities for validation of biological hypotheses through computer simulation. On the other hand, computer graphics community makes a great progress towards a photo-realistic real-time rendering of synthetic scenes. This enables the results of sophisticated mathematical experiments to be presented in almost self-explanatory way. By combining the best of both scientific worlds, we hold the tools to better understand our natural world, how to interact with it and eventually how to subdue it.

The focus of this dissertation is on the joint simulation of vegetation, soil, and weather. A novel multi-scale approach to modeling plants and their interactions with the environment is introduced, allowing for efficient simulations of large ecosystems controlled by temperature and precipitation. Additionally, a state-of-the-art cloud simulation is adopted and extended to capture bidirectional feedback through precipitation and evapotranspiration, modeling the water cycle between vegetation and the atmosphere. A novel soil model is proposed to describe water infiltration and uptake by individual plants. The results demonstrate a range of ecoclimate phenomena, including geomorphic controls, forest edge effects, the Foehn effect, and variations resulting from deforestation and drought. The method's plausibility is validated through numerous experiments and by comparing results to studies in ecology and climatology.

The following three chapters present the results of collaborative research in which I actively participated. For each chapter, I will highlight my primary contributions to the publications. All of these publications were composed and issued during the course of preparing this dissertation.

In particular, chapter 2 is based on the publication "Synthetic silviculture: Multi-scale modeling of plant ecosystems" of which I am the main author. My contributions to this publication include designing a modular plant representation that utilizes self-similarities of branching structures, making it efficient and versatile for large ecosystem simulations. I introduced a novel multi-scale approach to modeling plants and their interactions with the environment, which is controlled by average annual temperature and annual precipitation. I developed a tree growth model, and implemented a gradient-based optimization for ecosystem growth simulation. Additionally, I created an interactive simulation tool with real-time visualization, using modern GPU features such as Geometry Shaders and geometry instancing. I developed a parametrical tree model and designed a variety of plant species using it. I generated some of the results, including diagrams, tree growth visualization, and various forest simulations. I also performed validation of the results according to biological laws.

Chapter 3 is based on the publication "Stormscapes: Simulating Cloud Dynamics in the Now" of which I am a co-author. My contributions to this publication include conducting research on cloud models and tools for simulation of computational fluid dynamics. I also implemented realistic real-time cloud rendering which models light scattering, and generated results of cloud formation using real-time wind data.

Chapter 4 is based on the publication "Ecoclimates: Climate-response modeling of vegetation" of which I am a co-author. My contributions to this publication include designing an extension of the soil model that allows for the modeling of diffusion and advection of water in the soil and on its surface. I also implemented the combination of ecosystem, cloud, and soil models. I proposed a solution that simulates plant growth and cloud dynamics on different time scales, which captures substantial characteristics of both phenomena, while still preserving their interactions. I developed the interactive simulation tool, utilizing the possibilities of GPU computing. Additionally, I generated some of the results including the preparation of scenes and simulation of vegetation response to climatic changes, and assisted in validating the results according to existing research.

2 Synthetic Silviculture: Multi-scale Modeling of Plant Ecosystems

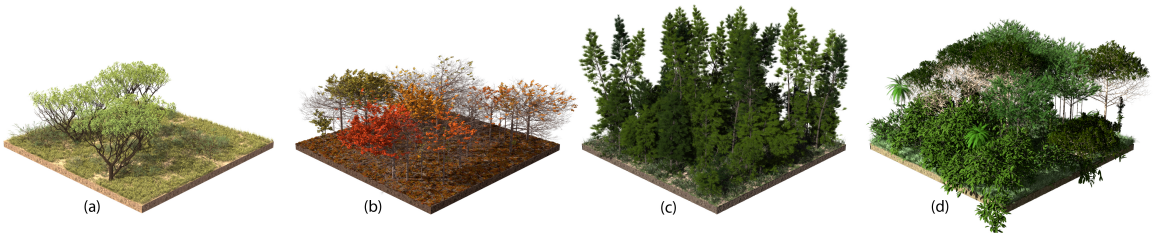

Figure 1: Ecosystems of different biome types generated with our framework: a savanna with grass and smaller trees (a), a deciduous forest composed of maple trees (b), a boreal forest with tall pine trees (c), and a rain forest scene with a large variety of species and high density of biomass (d). Our framework exploits inter- and intra-plant self-similarities to model plants and thereby allows us to interactively generate complex ecosystems while maintaining biologically plausible branching structures.

Due to the enormous amount of detail and the interplay of various biological phenomena, modeling realistic ecosystems of trees and other plants is a challenging and open problem. Previous research on modeling plant ecologies has focused on representations to handle this complexity, mostly through geometric simplifications, such as points or billboards. In this chapter we describe a multi-scale method to design large-scale ecosystems with individual plants that are realistically modeled and faithfully capture biological features, such as growth, plant interactions, different types of tropism, and the competition for resources. Our approach is based on leveraging inter- and intra-plant self-similarities for efficiently modeling plant geometry. We focus on the interactive design of plant ecosystems of up to 500K plants, while adhering to biological priors known in forestry and botany research. The introduced parameter space supports modeling properties of nine distinct plant ecologies (e.g. deciduous forest, boreal forest, tundra, etc.) while each plant is represented as a 3D surface mesh as required by commodity rendering systems. The capabilities and usefulness of our framework are illustrated through numerous models of forests, individual plants, and validations.

2.1 Introduction

Modeling trees and plants with all their nuances in structure and appearance is a thoroughly studied, and yet ongoing topic in visual computing. At the scale of plant ecosystems, this task is made even more challenging not only due to the enormous complexity of geometric detail, but also because of the intricacies of biological phenomena that affect how plants grow and interact. While existing approaches often model plant ecosystems by simplifying the involved geometry into more organized and hierarchical representations, such as voxels or layers, many applications benefit from detailed models that retain a plants' structure, faithful to all its defining features. This ranges from forests as content in 3D simulators and games, over urban and environmental planning applications, to research on ecosystems in forestry, and more recently the training of autonomous agents in virtual environments [1]. Detailed models of plant ecosystems, that even enable interactions with individual plants and their branches and leaves, play a key role in many situations. However, the computational costs for modeling these ecosystems is often beyond the capabilities of commodity rendering hardware. Furthermore, modeling the branching structures resulting from complex plant interactions as

part of the growth process – inevitable for realistic ecosystems – requires in-depth knowledge of the biological processes, which is an intractable requirement for most content creators.

Traditionally, plant ecosystems are simulated by jointly generating plausible distributions of plant species and modeling their geometry [2]–[4]. Several approaches exists to capture the various levels of abstraction, such as volumetric textures [5], voxels [6], or branch templates [7]. Choosing the appropriate level of detail scheme is critical for modeling plant ecosystems and a few approaches have been proposed to enable simplifications, while also adhering to plant structure [8], [9]. Only more recently methods focus on realistic geometric representations for trees with an emphasize on individual parts [10], [11], and interactive authoring [12], [13] to enable large-scale ecosystem modeling.

Methods for ecosystem modeling mostly describe trees in more abstract terms, e.g. as single value functions to model biological processes. More detailed representations model trees with a set of discrete elements that can express more complex phenomena, such as self-shadowing or apical control [14]. Existing multi-scale representations allow to model tree processes at various levels of detail [15]. However, these methods have not been shown the ability to jointly capture realistic plant ecosystems composed of detailed representations for individual plants.

In this chapter, we present a novel multi-scale approach for the large-scale modeling of plant ecosystems. Our method is based on leveraging self-similarities of branching structures for both, single plants and entire forests. We define branch modules to capture characteristic branching patterns of various species and combine multiple modules to model the whole branching structure of individual plants. Unlike previous approaches, where branch patches are used to represent the full surface geometry of branch parts, our modules only represent the topology of branching structures. This allows us to adapt the modules faithfully to the conditions of each individual plant and as required to simulate phenomena such as forest patterns, plant interactions, growth, and tropisms. To efficiently model large-scale ecosystems we then reuse the modules across the same plant and for the entire ecosystem by combining them through a non-convex optimization scheme, conditioned on biological priors, such as the availability of resources and collisions of branches.

The branch modules allow us to model complex and diverse plant biomes, ranging from tundras and deserts to boreal and deciduous forests. We introduce temperature and precipitation as a two-dimensional effortless means of control for modeling the diversity of different ecosystems. In forestry research, temperature and precipitation are considered as primary factors for plant growth and development. While temperature defines the overall fertility and diversity of species, variations in precipitation are responsible for the density of biomass [16]. We use these parameters to adapt the branch modules during the growth process for each plant and to select trees species common for each type of biome. Our modeling framework allows us to interactively design large-scale ecosystems. This is meant to provide an efficient feedback-loop for content creators to design the ecosystem.

Figure 1 shows examples of plant ecosystems simulated with our pipeline. In summary our contributions are (1) we advance the state-of-the-art in ecosystem modeling by introducing a modeling and editing framework that enables generating the diversity of nine biomes ranging from tundra to tropical rainforest, (2) a novel approach for modeling the geometry of plant ecosystems with unparalleled fidelity, (3) a representation for trees and plants based on self-similar branch modules that lends itself well to effcient rendering, (4) we evaluate our growth model by comparing simulation results to real and simulated data.

2.2 Related Work

Faithfully modeling plant ecosystems has been a motivation of computer graphics research for decades. While early approaches predominantly focus on modeling the branching structure of sin-

gle plants – fractals [17], repetitive patterns [18], and L-systems [19], [20], are prominent examples – recent methods provide more principled ways to model trees and plants. While sketch-based techniques provide content creators with the artistic freedom to model plants according to their requirements [21]–[23], data-driven methods have proven to be an efficient way to capture plants at convincing and plausible levels of detail. Today, advanced methods exist to reconstruct plants from images [24]–[27], videos [28], and laser-scanned point sets [7], [10].

It has been recognized that the underlying biological processes play an important role for producing realistic models of vegetation. This ranges from biological priors in procedural models [29] and growth simulations [30], to modeling the environmental response [31], [32] and motion of plant models [33]–[35]. Pirk et al. [36], [37] show the interaction of plant models with fluid dynamics to simulate realistic sway-motions and the combustion of tree models. Hädrich et al. [38] model the behavior of climbing plants and their adaptation to support structures and surfaces. Wang et al. [39] go even further and propose a realistic solver for the biomechanical properties of plant materials.

Due to the enormous complexity of plants, not only in their geometric detail, but also in their materials, and the involved biological phenomena, modeling large ecosystems is challenging. Many of the existing methods for modeling plant populations focus on jointly computing plant distributions and the geometry for each plant [3]. Modeling concepts like L-systems [40], Xfrog [41], or AMAP [42] readily model plant structures, while also adhering to biological attributes of plant species. Furthermore, several approaches address the rendering of ecosystems at different scales [43], [44]. But only more recent approaches also consider plant-plant interactions in the growth process of ecosystems and environmental factors [45]. Unlike the existing approaches, our method is a more holistic approach to ecosystem design, including realistic distributions, detailed plant geometry, and an intuitive parameter space to model different biomes.

To efficiently render ecosystems, specifically at a larger scale, selecting the appropriate level of detail is of utmost importance. Several approaches exist to represent ecosystems at different levels of abstraction, such as points and lines [46], images [47], [48], or voxels [49], to reduce the geometry necessary to render single plants and to even support processing large amounts vegetation at interactive rates. Leveraging the repetitive and self-similar nature of plants, has also been a focus of plant modeling research [42]. Other methods simplify the foliage of plants while considering species relevant properties [8] and camera setups [9]. Similar to these approaches, our framework allows us to efficiently process large amounts of vegetation, but it is complementary in that we focus on the interaction of plants in their growth process to generate more realistic branching structures.

Finally, research in botany and forestry studies models of ecosystems with an emphasis on the biological processes of plants and biomes ranging from developmental attributes [50], availability of resources [51], diversity and influence of plant species [52], plant productivity [53], to the impact of climatic changes [54]. Only a few methods are based on detailed models of trees and plants. As a recent example, Eloy et al. [55] use articulated plant models to study the effect of environmental factors, such as wind and light. Similar to our approach they explore the relationship of allometries and self-similarities; however, unlike them, our method also supports modeling ecosystem types at interactive rates, which is more suited for applications in computer graphics.

2.3 Overview

The core idea behind our approach is to employ a multi-scale representation for plant ecosystems based on branch modules defining the skeletal graphs of branching structures. Each module can be combined with other modules in order to form the graph of a plant. To find plausible combinations of modules, we attach them through a non-convex optimization scheme during the growth process, that considers a number of biological factors. The combined modules are then adapted and pruned

according to tropisms, developmental changes, and collisions with other modules of neighboring plants.

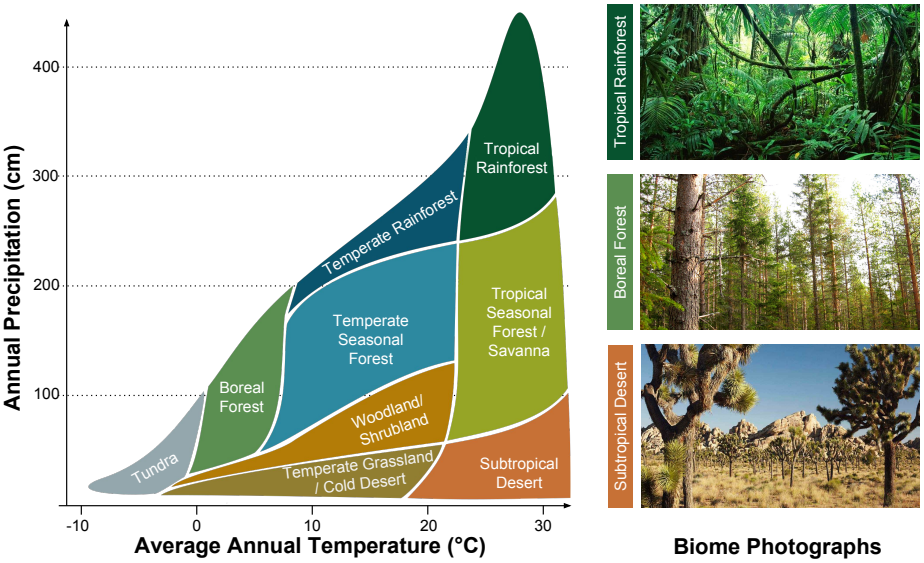

Figure 2: Temperature-precipitation diagram: we introduce temperature and precipitation, as a lightweight means of control for modeling the diversity of ecosystems. While temperature defines the overall fertility and diversity of species, variations in precipitation are responsible for the density of biomass. The photographs show characteristic biomes located in the diagram.

To create different types of plant biomes we introduce temperature and precipitation as parameters for ecosystem design. As shown in Fig. 2, temperature and precipitation span a two-dimensional parameter space that can be used to characterize plant ecosystems. Based on both parameters, we select branch modules along with their allometric properties and model the availability of plant species. Furthermore, we simulate the growth process of the entire ecosystem to model branching structures resulting from complex plant-plant interactions.

While being constrained and adapted by individual requirements of each plant, a module can occur multiple times across the same plant as well as across the entire ecosystem. The use of branch modules allows for GPU instancing which still retains enough flexibility to dynamically adapt each module to its specific environment while keeping a very light memory and performance footprint. Altogether, this results in realistic models of large-scale ecosystems with plausible branching structures.

2.4 Multiscale Modeling of Growth

We present a method to efficiently simulate the growth of plant ecosystems that captures essential biological properties of plant growth for both, individual plants and plant populations. In this section we discuss biological concepts related to plant growth.

2.4.1 Single Plant Growth

Our formal description of plant growth is based on two biological hypotheses. Sachs [56] proposes that plant form is the result of self-organization of branches. On the other hand, Barthélémy [57] postulates that tree architecture can be described as hierarchies of self-similar elements. Barthélémy calls these elements architectural units and defines them as a set of morphological and physiological features. Hence, plant form is the result of a specific configuration of architectural units. We combine the concepts of self-organization and self-similarity of branches in the following way.

We assume that the deterministic development of architectural units repetitively produces branching structures leading to self-similarity. This process is analogous to the development of mammals where the morphology of the same species is similar, *i.e.,* development of one head, two arms and two legs. In contrast to the development of architectural units, the development of the whole plant is unpredictable and plastic, *i.e.,* responsive to environmental cues (*e.g.,* light). Specifically, we describe plant form as the result of a multi-scale development which is deterministic at the scale of architectural units and self-organizing at the scale of the whole plant.

Single plant growth is commonly separated into primary growth, which refers to the lengthwise extension of shoots, and secondary growth, which describes the radial growth of branches. Most plant shoots produce branches, which emerge from lateral buds attached to the shoot axis. Diverse plant forms can be explained by apical buds inhibiting lateral buds and is referred to as *apical control*. Moreover, the overall growth potential of buds and shoots is called *vigor*, which may change over time; a phenomenon which can be assessed as the branch's *physiological age*. The adaptation of growth direction of branches to environmental stimuli is called *tropism*, most prominent categories of tropism are photo- and gravitropism (response to light and gravity). The growth of branches can further be classified as *determinate*, where buds become flowers thereby terminating further growth (determinacy), and *indeterminate*, where branches may grow indefinitely. Caraglio and Barthélémy [58] provide an overview of these concepts.

In summary, we describe single plant growth based on the following biological concepts: (1) competition of architectural units for light; (2) apical control; (3) gravitropism and phototropism; (4) determinacy (effects of flowering on tree architecture).

2.4.2 Plant Population Growth

Ecosystems are commonly characterized by the average annual temperature and annual precipitation (Fig. 2). Nine forest biomes composed of different plant species are defined as: desert, tundra, savanna, grassland, shrubland, boreal forest, temperate seasonal and rainforest, as well as tropical seasonal and rainforest. The variation of plant species is due to different *climatic adaptation* traits exhibited by the plants [59].

Growth of plant populations in an ecosystem is often described in terms of ecological successions, that describe the change in plant species compositions at a given location in the ecosystem [60]. A *succession* is defined by developing populations of grasses, forbs, and shrubs. These plants are gradually replaced by pioneering tree species, which grow slower but are more *shade tolerant*. This replacement of species continues until a set of environmentally well-adapted climax species establishes themselves as the dominant plant species. The climax species usually forms the canopy of the forest. Subsequent disturbances of the forest canopy, *e.g.,* as a result of fire or wind damage, lead to diverse microclimates as various plants try to exploit the newly available space for growth. This pattern of plant growth is called *gap dynamics* [61]. Fig. 3 and 12 show an example of this phenomenon.

Apart from temporal forest patterns, such as successions, ecologists also study spatial patterns. Plants employ a number of *seed dispersal strategies*, such as via wind, water, and animals, which naturally results in different spatial seeding patterns. However, plants are rarely distributed at

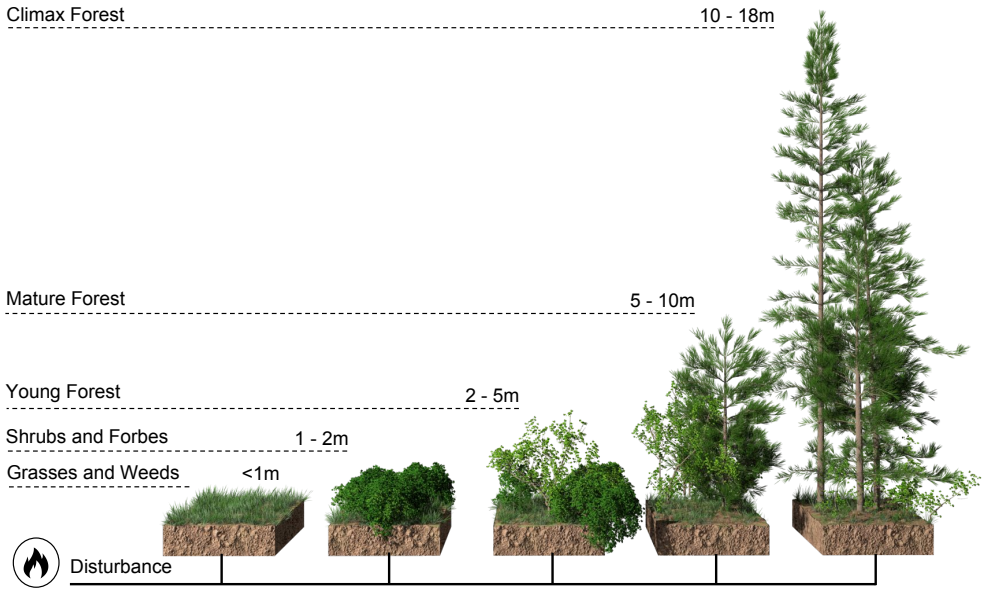

Figure 3: Successional stages of an evolving plant ecosystem: after the ecosystem is disturbed, e.g. through fire, populations of grasses, forbs, and shrubs develop. These plants are gradually replaced by pioneering tree species, which grow slower but are more shade tolerant. This replacement of species continues until a set of environmentally well-adapted climax species establishes themselves as the dominant plant species in the ecosystem.

random in a forest but are classified as either *over-dispersed* or *clustered*. Over-dispersed patterns emerge due to the competition of plants for the same resources, such as light. Interestingly, the strength of inter- and intra-species competition may not only depend on the distance (isotropy) but also on the direction between plants (anisotropy). An example is a treeline, where with increasing elevation a transition from trees to shrubs can be observed. Below the treeline trees are over-dispersed due to the competition for resources, while above the treeline the environment becomes so inhospitable that plants tend to aggregate in clusters around favorable growth conditions [62]. In summary, we assume that forest growth patterns emerge as a result of a number of variable plant species traits: (5) climatic adaptation, (6) shade tolerance and (7) seeding strategy.

2.5 Self-Similar Plant Models

We use the concept of architectural units as a data structure referred to as *branch modules* to describe plant growth as a multi-scale process. A plant is represented as a graph of branch modules (plant scale), where each module formally expresses the *morphology* and *physiology* of branching patterns (module scale). Branch morphology is represented by generalized cylinders that are generated using a parametric definition, whereas, branch physiology is defined by variable parameters for each module.

Modules can be used multiple times across the same plant and the entire ecosystem. Repeatedly using the same modules to define plants is based on the assumption that branching structures are self-similar and hierarchical. Plant growth is described at both plant and module scale. At plant scale, we add and remove branch modules to express development according to the biological concepts of competition for light (1) and apical control (2). We define a single scalar variable vigor $\bar{v}$

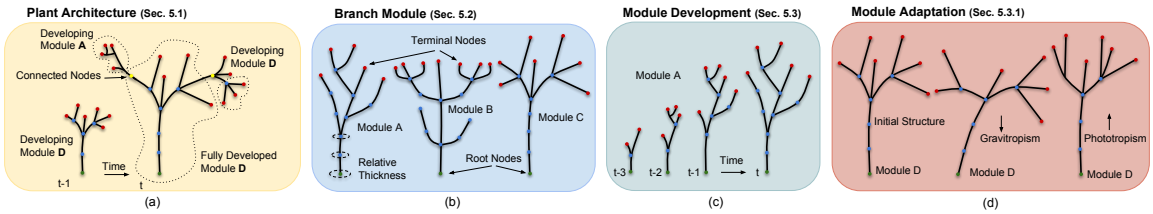

Figure 4: Self-similar plant models: we define plant architectures as collections of branch modules exploiting the self-similarity of plant structure (a). Branch modules are represented as graphs of nodes and edges (b) and structural parameters (thickness, length). We construct the geometry and develop them in time by interpolating structural parameters (c). The geometry of individual modules is adapted to model environmental effects, such as gravi- and phototropism (d).

for branch modules and calculate it based on the extended Borchert and Honda model (Sec. 2.5.1). At plant scale, growth is thus defined as a process of self-organization.

In contrast, at module scale growth is expressed deterministically by interpolating morphological parameters from axiomatic to their final values (Sec. 2.5.3, Fig. 4 b). Specifically, we interpolate positions, diameters and lengths of branches to represent changes of morphology based on the concepts of tropisms (3). Moreover, we express the effects of flowering on the branching structure (4) by choosing an appropriate branch module based on the parameter determinacy D. While high values of D result in monopodial (single trunk) forms, low values produce sympodial (multi trunk) branching patterns. As is the case at plant scale, physiology of branches is defined with vigor v.

2.5.1 Plant Architecture

A plant model in our method is represented as an ordered tree graph of connected modules U referred to as the module architecture (Fig. 4, a) with root module u_{root}. This architecture is developed during the simulation (Fig. 5, c). At each simulation step we first estimate the light exposure Q for each module and calculate its growth potential vigor $\bar{v}$. Then, we determine how quickly each module develops (i.e. the physiological age) and whether, where, and how to attach or detach modules.

2.5.1.1 Light and Vigor Distribution We assume that plant growth is constrained by light availability (space). To estimate the available space for module growth, we define spherical bounding volumes B_u for each module (positions are computed using center points of their geometries). Then, we calculate the intersection volume $V_{\mathsf{intersect}}$ between B_u and all intersecting neighboring bounding volumes B_w. Finally, we sum up the intersection volumes for each module, as

$$f_{\mathsf{collisions}}(u) = \sum_{u \neq w \in U} V_{\mathsf{intersect}}(B_u, B_w)\,, \tag{1}$$

in order to obtain a measure of the light exposure $Q(u)$ which is described by an exponential decay $Q(u) = \mathsf{exp}(-f_{\mathsf{collisions}}(u))$.

For the simulation of plant growth we describe the amount of vigor for each branch module as a scalar vigor quantity $\bar{v}$ at plant scale. Specifically, we adapt the extended Borchert-Honda method to the scale of branch modules instead of branch segments. In this method, a basipetal (tip-to-base) pass from tips to root accumulates a value of total light exposure Q_{total} in u_{root}, summing up light fluxes at each branching point $Q(u) = Q(u_m) + Q(u_l)$. This value is then redistributed as the vigor $\bar{v}$ in an acropetal (base-to-tip) pass calculating vigor fluxes $\bar{v}(u_m)$ and $\bar{v}(u_l)$ at each module

intersection ($\bar{v}(u_l) = \bar{v}(u) - \bar{v}(u_m)$). The vigor $\bar{v}(u_m)$ is calculated as a weighted function, where the weight λ represents apical control:

$$\bar{v}(u_m) = \bar{v}(u) \cdot \frac{\lambda Q(u_m)}{\lambda Q(u_m) + (1-\lambda) Q(u_l)} \,. \tag{2}$$

Values of $\lambda > 0.5$ result in excurrent architectures, whereas $\lambda \leq 0.5$ in decurrent architectures [14]. We assume that each plant is limited in growth potential by a maximum value of vigor $\bar{v}_{\mathsf{rootmax}}$, *i.e.,* we never allocate more than this amount of vigor to the root module u_{root}.

Branch modules can also be removed from the plant architecture. We define a shedding threshold ($\bar{v}_{\mathsf{min}}$) that defines when a module is shed ($\bar{v} < \bar{v}_{\mathsf{min}}$). Additionally, we define the age of a plant for each plant model as p_t (initially $p_t = 0$). When $p_t \geq p_{max}$ we linearly interpolate $\bar{v}_{\mathsf{rootmax}}$ to zero using a constant step size. Hence, the vigor allocated in each simulation step to the plant model is decreased until all modules are shed from the architecture, representing gradual plant senescence.

2.5.1.2 Orienting Modules Due to the exponential growth of the module architecture, modules and their associated branching segments could eventually collide. However, natural branches tend to avoid collisions while also exhibiting tendencies of growing in certain directions [63]. Hence, there seems to be a balancing mechanism between different branch orientation strategies. To capture this important phenomenon we propose an optimization process for determining module orientations that takes into account both, the constraints of space and the effects of tropisms.

We apply several optimization steps of the iterative gradient descent method to find an optimal orientation for a new module. A module's orientation is represented using three Euler angles. A default starting orientation (*i.e.,* orientation of the parent module) is chosen as the first step of the optimization process. We define $f_{\mathsf{distribution}}$ as a weighted sum

$$f_{\mathsf{distribution}}(u) := \omega_1 \cdot f_{\mathsf{collisions}}(u) + \omega_2 \cdot f_{\mathsf{tropism}}(u) \,, \tag{3}$$

in which $\omega_{1,2} \in \mathbb{R}_+$ are weights controlling the impact of the optimization criteria. We optimize for spatial constraints using $f_{\mathsf{collisions}}$ according to Eq. 1 and constraints emerging from tropisms using

$$f_{\mathsf{tropism}}(u_\alpha) = \|\mathsf{cos}(\alpha_{\mathsf{tropism}}) - \mathsf{cos}(u_\alpha)\| \tag{4}$$

with tropism angle α.

We choose a default starting orientation (i.e. orientation of the parent module) for the first step of the optimization process. Let the Euler angles of module u be denoted with $\rho_u = [\varphi_u, \theta_u, \psi_u]$. The module u is rotated by $\rho = [\varphi, \theta, \psi]$ such that one obtains u': $\rho_{u'} = \rho_u + \rho$, i.e. $[\varphi_{u'}, \theta_{u'}, \psi_{u'}] = [\varphi_u + \varphi, \theta_u + \theta, \psi_u + \psi]$.

We write $u' = \mathsf{rot}(u, \rho)$ and optimize the distribution by finding a local minimum of a distribution quality function ($f_{\mathsf{distribution}}$). In a single step, we iterate through all the modules separately. Let $u^{(i)}$ be the module u in the i-th step:

$$\rho^* \in \left\{ \rho \in \mathsf{P} \;\middle|\; f_{\mathsf{distribution}}(\mathsf{rot}(u^{(i)}, \rho)) = f_{\mathsf{min}} \right\} , \tag{5}$$

$$f_{\mathsf{min}} = \mathsf{min}_{\rho \in \mathsf{P}} \left\{ f_{\mathsf{distribution}}(\mathsf{rot}(u^{(i)}, \rho)) \right\} . \tag{6}$$

We make use of $\mathsf{P} = \{[\alpha, 0, 0], [-\alpha, 0, 0], [0, 0, \alpha], [0, 0, -\alpha]\}$ with a small angle α. Finally, we apply a rotation of the module: $u^{(i+1)} = \mathsf{rot}\left(u^{(i)}, \rho^*\right)$. After a few steps or $f_{\mathsf{distribution}} < \mathsf{error}$, we apply the most recently obtained orientation to the module. The function $f_{\mathsf{distribution}}$ is defined as a weighted sum given by Eq. 3.

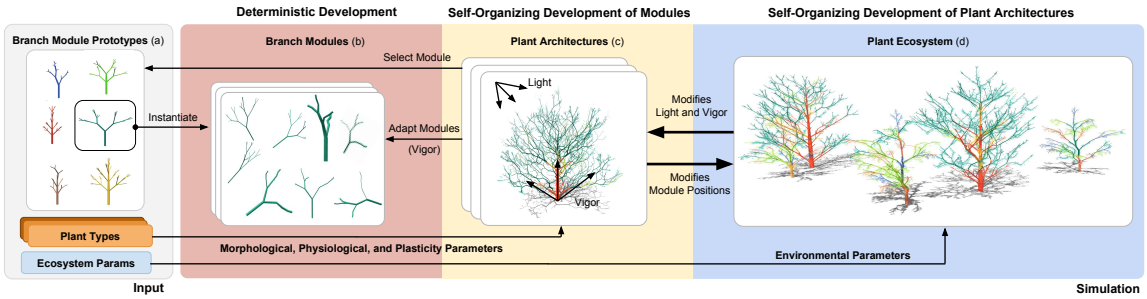

Figure 5: Multi-scale representation: we define module prototypes to represent common branching patterns agnostic to species (plant types) and developmental stages (a). We generate branch modules from prototypes and adapt them (b). To model a plant we combine modules to an architecture (c); prototypes and modules are used several times for the same plant and across a plant ecosystem (d). We simulate the growth of each module and plant as connected sets of modules with morphological and physiological parameters. Plant architecture development in the ecosystem is defined via plasticity parameters. In this example the prototypes and modules are color-coded to indicate module instances of the same prototype.

2.5.2 Branch Module Prototypes

We define the topology of a branching structure as a module prototype. The prototypes are used as templates to instantiate branch modules that define the geometry (Fig. 5, a, b). This allows us to represent trees with just a small number (we used 9) of prototypes instead of modeling all their individual branching structures.

A branch module is defined as a tree in the sense of a connected acyclic graph $G = (N, E)$, where N and E are sets of nodes and edges (referred to as branch segments). Each edge $e \in E$ connects two nodes $n_1, n_2 \in N$ and represents an individual branch segment $e = (n_1, n_2)$. The module has a single root node $n_{\text{root}} \in N$ and terminal nodes $n_{t_i} \in N$ serving as connectors for other modules during the growth process.

We provide a set of module prototypes $S = \{G_1, G_2, \ldots, G_{|S|}\}$. A module prototype can either be generated procedurally or manually designed by an artist (examples are shown in Fig. 5, a). A branch module is an instance of a specific module prototype $G_i \in S$ and describes the branching structure along with parameters associated with each node n; including position, physiological age, and a thickening factor (ϕ). The parameters associated with each node n describe how to generate the surface mesh for each branch segment e.

2.5.2.1 Selecting Modules To attach a new module to a terminal node of an existing fully developed module, we create a new module instance u_{new} selected from the set of module prototypes S (Sec. 2.5.2). The module prototypes contained in S are positioned in a special parameter space referred here as the morphospace that is spanned by plant type parameters apical control λ and determinacy D. The concept of a theoretical morphospace was discussed by McGhee [64] and in our case describes the variations of self-similar branching structures due to flowering and apical control. We define nine regions of

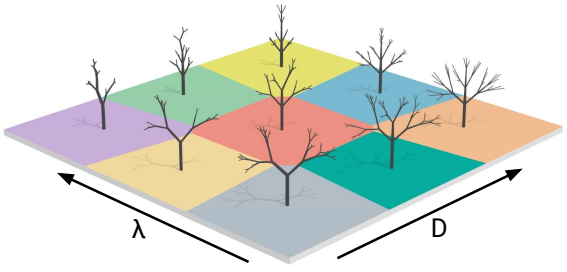

prototype modules in the morphospace. Regions are calculated using Voronoi partitioning where points of cells are given by prototype positions (chosen arbitrarily; see inset figure for a geometric illustration). In order to generate a new branch module, we determine its position in the morphospace as λ and $D' = \bar{v}(u_{\mathsf{parent}}) \cdot D / \bar{v}_{\mathsf{max}}$. This means, that new modules attached to vigorous parent modules tend to express more deterministic module prototypes providing a means for intra-architectural variation.

2.5.3 Module Development

Once we have calculated a vigor value for each branch module, we determine structural changes to the module architecture. Each module u is assigned a growth rate $\Upsilon(u)$ specifying how quickly a module is developed:

$$\Upsilon(u) = \mathsf{S}((\bar{v}(u) - \bar{v}_{\mathsf{min}})/(\bar{v}_{\mathsf{max}} - \bar{v}_{\mathsf{min}})) \cdot g_{\mathsf{p}} \,, \tag{7}$$

in which the vigor $\bar{v}(u)$, clamped to $\bar{v}_{\mathsf{max}}$, is smoothly interpolated by a sigmoid-like function $\mathsf{S} : x \mapsto 3x^2 - 2x^3$, and g_{p} denotes the growth rate of the whole plant. Consequently, modules may develop at different rates, taking into account the availability of light and apical control. The physiological age (Sec. 2.4.1) of a newly created module u is defined by

$$a_u(t_u) = \int_0^{t_u} \Upsilon(u) dt \tag{8}$$

appropriately measuring its real biological state. It is initially set to $a_u = 0$. The chronological age of the module, i.e. the time since its creation, is denoted by t_u. As simulation time proceeds, a_u is increased until a maximal value a_{mature} is reached (Fig. 4, c). Any subsequent growth is expressed via the attachment of new modules to the fully developed one. Please note, that unlike the chronological age, the physiological one is not a quantity of the dimension "time".

For any module u where $a_u > a_{\mathsf{mature}}$, we calculate the light exposure q for all terminal nodes n_i by $q(n_i) = Q(u)/\#n$, in which $\#n$ denotes the number of terminal nodes of module u. Next, we calculate vigor values v for all terminal nodes of the module u using the extended Bochert-Honda model. Here v denotes vigor at module scale as opposed to $\bar{v}(u)$ at plant scale. At each terminal node n with vigor $v > \bar{v}_{\mathsf{min}}$, we attach a new branch module. The diameter of the terminal nodes with the attached modules is set to the diameter of the root node of the child module.

To obtain a geometric representation of a module during the growth process, we simulate its physiological age. Unlike the self-organizing development of the module architecture (Sec. 2.5.1), the development of branch modules is expressed deterministically. We calculate intermediate growth stages by interpolating branch diameters and branch lengths. For a branch b, its physiological age a_b is defined by

$$a_b = \mathsf{max}(0, a_u - a_n) \,, \tag{9}$$

in which a_n is the physiological age of the end node of the branch (which describes when the branch starts to grow). The branch's diameter d_b is defined by

$$d_b = \begin{cases} \sqrt{\sum_{c \in C_b} d_c^2}, & C_b \neq \emptyset \,, \\ \phi, & \text{otherwise} \,, \end{cases} \tag{10}$$

in which C_b is the set of children of b. The branch's length ℓ_b is defined by

$$\ell_b = \mathsf{min}(\ell_{\mathsf{max}}, \beta \cdot a_b) \,, \tag{11}$$

in which β a scaling coefficient and ℓ_{max} the maximum length a branch can attain. Please note that Eq. 10 is a specific case of the Pipe Model [65], where parameter $n = 2$. Once all the branch segment parameter values are obtained we construct a surface mesh as generalized cylinders.

2.5.3.1 Module Adaptation We simulate a module's response to different kinds of tropism allowing for the realistic capturing of plant growth [42]. Positions and orientations of branch segments are transformed in order to account for the effect of tropisms on individual branches (Fig. 4, d). Given a node n and the age of the corresponding branch segment, we define the tropism offset as

$$\boldsymbol{\tau}_{\mathsf{offset}}(a_b) = \frac{g_1 \cdot \boldsymbol{g}_{\mathsf{dir}} \cdot g_2}{a_b + g_1}\,, \tag{12}$$

where $\boldsymbol{g}_{\mathsf{dir}}$ is the normalized direction of gravity, $g_{1,2}$ is the strength of tropism. The offset $\boldsymbol{\tau}_{\mathsf{offset}}$ is added to the current positions of the nodes. A negative value of g_2 represents gravitropism, a positive value phototropism.

2.6 Ecosystem Simulation

In this section we describe how our multi-scale plant representation can be used to model complex plant ecosystems based on individual plant models that dynamically adapt according to developmental traits, terrain features, and climatic conditions.

2.6.1 Plant Types and Biomes

We use our multi-scale plant representation to model different plant species, referred to as *plant types*, as a set of values for structural and environmental parameters. The parameters allow us to constrain the adaptation of module prototypes to generate plant graphs with features common to plant species, such as characteristic branch lengths or branching angles. A plant model is generated as an architecture of instantiated prototypes by individually developing and adapting them according to their unique location in the plant graph and their environment, as described in Sec. 2.5. A selection of plant types used in this chapter and their corresponding parameters are shown in Fig. 6 and Tab. 1. For finding these parameter values we rely on existing literature [14], [58].

Fig 6	p_{max}	$\bar{v}_{rootmax}$	g_p	λ/λ_{mature}	D/D_{mature}	F_{age}	α	ω_2	g_1	ϕ	β
a	20	42	0.19	0.62/-	0.25/-	0	0.52	0.63	-0.38	0.57	0.47
b	200	78	0.30	0.84/-	1.0/-	0	0.52	0.63	-1.2	1.00	0.79
c	80	11	0.80	1.0/-	1.0/-	0	0.9	0.5	1.0	5.00	1.95
d	16	1.7	0.23	0.44/-	0.31/-	0	1.0	1.0	1.0	5.00	3.00
e	430	600	0.15	1.0/0.5	1.0/0.33	58	0.52	0.63	0.56	3.00	1.23
f	550	450	0.20	0.76/-	0.82/-	0	0.17	0.5	0.47	1.20	1.90
g	550	700	0.20	0.9/0.5	0.93/0.74	55	0.17	0.5	0.47	1.38	0.94
h	500	570	0.24	1.0/0.5	1.0/0.5	55	0.5	0.27	-0.66	1.38	1.29
i	950	900	0.12	0.87/0.34	0.93/0.55	57	0.66	0.14	0.2	1.41	1.29
j	950	600	0.14	1.0/0.5	1.0/0.51	57	0.45	0.63	-0.9	0.82	0.93
k	950	600	0.14	1.0/0.5	1.0/0.51	57	-0.2	0.63	-0.9	0.82	0.93
l	1000	815	0.19	0.92/0.7	0.59/0.56	80	-0.19	0.72	-0.21	5.00	1.54
m	130	400	0.21	0.88/0.43	0.9/0.7	66	0.85	0.55	0.9	1.42	1.11
n	52	200	0.55	0.96/0.43	0.48/0.7	0	-0.27	0.43	0.73	1.50	2.50
o	300	600	0.20	0.8/-	0.86/-	0	-0.19	0.81	1.0	1.00	1.60
p	450	450	0.15	1.0/0.5	0.66/0.33	135	0.52	0.32	0.42	1.50	1.06

Table 1: Parameter values for plant types used to generate results for Fig. 6.

A key aspect of plant ecosystem simulation is the virtual environment. It is described by the plants that occupy it (instantiated plant types) and their locations in a spatially partitioned Euclidean space. We describe climatic conditions as the averaged annual parameters temperature and precipitation for the virtual environment. Furthermore, we model terrain with variable elevation based on a height map and represent it as a surface mesh. Additionally, we define a binary soil map to exclude areas of the terrain to be covered by vegetation, to account for natural (*e.g.,* mountains or water) and unnatural (*e.g.,* streets) landmark features (0 represents open terrain; 1 indicates blocked terrain).

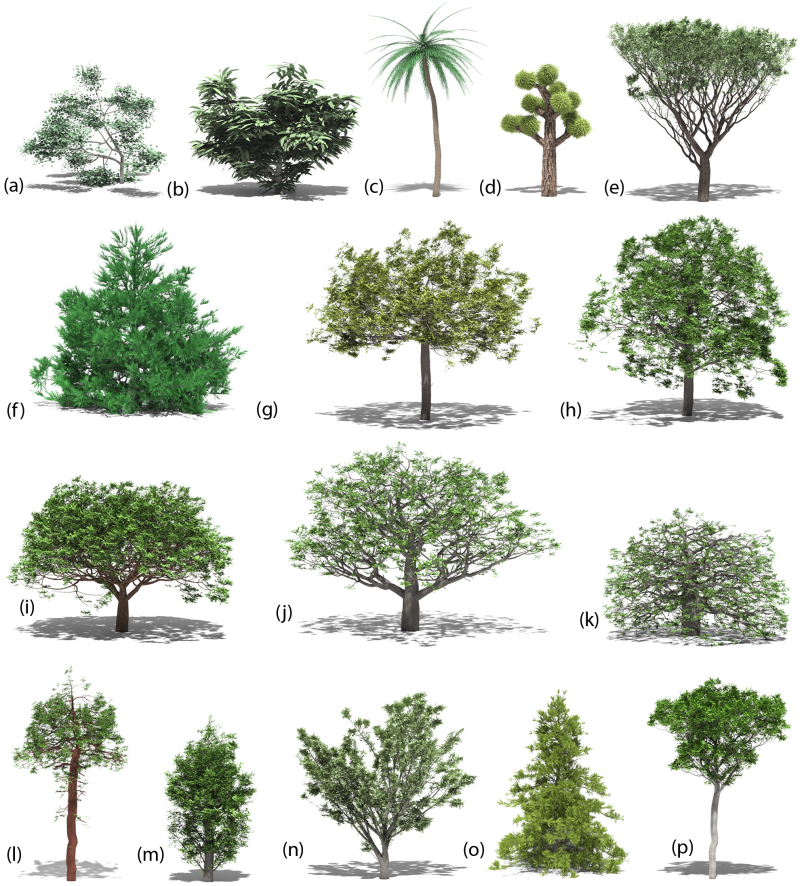

Figure 6: A selection of various plant models generated with parameter configurations reported in Tab. 1.

As described in Sec. 2.4 and shown in Fig. 2, we define the 9 most common plant biomes desert, tundra, savanna, grassland, shrubland, boreal forest, temperate seasonal, and rainforest, as well as tropical seasonal and rainforest. We select plant species in a biome based on their sensitivity to temperature and precipitation. We define parameters of climatic adaptation for each plant type and report them in Tab. 2. We manually select values for temperature and precipitation sensitivity according to Bassuk et al. [66] and use them to compute the probability of a plant to appear in a biome.

2.6.2 Global Shadowing

Based on the optimization of module orientations (Sec. 2.5.1.2) our method allows us to model local interactions of plants. These interactions are defined by bounding volumes that are limited by their geometric extent and do not account for shadowing over larger distances, such as branches in the crown, shadowing the understory. To allow for long distance interactions between individual plant types, we use shadow propagation [14]. We spatially partition the environment into a uniform grid of

Fig.	Seeding Frequency	Seeding Radius	s_{tol}	T_A	P_A
9 a	3.0	1.0	0.9	28.0	4100
9 b	3.0	9.0	0.9	28.0	4100
9 c	3.0	1.0	0.1	28.0	4100
9 d	3.0	9.0	0.1	28.0	4100
16 (I)	5.0	8.0	0.15	8.0	672
16 (II)	2.0	3.0	0.45	12.0	672
16 (III)	1.0	3.0	0.6	16.0	672

Table 2: Plasticity parameters for plant types used to generate the results shown in Fig. 9 (a-d) and 16. (I)-(III) refer to the three plant types, shrub, conifer, deciduous tree.

cells, where each cell describes the availability of light at a particular location. Whenever a module is associated with a cell, values of light availability Q_G for this grid cell and all cells underneath are updated. Unlike previous approaches, we apply the method at the scale of modules instead of buds and extend the shadowing cone into the bottom-most cells in the grid (approx. 2 meters). Therefore, we calculate effective light exposure values $Q_{\mathsf{eff}} = \mathsf{lerp}(s_{\mathsf{tol}}, 1, Q \cdot Q_G)$ that are used instead of values Q in case global shadowing is activated for a scene (s_{tol} denotes the shade tolerance of the plant type). An example of two plants interacting with each other and an obstacle is shown in Fig. 7.

Figure 7: A conifer and a deciduous tree are interacting with each other and an obstacle (house). By modeling plants with branch modules our method is able to maintain realistic branching structures throughout the simulation.

These long-distance, spatial interactions enable modeling successions. An example with three plant types is shown in Fig. 3: a fast growing shrub with a low s_{tol} value, a coniferous tree with a medium s_{tol} value, and a slow growing coniferous tree, with a high s_{tol} value. During 500 years of simulation time, several distinct successional stages emerge. Finally, the shade tolerant conifer grows tallest and establishes itself as the climax species. Our growth model is capturing temporal forest growth patterns where plant type compositions may change over simulation time (Sec. 2.4.2, (5)). Although, a state of homeostasis is reached at some point further variations in composition appear when large trees are removed from the virtual environment forming a gap in the canopy. The subsequent growth into the gap is called *gap dynamics*. In case the forest stand is composed of uniformly aged trees, many plants might be removed simultaneously. This phenomenon creates large gaps and is known as *cohort senescence* [67] (Fig. 16).

2.6.3 Flowering and Seeding

In addition to defining structural growth of plants, we also model the ability of plants to reproduce. We use a flowering age parameter to indicate when in the simulation a plant type reaches maturity. Once this threshold has been reached a new plant model is generated periodically (param-

eter seeding frequency) in a circular area around the position of the plant (parameter seeding radius, Tab. 3); the positions are computed based on a Gaussian distribution function (Fig. 8, left). Furthermore, we use the flowering age of a plant to determine changes to its structural growth. Specifically, we calculate $F_{\text{eff}} = F_{\text{age}} \cdot \bar{v}_{\text{rootmax}}/\bar{v}_{\text{root}}$ to determine the flowering age to allow vigorous plants to reach maturity quicker than less vigorous ones (F_{age} is a user-controlled parameter). Since the event of buds turning into flowers ends their ability to continue branch growth, it has impact on the plant architecture. We model this phenomenon of maturity by adapting *apical control* (λ) and *determinacy* (D) with λ_{mature} and D_{mature}. In Fig. 8 (right) high apical control and determinacy values have been replaced with smaller values to describe the growth pattern of Baobab trees.

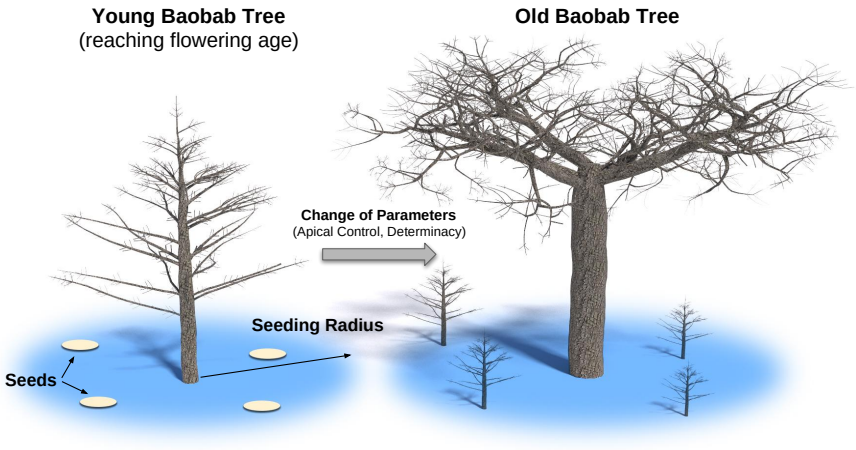

Figure 8: Flowering and Seeding: a 200 year old Baobab tree reaching maturity is seeding new plant models in a circular area around it (left). A 450 year old Baobab tree after changing the growth parameters apical control and determinacy (right). Flowering impacts the structure of the tree crown.

Seeding enables the representation of spatial forest patterns in our method. *Over-dispersion* emerges naturally as plant models compete in the virtual environment for space. By adjusting *shade tolerance* values a progression from tightly packed forest patterns to more distributed ones is simulated. Clustering patterns of forest growth can be obtained by varying the values of seeding radius. Lower values will result in a clustered and higher values in a homogeneous distribution (Fig. 9, a-d). More unusual patterns, studied as *labyrinths* and *gaps* [68], emerge due to cohort senescence of plants (Fig. 9, e-f). Finally, it is possible to set these parameters for each plant type resulting in varied forest patterns (Fig. 9, g-h).

2.6.4 Climatic Adaptation

We define the climate of an environment to model different biomes (climate space). We assume a constant temperature T and precipitation P across the simulation. While precipitation is defined as a constant for the whole virtual environment, the temperature T is given by a linear function $h \mapsto T(h) = T(0) + \gamma \cdot h$ of the elevation h with a constant negative slope parameter $\gamma < 0$. Appropriate measurements for γ can be found in the literature [69]. A sensitivity towards temperature and precipitation is defined for each plant type as T_A and P_A. We compute the probability of a plant appearing in a biome by 2D Gaussian kernel (adaptation) functions in the climate space. This is

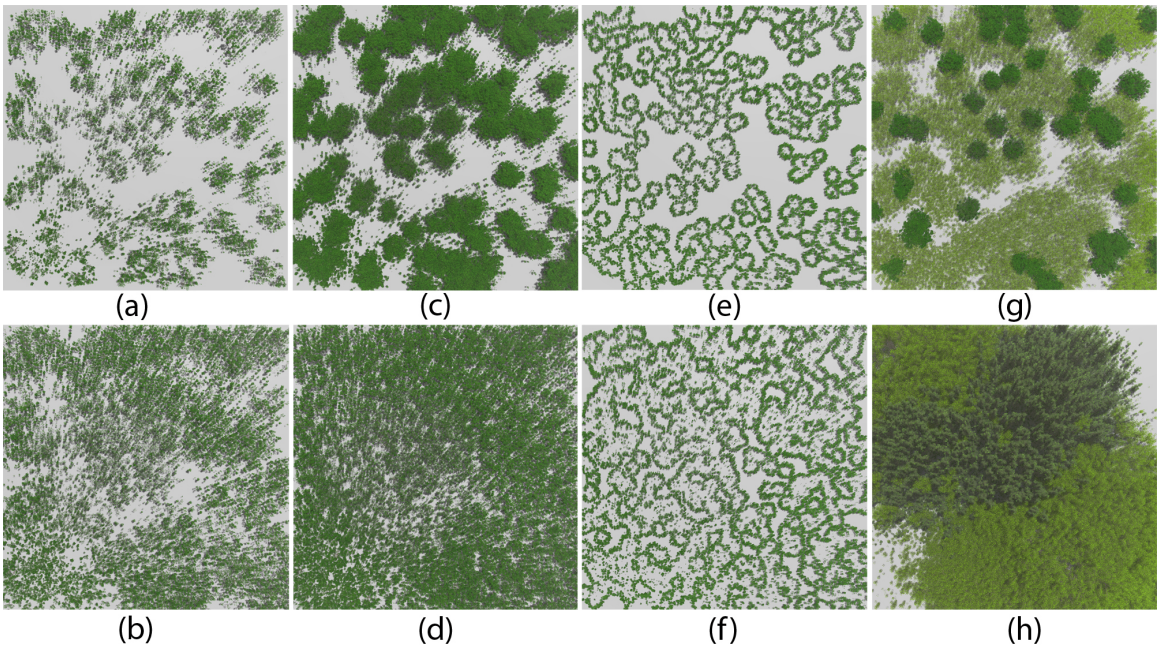

Figure 9: Bird's eye view of simulated plant populations. Different forest patterns emerge due to plasticity parameter changes: smaller seeding radius (top row); higher seeding radius (bottom row). (a)-(b): small s_{tol} values; (c)-(d): high s_{tol} values. (e)-(f): gaps and labyrinths emerge due to senescence. (g)-(h): variable plasticity parameter settings of two species resulting in different plant distributions.

analogous to a Gaussian mixture model by setting up corresponding parameter values:

$$o = \frac{\mathcal{N}_T(T) \cdot \mathcal{N}_P(P)}{\mathcal{N}_T(T_A) \cdot \mathcal{N}_P(P_A)}\,, \tag{13}$$

where $\mathcal{N}_T(\cdot)$ and $\mathcal{N}_P(\cdot)$ denote the normal distributions of temperature (mean is T_A) and precipitation (mean is P_A); see Table 3. Fig. 10 (b) illustrates the design of climatic adaptation by setting the mean and variance values for the adaptation functions of a plant type. For each plant type in the virtual environment we use the difference of the adaptation function and the position in climate space to linearly scale the $\bar{v}_{\mathsf{rootmax}}$ and seeding frequency parameter with probability o.

Parameter	**Explanation**	**Range**	**Unit**
Temperature	Avg. yearly temperature.	-10 - 33	°C
Precipitation	Yearly precipitation.	10 - 4300	mm
Seeding frequency	Num. of seeds/seeding period.	1-10	1/year
Seeding radius	Radius of placing plant seeds.	0.01 - 100	m
Shade tolerance	Plant adaptation to shade.	0-1	-
Temperature Adaptation	Optimal habitat temperature.	-10 - 33	°C
Precipitation Adaptation	Optimal habitat precipitation.	10 - 4300	mm

Table 3: Environmental parameters for modeling ecosystems (top) and plasticity parameters for modeling plant adaptation (bottom).

Plant types with high values for climatic adaptation express their full $\bar{v}_{\mathsf{rootmax}}$ and seeding frequency parameter values in a virtual environment, whereas plants with lower adaptation value receive only a portion of their parameter values during simulation time. Well adapted plant types, therefore, grow more vigorously and reproduce at a faster rate, whereas less adapted species might not grow at all or at a very slow rate. This allows capturing anisotropic, spatial interactions between plants mentioned in Sec. 2.4.2. Fig. 16 illustrates how temperature changes (due to elevation increase) reduce vigor and seeding frequency. This results in the gradual segregation of the three plant types at different levels of elevation. Moreover, individual plant model architectures adapt to changes of temperature.

2.6.5 Interactive Design of Ecosystems

We create virtual biomes in two steps. First, the plasticity parameters values (Table 3) are selected for all plant types the user wants to have appear in the biome. We provide a library for various default plant types (Fig. 6). Moreover, the parameters characterizing the environment have to be defined. This includes setting the climatic conditions by selecting values for temperature T and precipitation P as well as specifying the number of initial plant models and the time step for the simulation. A plant can be modeled by setting values for temperature and precipitation sensitivity, shade tolerance, and seeding radius. Upon simulation start plant models are instantiated at random locations in the terrain using the plant types in the library.

All parameter values can be modified during the simulation resulting in an interactive authoring process to design a specific biome (Fig. 10). We also allow users to select and remove individual plants at any moment. Once a desired simulation state has been reached, the branching structures of the whole ecosystem can be exported. We only export the skeletal graph of the branch modules and their individual transformations along with metadata for connectivity, branch diameter, and plant type.

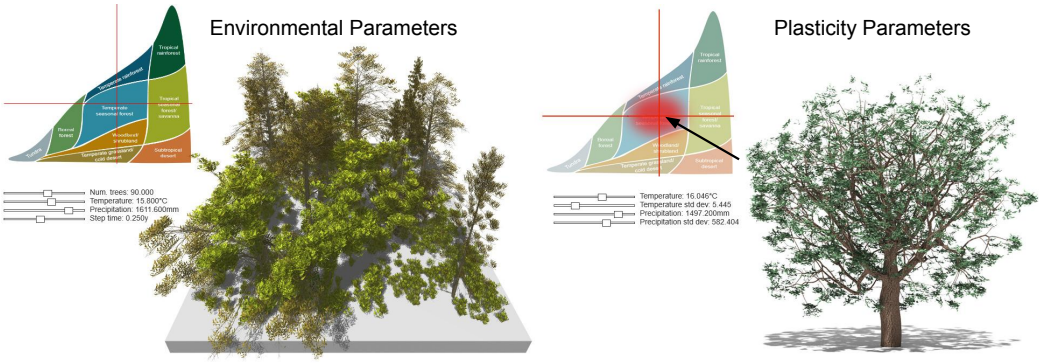

Figure 10: Screenshots of our interactive modeling tool. Environmental parameters (temperature and precipitation) are used on ecosystem level (left) to specify the climate. For each plant type plasticity parameters are set to describe the interaction with the environment (right).

2.7 Implementation and Results

We implemented our interactive framework in C++ and DirectX. To generate the results shown in the chapter we used an Intel(R) Core i5, 4×2.5GHz with 8GB RAM, and a NVIDIA Geforce

GTX 1050 GPU (4 GB RAM). We employ the instancing capabilities of DirectX to generate several instances of the same module and to transform and render them. Furthermore, we use a common shader pipeline of Vertex-, Geometry-, and Fragment Shaders along with the provided attributes of the nodes in the skeletal graph (branch thickness) to build and render intermediate branch geometry to provide users with visual feedback of the scene configuration. We used the *L3DT Terrain Editor* to generate a terrain mesh and a soil map for Fig. 16. Furthermore, we render the majority of the results shown throughout the chapter with Houdini. Table 4 reports the simulation times for the different components of our framework.

We implemented a framework to effortlessly generate ecosystems with plant interactions and realistic branching structures at interactive rates. Thereby, the framework allows users to efficiently explore the parameter space of the simulation. This allows for both, exploring natural phenomena related to plant ecosystem development as well as to generate complex forest geometry with high visual fidelity. Details of our framework and a screenshot of the developed user interface can be found in the Appendix 2.6.5.

Fig. #	P	PT	M	MP	B	N	TS	TR	TRO	TEMP	PREC	AGE
1 a	218	3	4.6	8	57.05	61.64	7	4	21	29.8	224.5	164
1 b	87	3	14.0	7	182.80	196.83	11	5	24	-2.1	267.4	273
1 c	611	3	34.4	4	392.45	435.50	14	19	32	6.0	940.1	382
1 d	1,248	6	18.9	7	215.97	113.89	45	12	36	28.0	3770.9	452
12 a	938	7	8.4	10	123.30	131.48	43	15	54	26.9	3055.9	389
12 b	926	7	7.40	10	111.78	118.89	43	15	52	26.9	3055.9	389
12 c	984	7	8.0	10	112.29	120.00	42	15	53	26.9	3055.9	423
12 d	950	7	7.6	9	97.13	104.60	42	15	53	26.9	3055.9	487
12 e	848	7	7.5	9	94.26	101.58	41	15	51	26.9	3055.9	543
11 a	147	2	2.9	3	30.39	33.35	4	3	19	-8.1	153	42
11 b	205	2	3.8	5	49.73	53.58	11	5	20	-2.6	310.3	145
11 c	264	3	4.1	4	48.16	52.23	10	4	22	-0.2	510.5	138
11 d	428	3	20.40	4	188.72	208.98	35	9	27	1.7	639.2	249
11 e	640	5	37.49	8	412.22	449.52	87	18	30	5.6	939.5	432
11 f	330	3	4.2	7	45.96	50.15	15	6	21	17.0	439.0	228
11 g	423	4	14.38	11	191.15	205.39	30	8	21	17.5	667.8	134
11 h	776	4	19.8	11	273.21	292.67	34	8	23	18.3	939.5	201
11 i	967	4	6.68	8	56.48	62.27	17	4	24	18.3	1239.8	223
11 j	1,404	3	9.23	4	103.45	112.47	20	7	24	18.3	1239.8	272
13 a	463	10	8.5	9	105.47	113.89	18	5	22	18.1	739.3	121
13 b	168	2	2.6	5	38.83	41.39	6	4	25	30.2	396.1	73
13 c	767	5	13.6	5	148.70	162.13	20	8	29	17.7	2526.8	486
16 g	468,199	3	2,271	15	23,283	26,776	18,796	3620	N/A	15.2	672.6	1400

Table 4: Performance settings and parameter values for figures in the chapter. P=Num. Plants, PT=Plant Types, M=Modules (K), MP=Module Prototypes, B=Branches (K), N=Nodes (K), TS=Time Simulation Step (ms), TR=Time Rendering (ms), TRO=Time Rendering Offline (min), TEMP=Temperature (°C), PREC=Precipitation, AGE=Simulation Age (years).

2.7.1 Results

In Fig. 1, 11, and 13 we show the final results produced with our modeling pipeline. The simulated plant populations show the characteristic features of the corresponding ecosystem types, ranging from small bushes and forbs in the *Savanna*, to tall growing pine trees for the *Boreal Forest* and densely populated plants in a *Rain Forest*. Altogether, our method is able to capture the properties of the nine biome types, introduced by the temperature-precipitation diagram (Fig. 2). As our method relies on representing branching structures as individual plants we can also produce realistic close-up renderings of the generated ecosystems, shown in Fig. 14.

We capture a variety of biological phenomena including successions, climatic adaptation, and gap dynamics. Moreover, our method is able to generate unique branching structures for each plant and the whole ecosystem. Fig. 3 and Fig. 12 show the successional stages of a developing ecosystem. During the simulation, plants die and decay, which opens space for existing and new

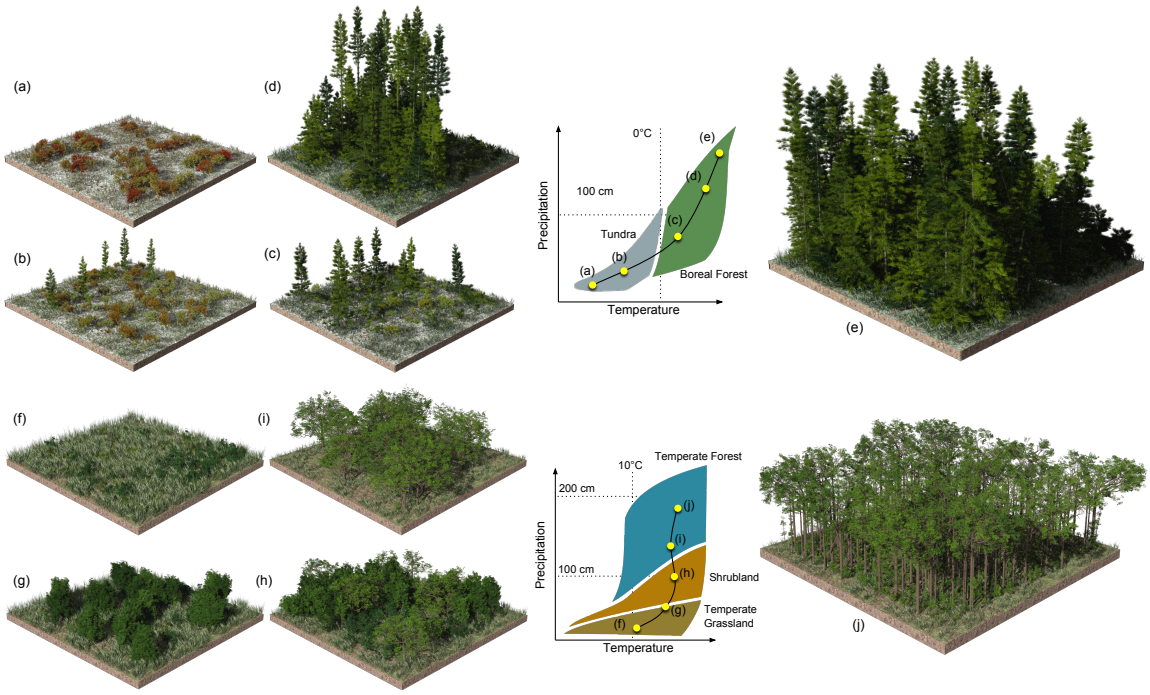

Figure 11: Biome transitions: by selecting temperature and precipitation our framework allows us to transition from one biome to another and thereby to generate a large variety of plausible ecosystems. The top row shows the transition from tundra to boreal forest (a)-(e), while the bottom row (f)-(j) shows the transition from temperate grassland to shrubland, and then to temperate forest. The diagrams show the locations of the corresponding biomes types in the temperature-precipitation diagram (Fig. 2). Each biome was simulated for a period of several hundred years.

Figure 12: Gap dynamics: starting from a fully grown plant population (a), a few plants are abruptly removed from the population and cause gaps in the ecosystem (b). This yields space to faster growing plants (palm trees) that quickly conquer the gaps (c), (d). Eventually, the well-adapted climax species (deciduous tree) establishes itself as the dominant species (e). The sequence shows the development over a period of 150 years.

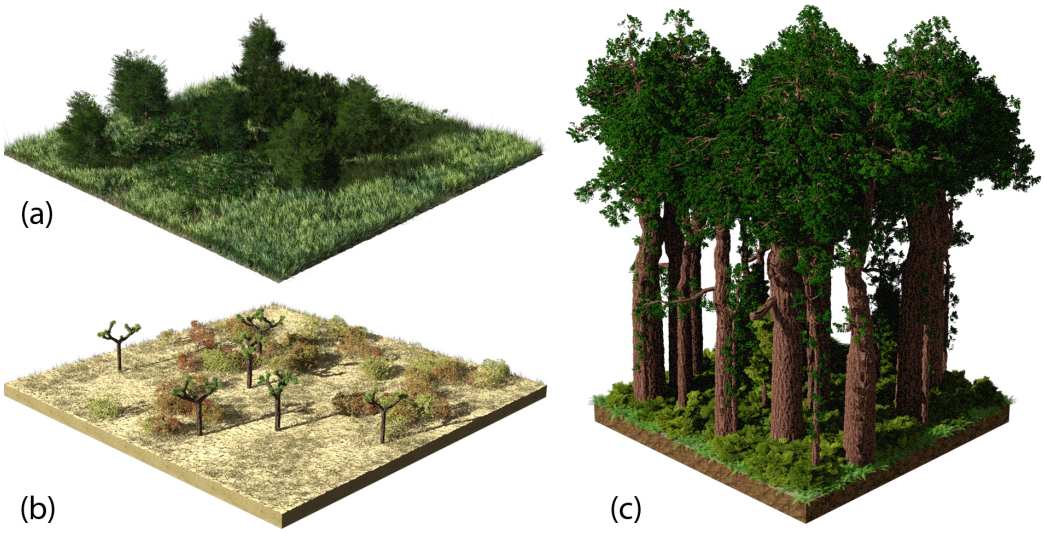

Figure 13: By selecting temperature and precipitation values we can generate other biomes. Here we show the results for a shrubland (a), a subtropical desert (b), and a temperate rainforest (c).

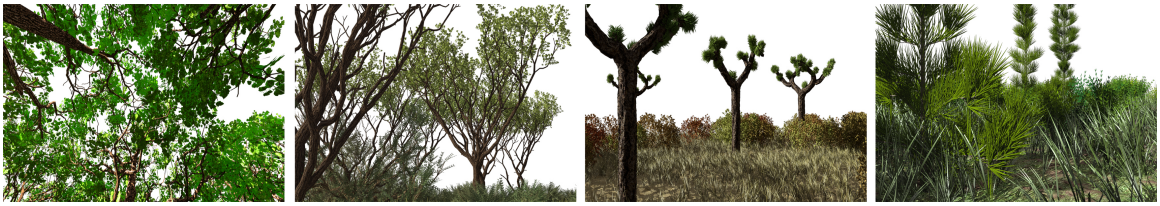

Figure 14: Close-up renderings of articulated branching structures. As our method relies on modeling plants based on individual branch skeletons we can produce complex in-forest renderings of the various biome types: temperate seasonal forest, savanna, desert, and boreal forest (left to right).

Figure 15: Tree architecture adapting to different environmental conditions: a solitary growing tree develops a wide crown covering the available space (a). When growing in more densely populated environments, it grows taller but less vigorous. It develops an asymmetric architecture due to the competition for light with neighboring plants (b, c).

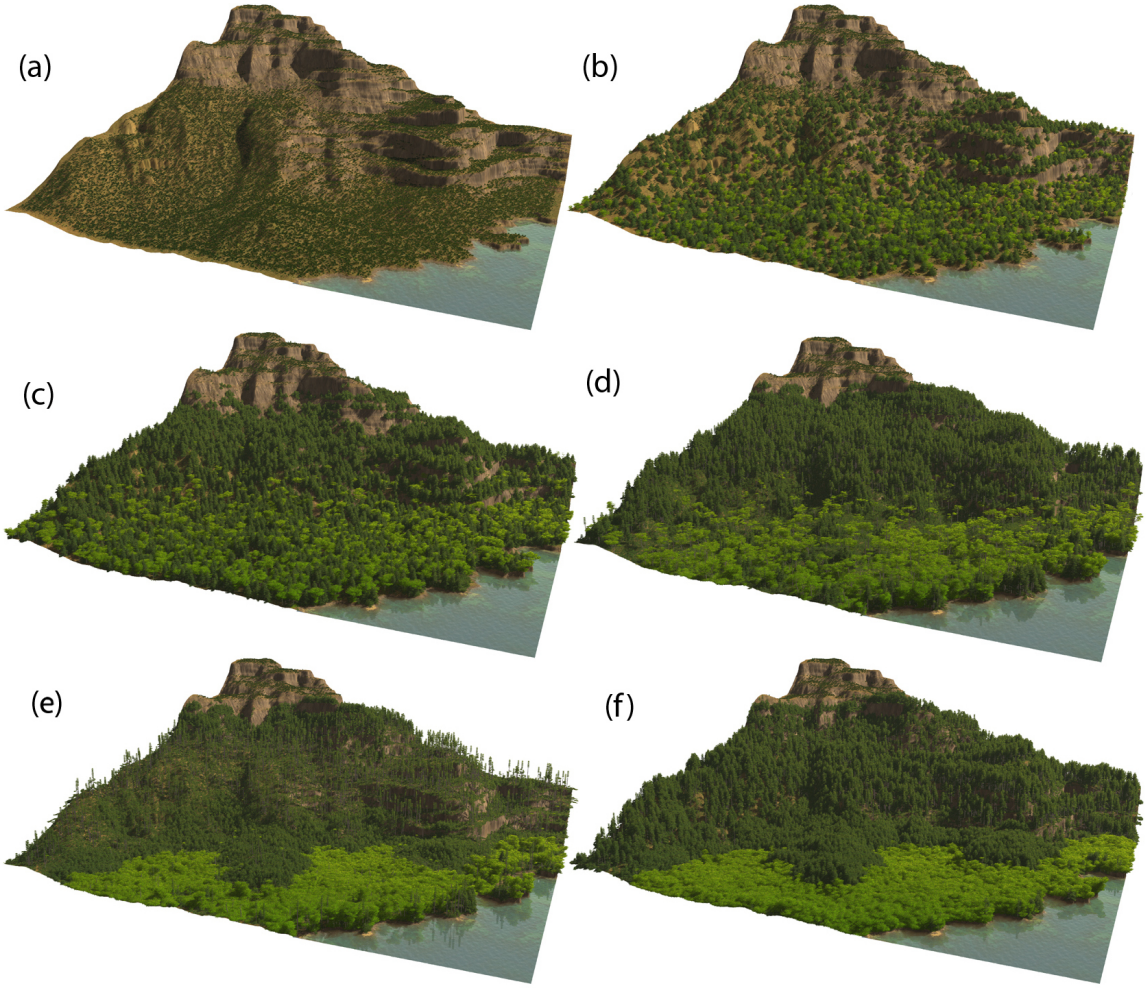

Figure 16: Temporal progression of a developing ecosystem composed of about 500K plant models and three plant types: a shrub, a conifer and a deciduous tree. We start the simulation with a mountainous environment devoid of vegetation such as is the case, e.g. after an ice-age. (a) fast growing shrubs populate all the terrain, (b) slower growing tree models start overshadowing shrubs at lower elevation levels, (c) a mixed forest of conifers and deciduous trees at lower elevations emerges, (d) the segregating forest forms a tree line with the cold-adapted shrub appearing only at the top of the mountain, (e) cohort senescence leaves large gaps in the conifer forest stand, (f) after several successions of trees a mixed age-forest emerges.

plants. In forestry this process is called gap dynamics and creates complex branching structures that are difficult to model manually. After an occurring disturbance of a plant ecosystem, new plants, such as grasses, forbs, and shrubs develop. Over time these plants are gradually replaced by pioneering tree species, which grow slower but are more shade tolerant.

The results in Fig. 11 show transitions through the temperature precipitation diagram. Our method is able to capture the variations of the different biome types, which allows to simulate plausible plant ecosystems. We show transitions from Tundra to Boreal Forest (a)-(e), as well as from Temperate Grassland to Temperated Forest (f)-(j).

The adaptation of branching structures according to varying distances to other plants is shown in Fig. 15. A plant growing together with surrounding plants develops a different branching structure compared to solitary grown plants. When growing in more densely populated environments, it grows taller but less vigorous and develops an asymmetric architecture due to the competition for light with neighboring plants.

In Fig. 16 we show a large-scale plant ecosystem developed on an initially empty terrain patch (e.g. the period of time just after an ice age). As we use instancing for the branch modules, we can model and render plant populations with up to 500K plants. Each plant is modeled with a unique branching structure interacting with neighboring plants and the terrain.

2.8 Evaluation, Discussion, and Limitations

We evaluated our framework based on visual and quantitative comparisons of plant ecosystem growth.

To validate the module orientation optimization algorithm, we calculate the intersection volume ratio of the bounding spheres of each module. We define it as the sum of volumes of intersections between modules divided by the total volume of all modules in the ecosystem. Fig. 18 (a), shows a comparison of ecosystem development with and without module orientation optimization. The naive approach increases quickly to a high percentage of volume intersection ratios indicating a high overlap of modules. Conversely, the approach with orientation optimization maintains volume intersection ratios below 5% throughout the simulation, indicating a very small overlap of module bounding volumes. We conclude that the optimization process successfully prevents most collisions of branches in the ecosystem. Usually, no more than 3 optimization steps are necessary to converge.

To evaluate self-thinning of plant populations, we compare our results to the logistic growth function [70]. We simulate the growth of 1,000 pine trees and measured the total biomass of the ecosystem (assuming a homogeneous wood density). Fig. 18 (b) illustrates that the curve resembles the logistic growth function. We also evaluate the self-thinning through comparison of simulation data for the ecosystem shown in Fig. 16 (d) to the 3/2 power law [71]. Results are shown in Fig. 17 and indicate a high-degree of correlation of the regression line (for plants with a diameter > 5 cm) and the 3/2 power law.

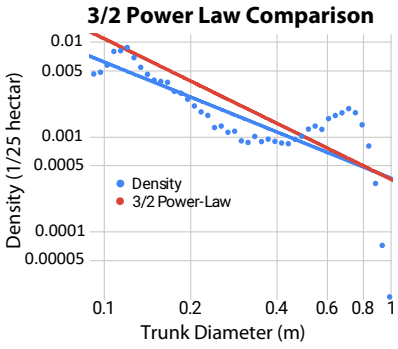

Figure 17: Comparison of simulation data for the ecosystem shown in Fig. 16 (d) to the 3/2 power law of self-thinning.

Tree structure is known to vary allometrically in branch lengths and diameters within the architecture. Therefore, we measured emerging allometries of tree height and trunk diameter as well as leaf dry mass and trunk diameter for a growing stand of simulated pine trees (Fig. 19). The results

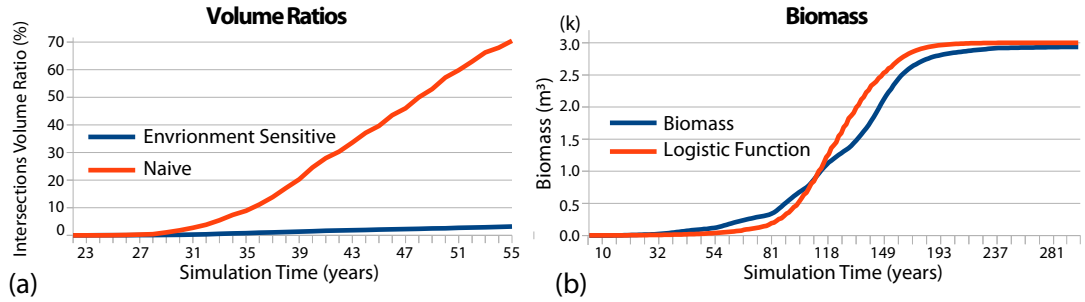

Figure 18: Measurements of a stand of 1,000 pine trees models. Comparison of intersection volume ratios between environment-sensitive and a naive forest growth model (a). Biomass of a plant population compared to logistic growth function with the parameters L = 3000, k = 0.0625, x_0=120 (b).

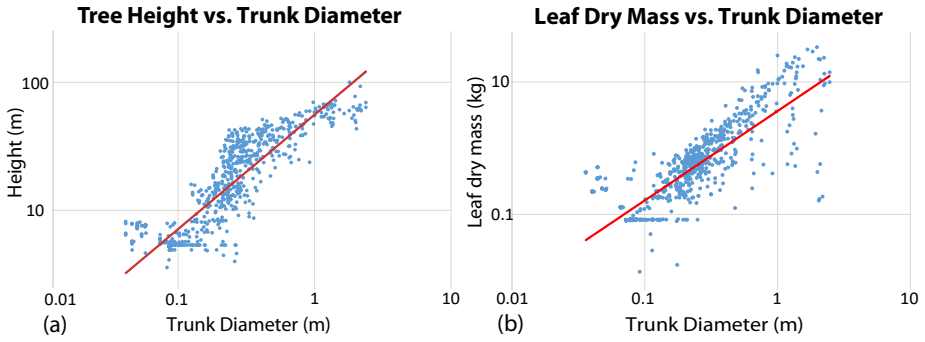

Figure 19: Emerging tree allometries of a simulated stand of about 1,000 pine tree models. (a): tree height vs trunk diameter; (b): leaf dry mass vs trunk diameter. Results conform with Eloy et al. (c.f. Figs. 6 a, b).

are in agreement to simulated and real data reported by other sources [55].

In Fig. 20 we report the results of modeling a single tree with variable numbers of branch modules as well as module prototypes with different complexity. Three examples of instantiated module prototypes are shown in the circles. Our multi-scale method allows balancing the deterministic development at module scale and self-organizing development at plant scale. Model (a) was generated with a few (99), but complex branch modules (deterministic development), while model (c) was simulated with many (1204) but less complex branch modules (self-organizing development). Model (b) represents the middle ground (294 modules). Even though the models were simulated with varying emphasis on these scales, all models (a-c) can be reproduced with similar visual fidelity and geometric complexity (about 200K polygons). This indicates the usefulness of the plant description given in Sec 4.1, i.e. plant architectures are the result of self-organization of self-similar architectural units. Balancing the number of modules and the complexity of prototypes thereby is a means to address accuracy and efficiency requirements for large-scale growth simulations. Furthermore, this can be seen as a compression scheme for branching structures.

To evaluate the modeling capabilities of our framework for single tree models, we compare our results to those produced by the procedural model of Stava et al. [29]. Their approach allows

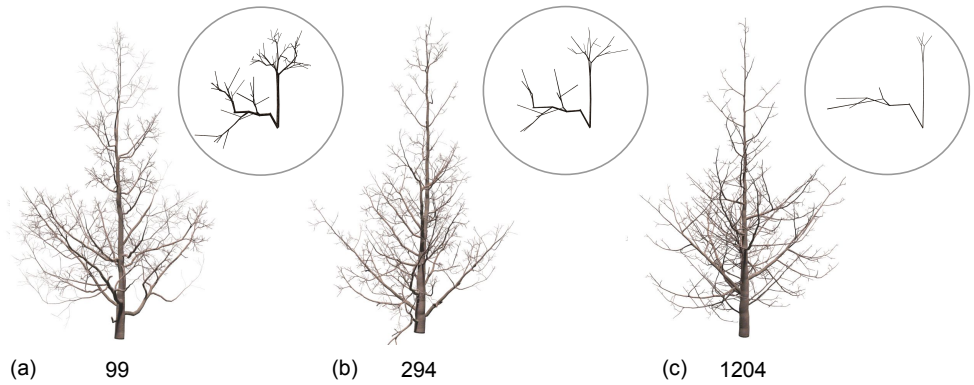

Figure 20: Results of modeling a single tree with variable numbers of branch modules (a: 99, b: 294, c: 1204) as well as module prototypes with different complexity. Three examples of instantiated module prototypes are shown in the circles. Despite the varying number of branch modules (99 vs. 1204), all models (a-c) can be reproduced with similar visual fidelity and geometric complexity.

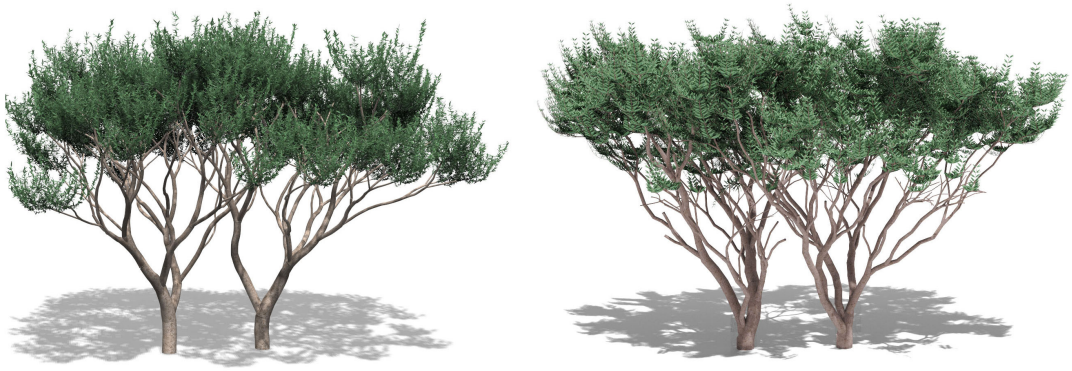

Figure 21: A comparison to the approach of Stava et al. [2014]. We use their procedural model to generate a tree model similar to the examples on the left. We decompose it into 10 modules and then use our modeling approach to replicate their modeling results. The figure shows the result of two trees growing together based on their (left) and our (right) method.

generating a large variety of plant species based on 25 parameters. While we aim at simulating ecosystems and not particular plant species, we use their method to generate plants, decompose them into branch modules, and then use our framework to produce new plants based on the generated modules. As we rely on the previously generated branching patterns, is not possible to directly compare the generated results, however, our module selection allows to connect the available modules so as to generate plausible branching structures, similar to state-of-the-art work in the field. In Fig. 21 we show the modeling results of plant-plant interactions of both systems (left: Stava et al. 2014, right: ours).

2.8.1 Discussion and Limitations

Our focus was to explore plant growth on the level of large-scale plant ecosystems. The visual results of our simulations evaluate the hypotheses stated in Sec. 2.4.1 that plant models can sufficiently be described as a collection of architectural units for ecosystem modeling. Branch modules facilitate

the instancing of geometry to efficiently design complex plant ecologies.

Moreover, our results indicate that the hypotheses given in Sec. 2.4.2 allow to produce complex plant ecosystem geometries that would be extremely challenging to model manually. Given our method it is now possible to explore the development of plant ecosystems, including temporal successions, gap dynamics, and spatial forest patterns.

Current methods for plant modeling mostly focus on more detailed representations of branch geometry and their development, while methods for modeling ecosystems often abstract away the complexity of single plant structures. Our method enables both: we can realistically model individual branching structures as well as biologically plausible forests. As a result, this allows us to evaluate ecological hypotheses formulated at the scale of branches instead of plants. This is novel and has the potential to stimulate future research in computer graphics and ecology.

We provide a library of plant types to model a range of plausible biomes. More realistic ecologies require a larger biodiversity that can only be obtained by manually defining more plant types. While we aimed at providing an efficient modeling tool, the introduced biological concepts to model plants and ecosystems are complex phenomena that require a range of parameters. While we limited the number of parameters, finding an appropriate configuration to author specific plant shapes can be challenging. The proposed parameters of our method allow us to generate a variety of biomes, however, we did not conclusively explore this parameter space.

2.9 Conclusion

We have presented a novel framework for large-scale ecosystem modeling that allows us to generate a variety of plant biomes of individual plants. We simulate the growth process of the entire ecosystem, which enables the plants to interact with their neighbors and in turn to generate plausible and complex branching structures. Our approach exploits the inherent self-similarity of plants to efficiently model large amounts of vegetation. We introduced plant modules as an efficient means of abstraction to define plant skeletons. Each module captures allometric properties that allows us to define convincing plants. We showed that the modules can be reused across single plants and across entire ecosystems.

Additionally, we have introduced a low-dimensional parameter space (2 environmental, 5 plasticity parameters), to efficiently design complex and diverse plant ecosystems. In combination with modeling plausible plant distributions this allows us to design different biome types, ranging from savannas and deciduous forests, to deserts and rain forests. The simulated ecosystems show a variety of properties also found in real forests, such as gap dynamics, successional stages, and self-thinning. Based on the introduced framework content creators can efficiently model complex ecosystems that can then be produced through commodity rendering software.

2.10 References

[1] M. Müller, V. Casser, J. Lahoud, N. Smith, and B. Ghanem, "Sim4cv: A photo-realistic simulator for computer vision applications," *IJCV*, vol. 126, no. 9, pp. 902–919, 2018.

[2] B. Lane and P. Prusinkiewicz, "Generating spatial distributions for multilevel models of plant communities," *Graphics Interface*, pp. 69–80, 2002.

[3] O. Deussen, P. Hanrahan, B. Lintermann, R. Měch, M. Pharr, and P. Prusinkiewicz, "Realistic modeling and rendering of plant ecosystems," *ACM Trans. Graph.*, pp. 275–286, 1998.

[4] O. Deussen, C. Colditz, M. Stamminger, and G. Drettakis, "Interactive visualization of complex plant ecosystems," *VIS '02*, pp. 219–226, 2002.

[5] E. Bruneton and F. Neyret, "Real–time realistic rendering and lighting of forests," *Comput. Graph. Forum*, vol. 31, no. 2pt1, pp. 373–382, 2012.

[6] M. Jaeger and J. Teng, "Tree and plant volume imaging - an introductive study towards voxelized functional landscapes," *PMA*, 2003.

[7] Y. Livny, S. Pirk, Z. Cheng, F. Yan, O. Deussen, D. Cohen-Or, and B. Chen, "Texture-lobes for tree modelling," *ACM Trans. Graph.*, vol. 30, no. 4, 53:1–53:10, 2011, ISSN: 0730-0301.

[8] B. Neubert, S. Pirk, O. Deussen, and C. Dachsbacher, "Improved model- and view-dependent pruning of large botanical scenes," *Comp. Graph. Forum*, vol. 30, no. 6, pp. 1708–1718, 2011.

[9] J. Gumbau, M. Chover, I. Remolar, and C. Rebollo, "View-dependent pruning for real-time rendering of trees," *Computers and Graphics*, vol. 35, no. 2, pp. 364–374, 2011, ISSN: 0097-8493.

[10] K. Xie, F. Yan, A. Sharf, D. Deussen, H. Huang, and B. Chen, "Tree modeling with real tree-parts examples," *TVCG*, vol. 22, no. 12, pp. 2608–2618, 2016.

[11] X. Zhang, G. Bao, W. Meng, M. Jaeger, H. Li, O. Deussen, and B. Chen, "Tree branch level of detail models for forest navigation," *Comp. Graph. Forum*, vol. 36, no. 8, pp. 402–417, 2017, ISSN: 0167-7055.

[12] G. Cordonnier, E. Galin, J. Gain, B. Benes, E. Guérin, A. Peytavie, and M.-P. Cani, "Authoring landscapes by combining ecosystem and terrain erosion simulation," *ACM Trans. Graph.*, vol. 36, no. 4, 134:1–134:12, 2017, ISSN: 0730-0301.

[13] J. Gain, H. Long, G. Cordonnier, and M.-P. Cani, "Ecobrush: Interactive control of visually consistent large-scale ecosystems," *Comput. Graph. Forum*, vol. 36, no. 2, pp. 63–73, May 2017, ISSN: 0167-7055.

[14] W. Palubicki, K. Horel, S. Longay, A. Runions, B. Lane, R. Měch, and P. Prusinkiewicz, "Self-organizing tree models for image synthesis," *ACM Trans. Graph.*, vol. 28, no. 3, 58:1–58:10, 2009, ISSN: 0730-0301.

[15] C. Godin, "Representing and encoding plant architecture: A review," *Ann. For. Sci.*, vol. 57, no. 5, pp. 413–438, 2000.

[16] L. Amissah, G. M. J. Mohren, F. Bongers, W. D. Hawthorne, and L. Poorter, "Rainfall and temperature affect tree species distribution in ghana," *Journal of Tropical Ecology*, vol. 30, no. 5, pp. 435–446, 2014.

[17] M. Aono and T. Kunii, "Botanical tree image generation," *IEEE Comput. Graph. Appl.*, vol. 4(5), pp. 10–34, 1984.

[18] P. E. Oppenheimer, "Real time design and animation of fractal plants and trees," *Proc. of SIGGRAPH*, vol. 20, no. 4, pp. 55–64, 1986, ISSN: 0097-8930.

[19] A. Lindenmayer, "Mathematical models for cellular interaction in development," *J. Theor. Biol.*, vol. Parts I and II, no. 18, pp. 280–315, 1968.

[20] P. Prusinkiewicz, "Graphical applications of l-systems," in *Proc. on Graph. Interf.*, 1986, pp. 247–253.

[21] T. Ijiri, S. Owada, and T. Igarashi, "Seamless integration of initial sketching and subsequent detail editing in flower modeling," *Comp. Graph. Forum*, vol. 25, no. 3, pp. 617–624, 2006.

[22] M. Okabe, S. Owada, and T. Igarashi, "Interactive design of botanical trees using freehand sketches and example-based editing," in *ACM SIGGRAPH Courses*, San Diego, California: ACM, 2007, ISBN: 978-1-4503-1823-5.

[23] J. Wither, F. Boudon, M.-P. Cani, and C. Godin, "Structure from silhouettes: a new paradigm for fast sketch-based design of trees," *Computer Graphics Forum*, vol. 28, no. 2, pp. 541–550, 2009.

[24] B. Neubert, T. Franken, and O. Deussen, "Approximate image-based tree-modeling using particle flows," *ACM Trans. Graph.*, vol. 26, no. 3, 2007, ISSN: 0730-0301.

[25] D. Bradley, D. Nowrouzezahrai, and P. Beardsley, "Image-based reconstruction synthesis of dense foliage," *ACM Trans. Graph.*, vol. 32, no. 4, 74:1–74:10, 2013, ISSN: 0730-0301.

[26] P. Tan, G. Zeng, J. Wang, S. B. Kang, and L. Quan, "Image-based tree modeling," *ACM Trans. Graph.*, vol. 26, no. 3, 2007, ISSN: 0730-0301.

[27] P. Tan, T. Fang, J. Xiao, P. Zhao, and L. Quan, "Single image tree modeling," *ACM Trans. Graph.*, vol. 27, no. 5, 108:1–108:7, 2008, ISSN: 0730-0301.

[28] C. Li, O. Deussen, Y.-Z. Song, P. Willis, and P. Hall, "Modeling and generating moving trees from video," *ACM Trans. Graph.*, vol. 30, no. 6, 127:1–127:12, 2011, ISSN: 0730-0301.

[29] O. Stava, S. Pirk, J. Kratt, B. Chen, R. Měch, O. Deussen, and B. Benes, "Inverse procedural modelling of trees," *Comp. Graph. Forum*, vol. 33, no. 6, pp. 118–131, 2014, ISSN: 1467-8659.

[30] S. Longay, A. Runions, F. Boudon, and P. Prusinkiewicz, "Treesketch: Interactive procedural modeling of trees on a tablet," in *Proc. of the Intl. Symp. on SBIM*, 2012, pp. 107–120.

[31] R. Měch and P. Prusinkiewicz, "Visual models of plants interacting with their environment," in *Proc. of SIGGRAPH*, ACM, 1996, pp. 397–410.

[32] S. Pirk, O. Stava, J. Kratt, M. A. M. Said, B. Neubert, R. Měch, B. Benes, and O. Deussen, "Plastic trees: Interactive self-adapting botanical tree models," *ACM Trans. Graph.*, vol. 31, no. 4, 50:1–50:10, 2012, ISSN: 0730-0301.

[33] Y. Zhao and J. Barbič, "Interactive authoring of simulation-ready plants," *ACM Trans. Graph.*, vol. 32, no. 4, 84:1–84:12, 2013, ISSN: 0730-0301.

[34] E. Quigley, Y. Yu, J. Huang, W. Lin, and R. Fedkiw, "Real-time interactive tree animation," *TVCG*, vol. 24, no. 5, pp. 1717–1727, 2018, ISSN: 1077-2626.

[35] R. Habel, A. Kusternig, and M. Wimmer, "Physically guided animation of trees," *Comp. Graph. Forum*, vol. 28, no. 2, pp. 523–532, 2009, ISSN: 0167-7055.

[36] S. Pirk, T. Niese, T. Hädrich, B. Benes, and O. Deussen, "Windy trees: Computing stress response for developmental tree models," *ACM Trans. Graph.*, vol. 33, no. 6, 204:1–204:11, 2014, ISSN: 0730-0301.

[37] S. Pirk, M. Jarząbek, T. Hädrich, D. L. Michels, and W. Palubicki, "Interactive wood combustion for botanical tree models," *ACM Trans. Graph.*, vol. 36, no. 6, 197:1–197:12, Nov. 2017, ISSN: 0730-0301.

[38] T. Hädrich, B. Benes, O. Deussen, and S. Pirk, "Interactive modeling and authoring of climbing plants," *Comput. Graph. Forum*, vol. 36, no. 2, pp. 49–61, 2017, ISSN: 0167-7055.

[39] B. Wang, Y. Zhao, and J. Barbič, "Botanical materials based on biomechanics," *ACM Trans. Graph.*, vol. 36, no. 4, 135:1–135:13, Jul. 2017, ISSN: 0730-0301.

[40] P. Prusinkiewicz and A. Lindenmayer, *The Algorithmic Beauty of Plants*. Springer-Verlag New York, Inc., 1990, ISBN: 0-387-97297-8.

[41] B. Lintermann and O. Deussen, "Interactive modeling of plants," *IEEE Comput. Graph. Appl.*, vol. 19, no. 1, pp. 56–65, 1999, ISSN: 0272-1716.

[42] P. de Reffye, C. Edelin, J. Françon, M. Jaeger, and C. Puech, "Plant models faithful to botanical structure and development," *SIGGRAPH Comput. Graph.*, vol. 22, no. 4, pp. 151–158, 1988, ISSN: 0097-8930.

[43] P. Decaudin and F. Neyret, "Rendering forest scenes in real-time," ser. EGSR'04, Norrköping, Sweden, 2004, pp. 93–102, ISBN: 3-905673-12-6.

[44] K. Boulanger K. Bouatouch and S. Pattanaik, "Rendering trees with indirect lighting in real time," ser. EGSR '08, Sarajevo, Bosnia and Herzegovina, 2008, pp. 1189–1198.

[45] B. Beneš, N. Andrysco, and O. Šťava, "Interactive modeling of virtual ecosystems," ser. NPH'09, 2009, pp. 9–16, ISBN: 978-3-905674-11-8.

[46] G. Gilet, A. Meyer, and F. Neyret, "Point-based rendering of trees," ser. NPH'05, Dublin, Ireland, 2005, pp. 67–73, ISBN: 3-905673-29-0.

[47] O. Argudo, A. Chica, and C. Andujar, "Single-picture reconstruction and rendering of trees for plausible vegetation synthesis," *Comput. Graph.*, vol. 57, no. C, pp. 55–67, 2016, ISSN: 0097-8493.

[48] C. Andújar, A. Chica, M. A. Vico, S. Moya, and P. Brunet, "Inexpensive reconstruction and rendering of realistic roadside landscapes," *Comput. Graph. Forum*, vol. 33, no. 6, pp. 101–117, Sep. 2014, ISSN: 0167-7055.

[49] M. Jaeger and P. de Reffye, "Basic concepts of computer simulation of plant growth," vol. 17, 1992.

[50] R. H. Waring and S. W. Running, "Forest ecosystem analysis at multiple time and space scales," in *Forest Ecosystems (Third Edition)*, Academic Press, 2007, pp. 1–16, ISBN: 978-0-12-370605-8.

[51] J. I. Drever, *Surface and Ground Water, Weathering, and Soils*. Elsevier Science, 2005, ISBN: 9780080447193.

[52] M. Heydari and A. Mahdavi, "The survey of plant species diversity and richness between ecological species groups (zagros ecosystem, ilam)," vol. 9, 2009.

[53] F. L. Zhang, J. J. Wang, S. H. Liu, and S. M. Zhang, "Development of economic and environmental metrics for forest-based biomass harvesting," *IOP Conference Series: Earth and Environmental Science*, vol. 40, no. 1, p. 012 052, 2016.

[54] R. J. Keenan, "Climate change impacts and adaptation in forest management: A review," *Annals of Forest Science*, vol. 72, no. 2, pp. 145–167, 2015, ISSN: 1297-966X.

[55] C. Eloy, M. Fournier, A. Lacointe, and B. Moulia, "Wind loads and competition for light sculpt trees into self-similar structures," in *Nature Communications*, 2017.

[56] T. Sachs, "Self-organization of tree form: A model for complex social systems," *Journal of Theoretical Biology*, vol. 230, no. 2, pp. 197–202, 2004, ISSN: 0022-5193.

[57] D. Barthélémy, "Establishment of modular growth in a tropical tree: Isertia coccinea vahl. (rubiaceae)," *Philosophical Transactions of the Royal Society of London B: Biological Sciences*, vol. 313, no. 1159, pp. 89–94, 1986, ISSN: 0080-4622.

[58] D. Barthélémy and Y. Caraglio, "Plant architecture: A dynamic, multilevel and comprehensive approach to plant form, structure and ontogeny.," *Annals of botany*, vol. 99 3, pp. 375–407, 2007.

[59] R. H. Whittaker, *Classification of natural communities*, English. New York : Arno Press, 1977, Reprint of the 1962 ed. published in Plainfield, N.J., which was issued as v. 28, no. 1 of the Botanical review, ISBN: 040510426X.

[60] J. Andel, J. P. Bakker, and A. P. Grootjans, "Mechanisms of vegetation succession: A review of concepts and perspectives," *Acta Botanica Neerlandica*, vol. 42, no. 4, pp. 413–433, 1993.

[61] S.-I. Yamamoto, "Forest gap dynamics and tree regeneration," *Journal of Forest Research*, vol. 5, no. 4, pp. 223–229, 2000, ISSN: 1610-7403.

[62] H. Buckley, B. Case, R. Vallejos, J. Camarero, E. Gutiérrez, E. Liang, Y. Wang, and A. M. Ellison, "Detecting ecological patterns along environmental gradients: Alpine treeline ecotones," *CHANCE*, vol. 29, pp. 10–15, Apr. 2016.

[63] J. Digby and R. D. Firn, "The gravitropic set-point angle (gsa): The identification of an important developmentally controlled variable governing plant architecture.," *Plant Cell Environ*, vol. 18, no. 12, pp. 1434–40, 1995.

[64] G. R. McGhee, "Theoretical morphology: The concept and its applications," 1999.

[65] K. Shinozaki, K. Yoda, K. Hozumi, and T. Kira, "A quantitative analysis of plant form: The pipe model theory. ii. further evidence of the theory and its application in forest ecology," *Jpn J Ecol*, vol. 14, pp. 133–139, Aug. 1964.

[66] N. Bassuk, D. F. Curtis, B. Marranca, and B. Neal, "Recommended urban trees: Site assessment and tree selection for stress tolerance," *Cornell University, Department of Horticulture*, 2009.

[67] D. Mueller-Dombois, "A natural dieback theory, cohort senescence as an alternative to the decline disease theory," pp. 26–37, Jan. 1992.

[68] L. Mander, S. C. Dekker, M. Li, W. Mio, S. W. Punyasena, and T. M. Lenton, "A morphometric analysis of vegetation patterns in dryland ecosystems," *Royal Society Open Science*, vol. 4, Feb. 2017.

[69] N. Salzmann, S. C. Scherrer, S. Allen, and M. Rohrer, *Temperature, precipitation and related extremes in mountain areas*. Cambridge University Press, 2015, pp. 28–49.

[70] J. Vanclay, "Growth models for tropical forests: A synthesis of models and methods," *Forest Science -Washington-*, vol. 41, pp. 7–42, Jan. 1995.

[71] B. Zeide, "Analysis of the 3/2 power law of self-thinning," *Forest Science*, vol. 33, pp. 517–537, Jun. 1987.

3 Towards Modeling Complex Interactions between Weather and Vegetation

Figure 22: An aerial photograph of clouds over a forest. The vapor released by the foliage is an important factor in cloud formation. In return the clouds affect the sunlight and precipitation available to the plants.

3.1 Introduction

In Chapter 2 we presented our method for simulating vast ecosystems. The results shown that a great variety of biomes can be generated by adjusting temperature and precipitation. However, for a given scene these parameters were in principle uniform, allowing for a simple height-based temperature gradient. Therefore, we seeked to explore modeling of more environmental conditions that interplay with vegetation growth, e.g. wind, clouds, fog, mist, local variations of precipitation and temperature.

We decided to develop a cloud dynamics model, which allows for the simulation of evaporation, cloud formation and precipitation. Clouds are among the most common weather phenomena and have a close connection with vegetation (see Figure 22). The vapor released by the foliage is eventually condensing as fog or clouds. In return the clouds produce precipitation which is crucial for the growth of the plants. Depending on the cloud cover, a variable amount of sunlight is available to the plants. In result, all these factors induce local variations of humidity and temperature, and this way so called ecoclimates emerge. In Chapter 4 we show how to simulate ecoclimates by combining our models for vegetation and clouds.

3.2 Cloud Model

In this section we provide an overview of our cloud dynamics model, which can be divided into an atmospheric model that describes temperature and pressure changes as a function of altitude, a 0D thermodynamics model that determines local forces and the formation of clouds, and the fluid dynamic model that determines the motion of humid air in the atmosphere.

3.2.1 Atmosphere

The background atmosphere is determined by the temperature distribution and the fundamental hydrostatic equation [1] for compressible fluids.

3.2.1.1 Atmospheric Pressure The hydrostatic equation relates the density ρ of a fluid to the pressure gradient,

$$\mathsf{d}_z p = -\rho g \,, \tag{14}$$

in which $g \approx 9.81$ m/s^2 denotes the acceleration due to gravity. In an ideal gas, pressure p is related to density and temperature T as $\rho = p/(RT)$, where $R = \mathcal{R}/M$ is the specific gas constant, i.e. the ratio of the general gas constant $\mathcal{R}$ and the molar mass M. We introduce a temperature distribution analogous to the 'International Standard Atmosphere' (ISA) using the temperature lapse rate $\mathsf{d}_z T = \Gamma$, so that 14 can be integrated to

$$\int_0^z \frac{dp}{p} = \frac{g}{R}\int_0^z \frac{dz}{T(z)} = \frac{g}{R}\int_0^z \frac{dz}{T_0 + \Gamma z} \,, \tag{15}$$

yielding an equation for pressure as a function of altitude,

$$p(z) = p_0 \left(1 - \frac{\Gamma z}{T_0}\right)^{\frac{g}{R\Gamma}} \,. \tag{16}$$

3.2.1.2 Temperature Profile Interesting weather phenomena occur at an inversion layer at high altitudes, for which we introduce a second lapse rate Γ_1, valid beyond an altitude of z_1, so that the temperature profile is described as

$$\begin{aligned} 0 \le z \le z_1 : &\qquad T(z) = T_0 + \Gamma_0 z \,, \\ z_1 < z : &\quad T(z) = T_{z1} + \Gamma_0 z = T_0 + \Gamma_0 z_1 + \Gamma_1 (z - z_1) \,. \end{aligned} \tag{17}$$

An interesting stratification is given for $\Gamma_0 < 0$, $\Gamma_1 > 0$, then the temperature inversion at z_1 would act as an obstacle for the rising thermal, allowing the distinct flattened top (the 'anvil') of a cumulonimbus to form. Usually, we employ a simple inversion by making use of a single lapse rate Γ setting $\Gamma_0 := \Gamma$ and $\Gamma_1 := -\Gamma$.

3.2.2 Thermodynamics

The thermodynamics model based on first-principles provides local descriptions of air-water mixture properties, the temperature change of the rising thermal, the buoyancy and thus resulting local acceleration, and the phase transitions between vapor, cloud, and rain.

3.2.2.1 Generalities In the present model, the background air is assumed to be dry. Then its molar mass is constant with

$$\mathcal{M}_{\mathsf{air}} = 28.96 \text{ g/mol} \,. \tag{18}$$

The thermal (i.e. a column of rising air) is an air-water mixture, with a water vapor mole fraction X_V, and the water molar mass

$$\mathcal{M}_W = 18.02 \text{ g/mol} \,, \tag{19}$$

so that, using the water vapor mole fraction X_V, an average molar mass for the humid air in the thermal can be calculated as

$$\mathcal{M}_{\mathsf{th}} = X_V \mathcal{M}_W + (1 - X_V)\mathcal{M}_{\mathsf{air}} \,. \tag{20}$$

Mole fractions X and mass fractions Y are related through

$$Y_V = X_V \frac{\mathcal{M}_W}{\mathcal{M}_{\mathsf{th}}} \,. \tag{21}$$

Following Kessler [2], the amount of water in the atmosphere can be expressed in terms of the mass ratio q_i of water per mass unit of dry air, specifically vapor q_v, cloud q_c, and rain q_r. The mole fractions X_i are related to the mass ratios q_i via

$$X_i = \frac{q_i}{q_i + 1} \,. \tag{22}$$

3.2.2.2 Temperature in the Rising Thermal The warm and humid air in a thermal rises when it has a lower density than the surrounding air. The temperature profile of the atmosphere is prescribed and ultimately a function of the weather, whereas the rising thermal changes its local temperature because of its expansion to lower pressures at higher altitudes. Heat exchange with the surrounding atmosphere can be neglected, and the process is slow enough to assume an isentropic expansion to take place.

The change in pressure directly determines the change in temperature through the classical isentropic relations [3]

$$T_{\mathsf{th}}(z) = \hat{T} \left(\frac{p(z)}{\hat{p}} \right)^{\frac{\gamma_{\mathsf{th}} - 1}{\gamma_{\mathsf{th}}}} \,, \tag{23}$$

where $\hat{T}$ and $\hat{p}$ are the conditions at the ground. The isentropic exponent γ for water vapor and air are, respectively $\gamma_{\mathsf{air}} = 1.4$ and $\gamma_V = 1.33$, so that the isentropic exponent of the humid thermal is approximately

$$\gamma_{\mathsf{th}} = Y_V \gamma_V + (1 - Y_V)\gamma_{\mathsf{air}} \,, \tag{24}$$

where Y_V is the mass fraction of water in the thermal.

3.2.2.3 Buoyancy and Acceleration of the Thermal A difference in density between atmosphere and thermal will result in a vertical acceleration following Archimedes' principle. The humid thermal air parcel of volume V and density ρ_{th} experiences an upward lift force in air of density ρ_{air} of

$$L = V g(\rho_{\mathsf{air}} - \rho_{\mathsf{th}}) \,. \tag{25}$$

Then, the buoyant acceleration on this thermal parcel, from Newton's second law $F = ma$, is given by

$$B = \frac{L}{m} = \frac{V g(\rho_{\mathsf{air}} - \rho_{th})}{V \rho_{\mathsf{th}}} = g \left(\frac{\rho_{\mathsf{air}}}{\rho_{\mathsf{th}}} - 1 \right) \,. \tag{26}$$

We can treat thermal and air as ideal gases, for which

$$\rho = \frac{p}{RT} = \frac{p}{(\mathcal{R}/\mathcal{M})T} \,, \tag{27}$$

with the universal gas constant $\mathcal{R} = 8314$ J/g K and the gas molar mass $\mathcal{M}$. The pressure at every altitude is equilibrated between the thermal and the surrounding air, so that 26 can be simplified to

$$B = g\left(\frac{\mathcal{M}_{\mathsf{air}}}{\mathcal{M}_{\mathsf{th}}}\frac{T_{\mathsf{th}}}{T_{\mathsf{air}}} - 1\right). \tag{28}$$

The air temperature $T_{\mathsf{air}} = f(z)$ is specified by our atmospheric model, Eq. (17), and the thermal temperature from the cooling due to expansion, Eq. (23), the molar masses $\mathcal{M}_i$ as introduced in Sec. 3.2.2.1.

3.2.2.4 Condensation and Cloud Formation The initial water content rises with the thermal. However, the rising humid air in the thermal cools down as it gains altitude and loses capacity to keep the water vapor solved. When the partial pressure on the water vapor in the air drops below the saturation pressure at the local temperature, the excess water vapor that cannot be solved in the air anymore condenses into tiny droplets – clouds. This saturation mixing ratio $q_{vs}(T, p)$ can be approximated for the relevant temperature range as

$$q_{vs}(T, p) = \frac{380.16}{p}\mathsf{exp}\left(\frac{17.67T}{T + 243.50}\right) \tag{29}$$

for given temperature and pressure in Celsius respectively Pascal [4].

3.2.2.5 Heat Release from Condensation In order to account for the energy released by water vapor condensing into droplets when saturation is reached at the base of the cloud, the temperature of the thermal, 17 has to be extended. The energy release per condensed water mass fraction X_C is the latent heat L. The associated temperature increase ΔT_V then depends on the heat capacity, so that

$$T_{\mathsf{th}}(z) = \hat{T}\left(\frac{p(z)}{\hat{p}}\right)^{\frac{\gamma_{\mathsf{th}}-1}{\gamma_{\mathsf{th}}}} + \Delta T_V = \hat{T}\left(\frac{p(z)}{\hat{p}}\right)^{\frac{\gamma_{\mathsf{th}}-1}{\gamma_{\mathsf{th}}}} + \frac{L}{c_p}X_C\,. \tag{30}$$

Now, the heat capacity c_p of the air in the thermal is required. This is with respect to only the gaseous part of the thermal, i.e. dry air and water vapor X_V,

$$c_p^{\mathsf{th}} = \frac{\gamma_{\mathsf{th}}\mathcal{R}}{\mathcal{M}_{\mathsf{th}}(\gamma_{\mathsf{th}} - 1)}\,, \tag{31}$$

with the thermal air molar mass $\mathcal{M}_{\mathsf{th}}$ from 20, and the thermal air ratio of specific heats γ_{th} from 24.

3.2.2.6 Prediction of Cloud Boundaries This static model already allows for parameter studies and identification of relevant variables. Figure 23 shows how the relative humidity $\phi_{\mathrm{rel}} = q_v/q_{vs}$ and the buoyancy B determine the base and the top of the cloud. As an approximation for this initial exploration, the effect of latent heat is neglected. Specifically, the buoyancy is determined by the temperature gradient; the relative humidity in the thermal is controlled by the temperature and the vapor mass ratio q_v. Figure 24 shows a number of atmospheric profiles of temperature, density, buoyancy, vapor fraction, and relative humidity, to illustrate representative profiles for fog, stratocumulus, cumulus, and cumulonimbus clouds that can be created with this model.

Figure 24 further reveals the physical parameters that can be used to control the cloud dimensions. The cloud base is determined from the point where the relative humidity exceeds unity and

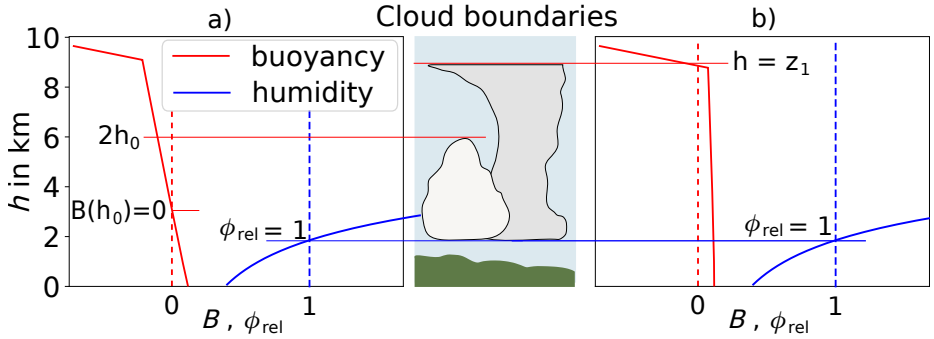

Figure 23: Illustration of relation between atmospheric profile data and cloud boundaries. A warm/ humid thermal will form on the ground and rise up, cooling down in the process. The cloud base will form at the point where the relative humidity ϕ_{rel} has increased to unity due to the reduced temperature. (a) the thermal will be accelerated upwards to neutral buoyancy $B(h_0) = 0$, and will be decelerated beyond. For the linear buoyancy profiles found here, the top of the cloud will be found where the thermal has come to rest at approximately $h = 2h_0$. (b) An inversion layer will stop the upward draft of the air that has not been decelerated, creating the characteristic flat anvil shape of the cumulonimbus cloud top.

the vapor condenses. The top is reached where the upward velocity of the rising thermal vanishes, with the altitude of vanishing buoyancy marking the mid-point altitude.

The temperature and density plots are mostly similar across fog, stratocumulus, and cumulus clouds. They differ for cumulonimbus as the temperature values of the thermal are higher relative to the atmospheric temperature values, which can be controlled by the temperature lapse rate Γ. The intersection point of the graphs indicates the altitude of the top of the clouds, which is several dozen meters for fog, 2 000 meters for stratocumulus clouds, 2 500 meters for cumulus clouds and 8 000 meters for cumulonimbus clouds. Alternatively, the top of the clouds is shown by the buoyancy graph. Relative humidity ϕ_{rel} defines the base altitude at which a cloud forms. Fog forms close to the ground surface, while cumulus and cumulonimbus clouds form at an altitude of 1 500 meters and stratocumulus at 1 800 meters. Analogously, this relationship can be expressed by the proportions of vapor fraction q_v and saturation mixing ratio q_{vs}. Varying the parameter values over time allows us to describe the temporal development of weather, such as the transition of fog to stratocumulus clouds. By additionally applying an external (rotating) wind field to the simulation we can transition to a typical summer afternoon thunderstorm.

3.2.3 Fluid Dynamics

The fluid dynamics model solves the motion of air in the atmosphere, as caused by external wind and differences in density.

3.2.3.1 Transport Equations The system of equations for fluid transport is developed from the principles of conservation of mass, energy, and Newton's second law. Following Boussinesq's classical assumption, we account for variable density in the source terms, but assume an approximately constant density in the flow dynamics due to the very low Mach numbers involved. From this follows directly that the momentum and energy equations are decoupled and can be solved independently. Our model is closed by using the water phase transport equations for vapor q_v, condensed cloud q_c,

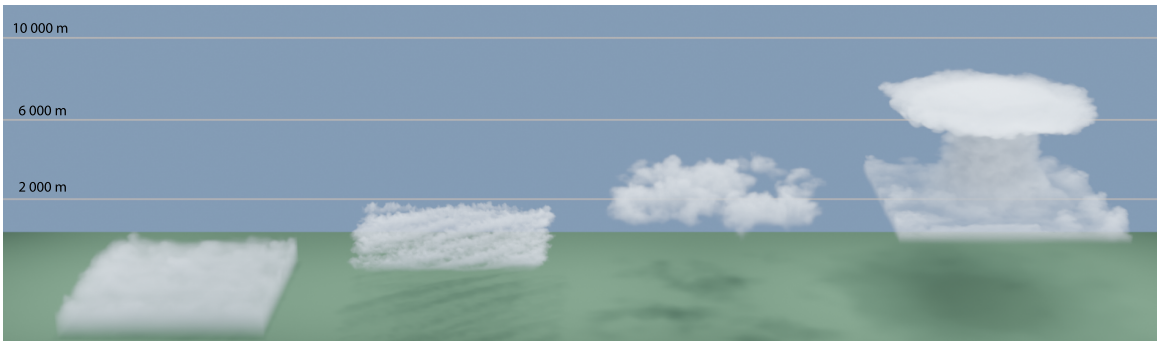

(a) Simulated fog, stratocumulus, cumulus, and cumulonimbus clouds (left to right). The corresponding altitude-temperature, -density, -buoyancy, -vapor fraction and -relative humidity profiles can be found below.

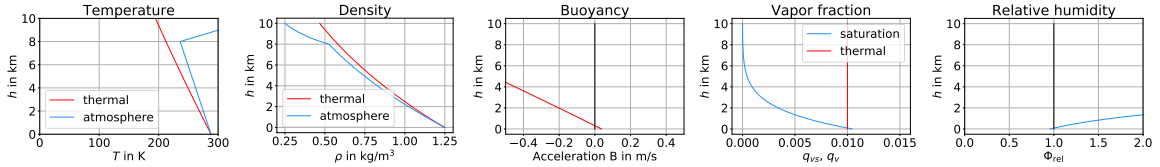

(b) Fog: Vanishing buoyancy at ground level prevents thermals from rising, a relative humidity of one at ground level causes formation of fog.

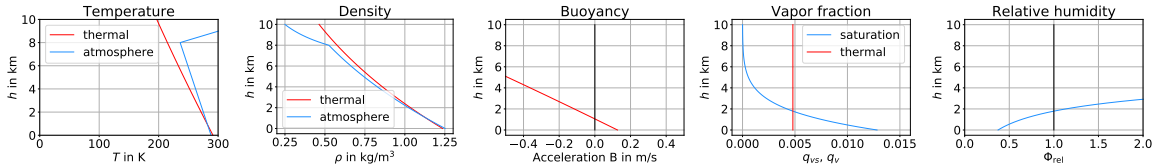

(c) Stratocumulus: Finite buoyancy at ground causes thermal to rise, with a top of 2000 m, and a base with $\phi_{\text{rel}} = 1$ at 1800 m.

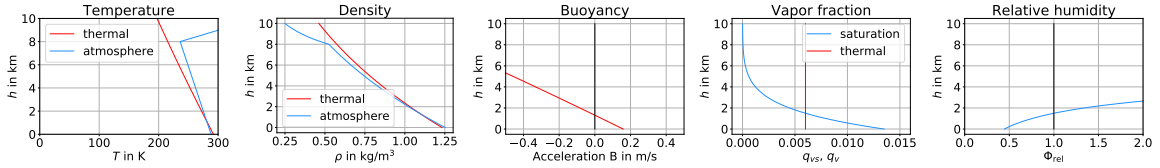

(d) Cumulus: Buoyancy at ground causes thermal to rise, the higher humidity increases the top to 2500 m, and reduces the base with $\phi_{\text{rel}} = 1$ to 1500 m.

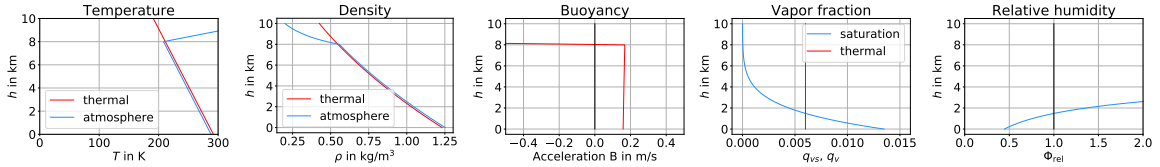

(e) Cumulonimbus: a higher temperature lapse rate causes a constant upward acceleration of the thermal to the inversion layer at 8000 m, while maintaining a base of 1500 m.

Figure 24: Simulation of the development of different cloud types (24a) and corresponding altitude-temperature, -density, -buoyancy, -vapor fraction and -relative humidity profiles: fog (24b), stratocumulus (24c), cumulus (24d), and cumulonimbus (24e) clouds. In accordance with Fig. 23, the cloud base is determined by the vapor reaching saturation conditions with the relative humidity ϕ_{rel} reaching unity; the top of the cloud is where the upward motion of the rising thermal has vanished.

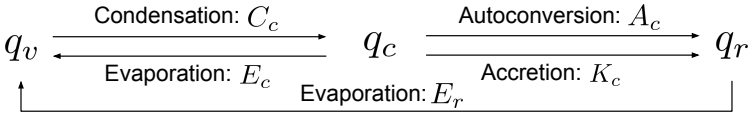

Figure 25: Illustration of Kessler's scheme [2] for modeling the transport between vapor, cloud water, and rain.

and rain q_r based on Kessler's classical model [2].

The simulation of fluids is an established and ongoing research topic within the computer graphics community. Among others, Bridson and Müller provided a detailed introduction to fluid simulation from a computer graphics' perspective in their SIGGRAPH course [5].

As usual, in our model, the fluid's state is described by a velocity field $\boldsymbol{u} : (\boldsymbol{x}, t) \mapsto \boldsymbol{u}(\boldsymbol{x}, t)$ which for given time $t \in \mathbb{R}_0^+$ and position $\boldsymbol{x} \in \mathbb{R}^3$ returns the corresponding local flow $\boldsymbol{u}(\boldsymbol{x}, t) \in \mathbb{R}^3$.

3.2.3.2 Mass The conservation of mass prescribes the continuity equation of a solenoidal velocity field as

$$\nabla \cdot \boldsymbol{u} = 0\,. \tag{32}$$

3.2.3.3 Momentum The change in momentum according to Newton's second law is expressed in terms of the Navier-Stokes equations, allowing for the solution of the temporal evolution of the velocity field,

$$\partial_t \boldsymbol{u} = -\boldsymbol{u} \cdot \nabla \boldsymbol{u} - \rho^{-1} \nabla p + \nu \nabla \cdot \nabla \boldsymbol{u} + \boldsymbol{b} + \boldsymbol{f}\,, \tag{33}$$

in which the density is denoted by ρ, the pressure by p, and the kinematic viscosity by ν. The first term on the right side of 33 describes phenomena caused by advection followed by a pressure and a viscosity term. Buoyancy is taken into account by the force $\boldsymbol{b} \in \mathbb{R}^3$ and other external forces are combined and described by an additional external net force $\boldsymbol{f} \in \mathbb{R}^3$. Please note, that the vector Laplacian in 33 is similarly defined as its scalar counterpart and simply acts component-wise.

3.2.3.4 Energy The conservation of energy in temperature form can be written [1] as

$$\partial_t \theta + (\boldsymbol{u} \cdot \nabla)\theta + \frac{L}{c_p \Pi} C_c = 0\,, \tag{34}$$

in which $C_c = \partial_t q_c + (\boldsymbol{u} \cdot \nabla)\, q_c$ denotes the rate of condensation. In 34, the latent heat is given by $L \approx 2.5$ J/kg, and the ratio $\Pi := T(t_0)/\theta$ of the absolute and the potential temperature is written as the Exner function used in atmospheric modeling. Π can be considered as a non-dimensionalized pressure.

3.2.3.5 Water Continuity The simplest model for rain, based on Kessler's methodology as illustrated in Figure 25, includes a third transport equation for a rain phase q_r in addition to vapor and cloud, along with source terms that couple the transport equations. Using the material derivative $\mathsf{D}_t \varphi = \partial\varphi/\partial t + \boldsymbol{v} \cdot \nabla\varphi$ [6], we can write

$$\mathsf{D}_t q_v = \quad -C_c + E_c + E_r\,, \tag{35}$$

$$\mathsf{D}_t q_c = \quad C_c - E_c - A_c - K_c\,, \tag{36}$$

$$\mathsf{D}_t q_r = \quad A_c + K_c - E_r\,, \tag{37}$$

with the source terms C_c describing condensation, E_c describing the evaporation of clouds, E_r describing the evaporation of rain, A_c describing autoconversion of raindrops from clouds, and K_c describing the accretion of cloud water due to falling drops. Kessler suggests models in the form $A_c = \alpha_A(q_c - a_T)$ with $a_T = 0.001$ kg/kg, and $K_c = \alpha_K q_c q_r$. Rain drops technically fall and are accelerated, but they reach a constant terminal velocity almost right away (≈ 10 m/s). We employ a constant vertical terminal velocity and the local lateral wind velocity.

3.3 Conclusion

We presented a novel approach to physically accurate simulation of clouds based on first-principles. Using our framework, we can simulate several different cloud types, their transitions, and complex cloud phenomena. With this method we are prepared for the next steps towards modeling complex interactions between weather and vegetation. In Chapter 4 we combine the simulation of ecosystems with cloud dynamics model and explore the feedback between plants and cloud formation.

3.4 References

[1] R. A. Houze, *Cloud Dynamics*, ser. ISSN. Elsevier Science, 1994, ISBN: 9780080502106.

[2] E. Kessler, "On the distribution and continuity of water substance in atmospheric circulations," in *On the Distribution and Continuity of Water Substance in Atmospheric Circulations*. Boston, MA: American Meteorological Society, 1969, pp. 1–84, ISBN: 978-1-935704-36-2.

[3] J. D. Anderson, *Modern compressible flow with historical perspective*, 3rd. McGraw Hill, 2003.

[4] M. K. Yau and R. R. Rogers, *A Short Course in Cloud Physics*. Elsevier Science, 1996, ISBN: 9780080570945.

[5] R. Bridson and M. Müller, "Fluid simulation: Siggraph 2007 course notes," pp. 1–81, 2007.

[6] P. K. Kundu, I. M. Cohen, and D. R. Dowling, *Fluid Mechanics*, ser. Science Direct e-books. Elsevier Science, 2012, ISBN: 9780123821003.

4 Ecoclimates: Climate-response Modeling of Vegetation

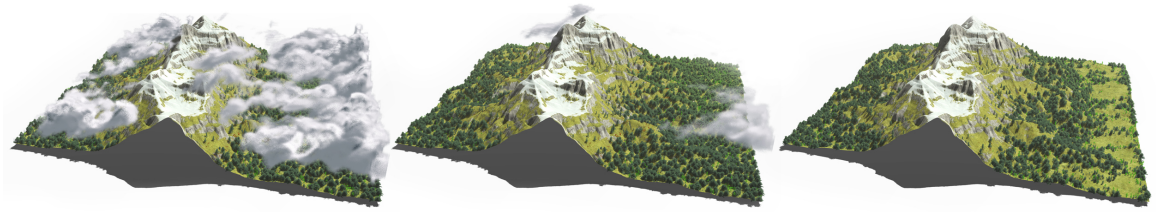

Figure 26: We simulate ecoclimates by combining models for vegetation, soil, and weather. This allows us to simulate complex and realistic outdoor landscapes with vegetation growth and weather dynamics (left, center). Our method can simulate over 500K plants with individual geometries at interactive rates (center). Additionally, we can also simulate the climate-response of vegetation, e.g. resulting in forest dieback (right).

One of the most intriguing problems is understanding the underlying principles of climatic changes. Over the last years, the role of forests in climatic change has received increased attention. This is due to the observation that not only the atmosphere has a principal impact on vegetation growth but also that vegetation is contributing to local variations of weather resulting in diverse microclimates. The interconnection of plant ecosystems and weather is described and studied as ecoclimates. In this work we take steps towards simulating ecoclimates by modeling the feedback loops between vegetation, soil, and atmosphere. In contrast to existing methods that only describe the climate at a global scale, our model aims at simulating local variations of climate. Specifically, we model tree growth interactively in response to gradients of water, temperature and light. As a result, we are able to capture a range of ecoclimate phenomena that have not been modeled before, including geomorphic controls, forest edge effects, the Foehn effect and spatial vegetation patterning. To validate the plausibility of our method we conduct a comparative analysis to studies from ecology and climatology. Consequently, our method advances the state-of-the-art of generating highly realistic outdoor landscapes of vegetation.

4.1 Introduction

Understanding the complex interconnection of plant ecosystems and their impact on the climate system plays a central role in predicting climate dynamics. While it is well understood that climatic variations cause changes in ecosystem distribution, structure and function, only recently it has been recognized that the composition of vegetation also impacts the development of weather, which – in turn – leads to the development of local climatic variation (microclimates) [1]. Researchers study the interconnection of plant ecosystems and their impact on the climate system as *ecoclimates*. Understanding these ecoclimates is a challenging and open research problem.

The primary goals of ecoclimate research are to understand the growth response and functioning of vegetation according to changing climatic conditions [2], the impact of vegetation on thermodynamics and the water cycle [3], and the feedback loop of vegetation and the climate [4]. Many of the current approaches for modeling ecoclimate processes rely on meteorological or macroclimate data, such as free-air temperature or open-field precipitation, that is measured in weather stations. However, recent studies indicate that climatic parameters in forests are determined to a greater degree by microclimatic rather than macroclimatic processes [5]. Furthermore, most of the analytical ecoclimate approaches do not leverage geometric representations of individual plants to explore

vegetation-climate interactions but instead treat plants as averaged populations.

In computer graphics, modeling plant ecosystems has a long tradition [6]–[9], that more recently also encompasses complex physical simulations, such as required for modeling wildfires [10], erosion feedback [11], or the interaction with fauna [12]. The goal of many of these methods is to employ detailed geometric representations to faithfully simulate the underlying physical or biological processes. The breadth of these approaches is a testament of the complexity of this undertaking. Simulating the growth response of vegetation according to climatic variations and the impact of vegetation on local weather and climate has not yet been studied in computer graphics. Closest to this objective is the method of Makowski et al. [13], who simulate the development of plant ecosystems in different climatic conditions. However, their method only simulates the feedback from the atmosphere to vegetation at a global scale disregarding the influence of the microclimate.

In this chapter, we propose a method to capture feedback loops between vegetation, soil, and the atmosphere at a local scale. We extend existing vegetation and atmosphere models and combine them with a novel soil model. This allows us to jointly simulate the hydrologic cycle, heat transfer, and light availability. We model tree growth interactively in response to gradients of water, temperature and light. As a result, we are able to capture a range of ecoclimate phenomena that have not been emergently modeled before, including geomorphic controls, forest edge effects, the Foehn effect and spatial vegetation patterning. This not only allows us to generate highly realistic outdoor landscapes of vegetation, but also to capture essential ecoclimate variations resulting from deforestation and drought.

Our framework allows us to interactively explore complex ecoclimate phenomena by explicitly considering climatic gradients. This is the first attempt that combines a detailed vegetation growth model with a climate representation comprised of a hydrological cycle, heat transfer, and a light model. Unlike existing methods in climatology that focus on physically detailed representations of these processes, our goal is to find a light-weight description that emergently captures ecoclimate-related phenomena. For this reason, we refrain from a detailed description of irradiance. Our approach considers the geometry of individual plants, the terrain, and cloud formation to simulate climates locally. We show that explicitly modeling 3D geometry and simulating physically and biologically plausible scenes enables studying microclimate phenomena.

To summarize, our contributions are as follows: (1) we propose a novel model for simulating ecoclimates that allows us to plausibly model vegetation-climate feedback loops for individual trees; (2) our method is the first to simulate gradients of water, temperature and light which allows capturing local phenomena of vegetation development, such as varying vegetation distribution at forest edges, the formation of spots, stripes, and gaps, as well as complex geomorphic effects; (3) we validate the plausibility of our method through numerous experiments and by comparing our results to studies from ecology and climatology.

4.2 Related Work

In this section, we aim to provide an overview of terrain and vegetation modeling, weather simulations, and modeling ecoclimates.

Vegetation Modeling. Modeling trees and plants has been content of computer graphics research for decades. A key objective of this research is to generate plausible and realistic branching structures of single plants and existing methods include fractals [14], repetitive patterns [15], L-Systems [16], and rule-based techniques [17]. On a different trajectory, data-driven approaches aim to reconstruct branching structures from images [18]–[22], videos [23], or laser-scanned point sets [24], [25]. Furthermore, it has been recognized that user-defined sketches provide an efficient means to generate realistic plant structures, while also considering artistic requirements [26]–[28]. More

recently, methods aim to further improve the realism of plant models [29] ranging from explicitly describing the environmental response of plants [30]–[32] to modeling with biological priors [33]. Previous work on plant dynamics ranges from modeling the growth process [34], [35], successfully capturing biophysical and biomechanical deformations [36], and addressing plant plasticity [37], to recent work on the machine learning-assisted acceleration of dynamic tree geometry [38]. Pirk et al. [39], [40] and Hädrich et al. [10] introduce methods for coupling plant models with fluid dynamics to capture the growth response in wind fields and the combustion process of plants. Similar to these methods our goal is to couple detailed plant models with fluid dynamics, however, unlike them we focus on large-scale ecosystems.

Plant Ecosystems. Methods for generating models of plant ecosystems aim to jointly compute plausible distributions of plants and to represent plants with an appropriate level of geometric detail [8], [9], [41]. A number of approaches exists that represent plant ecosystems as layers [42], voxels [7], volumetric textures [43], through more principled level of detail strategies [44], or based on simulating erosion feedback with vegetation [11]. Furthermore, it has been recognized that the artistic authoring of ecosystems plays an important role [45], [46], which can even be facilitated based on neural networks [47]. Furthermore, in forestry and ecology researchers widely explore stand-based, individual-based, and agent-based models of ecosystems at various scales of abstraction. The interested reader is referred to the surveys of Pretsch et al. [48] as well as Zhang and DeAngelis [49]. A related work to the method we propose can be found in Ch'ng [50]. The work of Makowski et al. [13] is the most advanced for simulating ecosystems with respect to climatic conditions and geometric representation of plants: different plant biomes are simulated based on individual, spatially-adapted plant instances and by considering temperature and precipitation as the driving factors of ecosystem development and plant growth. In contrast to this work, our goal is to simulate the weather-based growth response of individual plants and – in turn – to also simulate the impact of vegetation on weather.

Weather and Cloud Simulations. Physics-based approaches for cloud modeling employ Eulerian solvers to advect fluids for simulating different forms of clouds [51]–[53]. Due to the importance of clouds in various application domains, there exists a number of representations for clouds that range from particles [54]–[56], position-based dynamics [57] to layers [58], interpolation-based methods [59], and cellular automata [53]. However, despite these advances, simulating cloud dynamics remains a challenging research problem. Only very recently, Hädrich et al. [60] proposed a physically-accurate solver for various cloud types and their formations that even enables the simulation of precipitation in the form of rain. In this work, we apply this solver to simulate the interaction of fluid dynamics and vegetation.

Vegetation Climate Response. Research in forestry, botany, and ecoclimates focuses on understanding the complex interplay of vegetation and climate. A number of methods investigate the impact of climate and weather on vegetation to explain the dynamics and functioning of plants, for example when exposed to climate warming [2], [5]. Furthermore, climate can have a profound influence on the self-organization of plant ecosystems, which results in the formation of spatial patterns, such as labyrinths and gaps [1], [61]. Conversely, it has also been recognized that vegetation affects weather and thus the climate. To understand this phenomenon, research focuses on establishing models that allow us to investigate the impact of vegetation on the water cycle and the climate system [3], heat transfer [62] as well as on understanding microclimate dynamics [5]. Vegetation defines a complex surfaces that interfaces with the weather system. Therefore, a number of methods investigate the impact of ecosystem composition on the formation of clouds [63], [64]. Many of the existing approaches aim at defining accurate models for ecoclimates. However most of these methods cannot be directly applied to geometric models of plants or be used to simulate the emerging phenomena of coupling weather and ecosystem at interactive rates.

4.3 Overview

Our main goal is to increase the realism of plant ecosystem models by simulating the interaction of vegetation, soil, and weather as shown in Fig. 27. The interaction of these models allows us to define ecoclimates and to simulate the water cycle (Fig. 28).

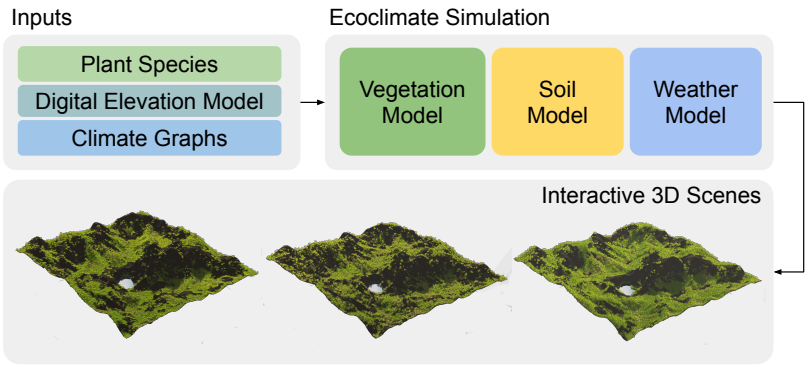

Figure 27: Framework overview: we employ models for vegetation, soil, and weather to simulate eoclimates. Our system operates at interactive rates and thereby allows users to efficiently explore configurations and parameters settings for plant species, terrain, and climate.

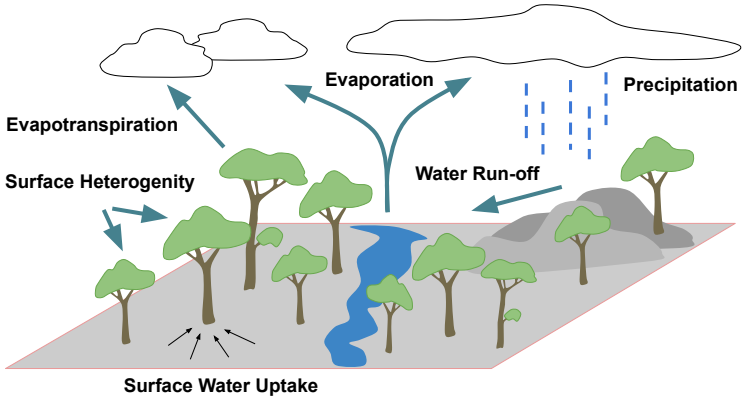

Figure 28: We define ecoclimates by simulating the water cycle, including effects such as the water infiltration and water uptake of plants from the soil, the evaporation and transpiration of water from the ground and from leaves. Our model can realistically simulate the interaction of vegetation and fluid dynamics, resulting in complex microclimates.

In our framework we have integrated and extended a tree growth model for large-scale plant ecosystems [13]. Tree models are composed of a number of self-organizing branch modules that define the 3D branching structure of a tree model. Modules can be instantiated and are used multiple times across the same tree as well as across other trees in the ecosystem. The advantage of this module-based representation is that it enables the efficient processing of large collections of plants. This means that we simulate the developmental process of the ecosystem as a collection of individually interacting plants, which results in unique and realistic branch geometry.

To simulate the atmosphere we integrated and extended a state-of-the-art method for simulating cloud dynamics [60], which allows us to capture various weather conditions and the formation of

clouds. We couple the atmosphere and vegetation model by introducing a novel soil model. The soil model describes water infiltration into the soil as well as the water uptake by individual plants, which in turn can transpire water back to the atmosphere. Important to our work is that the coupling of fluid dynamics and plant ecosystems enables us to locally define the interactions of plants and weather – plants respond to the changes in the weather model, while the weather model is simultaneously affected by the vegetation. Sampling the weather over time establishes the climate for a simulated ecosystem.

In summary, we couple a module-based representation for vegetation with a state-of-the-art atmosphere model and a novel soil model for water infiltration. This allows us to model the feedback loops between vegetation, soil, and atmosphere to simulate essential ecoclimate phenomena.

4.4 Ecoclimates

Relatively recently earth's climate has been described by a system of several interacting spheres [65]. The main components of this earth system are the atmosphere (air), hydrosphere (water), cryosphere (frozen regions of earth), biosphere (living organisms), pedosphere (soil), and anthroposphere (humans). The major mediators between these different spheres can be defined by temperature and water in various phases. In this work, we emphasize the role of the climate on the biosphere: the **ecoclimate**.

In the atmosphere, water undergoes phase transitions between condensed form and rain. When liquid water reaches the ground as rainfall some of it drains downward due to the force of gravity. This vertical flow of water is called **infiltration**. The water that infiltrates into the soil is stored as **soil water**. When the infiltration capacity of soil is exceeded, water collects as puddles in small depressions of the ground surface. When these are filled, water runs off over the ground surface as overland flow. Soil water returns to the atmosphere through **evaporation** from bare ground and **transpiration** from plants. Evaporation is understood as the physical process by which water turns from liquid to vapor in the air. Transpiration is evaporation of water held inside plants. Due to the difficulty in clearly separating these processes, they are also jointly referred to as **evapotranspiration**. Plants consume large amounts of water during growth. However, plants cannot grow if leaf pores (stomata) are not open. In case stomata have opened, water contained in the leaf may diffuse out as transpiration. If too much water is lost, the plant becomes desiccated and will die in case its internal water is not replenished through the roots from water in the soil. Therefore, plants have to compromise between the need to transpire and grow, and to prevent water loss and not grow.

The complexities of the hydrologic cycle on land can be reduced to a simple form in which the change in soil water ($\mathbf{\Delta} q_w$) is the balance between water input from rainfall (R), water loss from evapotranspiration (E), and water lost as runoff (q_o). This cycle has a major impact on vegetation growth patterns, such as **spatial self-organization** of plants due to climate variations, **forest edge effects** which are defined by stark climatic gradients, and the influence of the topography on vegetation (**geomorphic effects**).

Conversely, wet soil or dense vegetation matter creates a cool, moist atmospheric boundary layer which may feed back to increase precipitation. In addition, rough surfaces such as forests generate more turbulence of air flow compared to smoother surfaces such as grasslands. A smoother surface can lead to a warmer, drier atmospheric boundary layer and therefore to different cloud formation. The surface characteristics of a given geographic location are described as **surface heterogeneity**. This bidirectional coupling of ecosystems and climate occurs over a continuum of timescales from minutes to seasons to millennia.

4.5 Model

For a realistic 3D simulation of ecoclimates we formally describe cloud formation and plant growth at a detailed geometric scale. Our ecoclimate model is distinguished by a vegetation model based on space-constrained plant growth (Figure 29a), a soil model describing terrain hydrology (Figure 29b), and a weather model simulating fluid dynamics (Figure 29c).

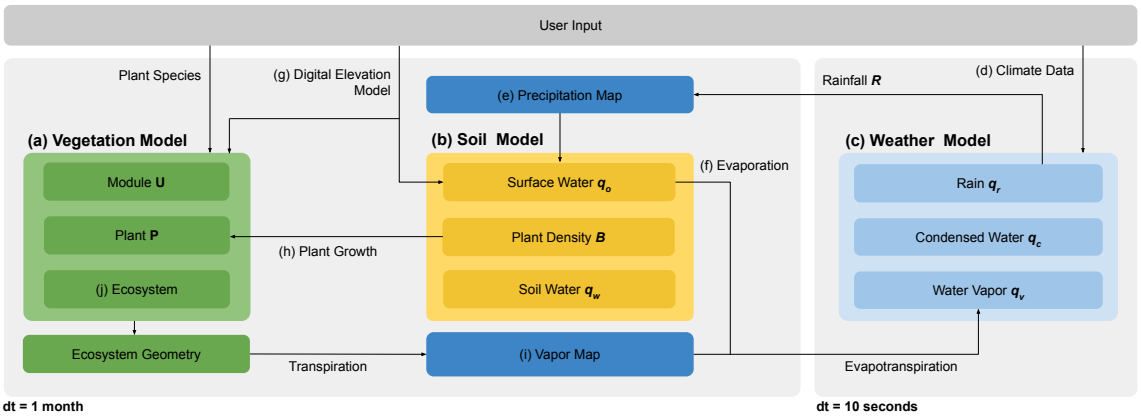

Figure 29: Detailed overview of our ecoclimate model. Our model can be distinguished by a vegetation (a), soil (b), and weather model (c). We explicitly describe the water cycle which mediates the feedback between the three models. While the weather model describes dynamic cloud formation over time scales of seconds the vegetation and soil model describe phenomena occurring on time scales of months. A user provides input in the form of a set of plant species, a digital elevation model and data describing macroclimatic variation over time. A description of the processes that our model is able describe and the underlying hypotheses expressed by our ecoclimate model is given in Section 4.5.3.

4.5.1 Spaces

To simulate ecoclimates based on the vegetation, soil, and weather models we rely on four different spaces as illustrated in Fig. 31. First, we define a continuous 3D space in which we embed a digital elevation model and vegetation geometry that is suitable for 3D rendering (Ecosystem Continuous Space). For most of our scenes we define terrains of size 4 km^2. Second, we use a 3D voxel space with a resolution 1.5 m to compute light exposure and temperature values to express plastic development of plants (Ecosystem Voxel Space). Third, we define 2D grids with a resolution 1.5 m to store values for average monthly vapor and precipitation over the terrain (Vapor and Precipitation Maps). Finally, we use a 3D voxel space with a resolution 20 m for our cloud simulation (Weather System Voxel Space). Exchange of water quantities between *Weather Voxel Space (WVS)* and *Ecosystem Voxel Space (EVS)* is facilitated via vapor and precipitation maps. The use of precipitation and vapor maps to express components of the hydrological cycle instead of operating on the respective 3D grids improves the computational efficiency of our method. The local storage of water, light exposure and temperature values defines the microclimate in our method.

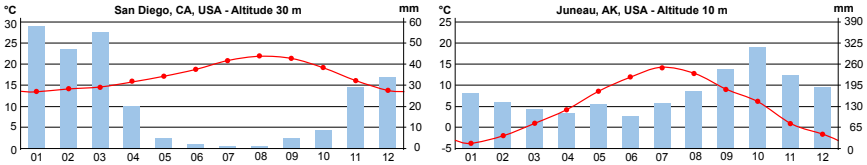

Figure 30: We use the monthly average temperature (red) and precipitation (blue) as input to our framework. Two different temperature and precipitation graphs for San Diego and Juno shown as example inputs.

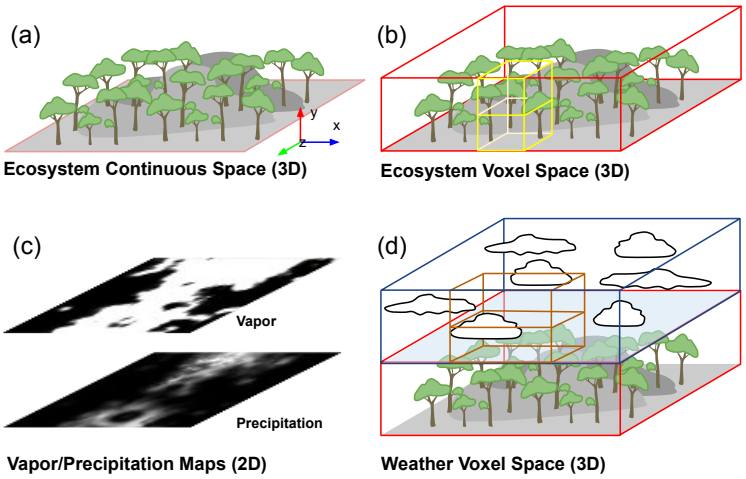

Figure 31: Mathematical spaces used in our framework. We use a continuous space to embed terrain surface and vegetation meshes used for 3D rendering (a); a discrete 3D grid composed of cubic voxels to store temperature and light information relevant to computing ecosystem development (b); a vapor and precipitation map to transfer data about water and temperature between individual models of our method (c); and a discrete 3D grid composed of cubic voxels for calculating the dynamics of fluid motion (d).

4.5.2 Input and Output

Our framework allows us to interactively explore ecoclimates. To define an ecoclimate a user can specify a terrain (digital elevation model) and a set of plant species. We use the the method of Makowski et al. [13] to design a set of plant species P. This method requires setting a number of parameter values that define plant growth in an ecosystem, such as for shade tolerance, precipitation and temperature adaptation.

A macroclimate is defined as a set of monthly average values for temperature and precipitation describing climatic variation during an average year. Examples of two macroclimates for different geographic locations are shown in Fig. 30. Moreover, a user can specify a wind field that defines additional input for the fluid dynamics. Our framework allows to specifiy a wind vector f_w applied to all grid cells of the *Weather Voxel Space*. The wind field can either be defined manually or obtained from online weather services as shown in Hädrich et al. [60].

The output of our algorithm is terrain surface mesh and a set of 3D plant models with their geometry adapted to their environment. Plant models are defined as sets of branch modules which are used multiple times across the same plant and within the entire ecosystem. Each module is

individually adapted to its location in the plant and its geometry is generated on the GPU. This way modules can be instantiated, which facilitates the efficient rendering of large plant collections. In addition, condensed water q_c in the *Weather Voxel Space* is rendered as clouds using volume ray marching.

4.5.3 Hypotheses

We aim to create an ecoclimate model that expresses realistic vegetation growth and cloud dynamics, as well as the feedback loops between them. This feedback is mediated by water and temperature quantities stored in the *Ecosystem Voxel Space*, vapor and precipitation maps, and the *Weather Voxel Space*. In the following we list the major hypotheses described by our formal model:

1. Water is treated as an extensive quantity that can vary according to global weather influx as defined by the macroclimate input (Fig. 29d, Sec. 4.5.7).
2. Water in the atmosphere undergoes phase transitions between vapor q_v, rain q_r, or in condensed form q_c as proposed by the Kessler scheme [66] (Fig. 29c, Eqs. 47, 48, 49).
3. Rain R increases the amount of surface water q_o (Fig. 29e, Eq. 44).
4. Surface water q_o moves by diffusion, is advected by the slope of the terrain v, evaporates back into the air as q_v, and can infiltrate into the soil (Fig. 29b, f, g, Eq. 44).
5. Water infiltration into the soil is proportional to the density of plants B (Fig. 29b, Eq. 43).
6. Plants P take up soil water q_w and transpire it as q_v to grow (Fig. 29a, h, i, Eq. 43).
7. Plant growth is expressed by competition for light, apical control, tropisms, flowering, climatic adaptation, shade tolerance and seed dispersal (Fig. 29i). For a more detailed explanation please see Makowski et al. [13] (Secs. 5.2-5.3, 6.1-6.4).
8. Plants P decrease light exposure and temperature (Fig. 29j, Sec. 4.5.5.1). For a more detailed explanation please see Makowski et al. [13] (Sec. 6.2).

Hypotheses (1-5) are described by partial differential equations. Whereas, hypotheses (6-8) are described by a discrete, graph-based method. Both the continuous and discrete formalism exchange quantities between each other. Specifically, the density of plants B is computed from the number of plants P and the growth of plants P is modulated by the soil water q_w. This means that we use a coupled continuous and discrete formalism to describe the major empirical hypotheses underlying our ecoclimate model.

4.5.4 Time Scales and Model Integration

It is important to note that our ecoclimate model operates on two different timescales. The simulation of vegetation development and water cycle in the soil takes place at a timescale of one month Δt_E (Fig. 32 indicated by green horizontal line). This timescale allows us to simulate the long-term development of plant ecosystems and consequently the vapor maps necessary for computing corresponding weather variations for a given month. To simulate the annual variation of climate, we define 12 unique weather conditions for each month by defining macroclimatic vapor and heat emission (Sec. 4.5.7). For each month we simulate weather at a small time scale (10s-60s) until we obtain a plausible sample of the local weather conditions for a given day. Sampling monthly

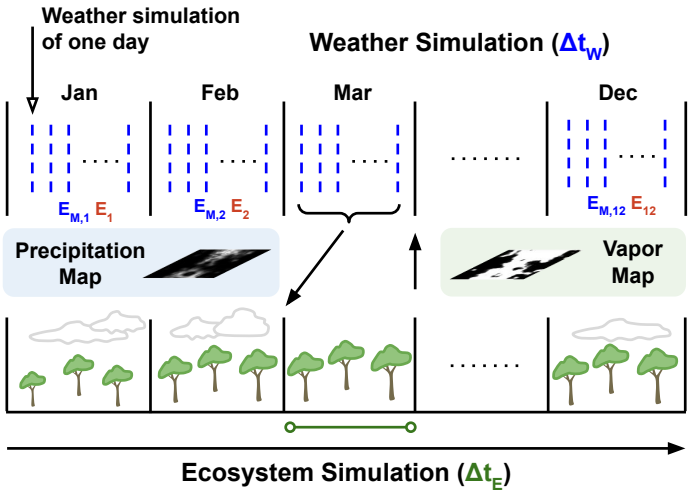

Figure 32: We simulate ecoclimates at two time scales. First, we sample daily weather conditions by simulating weather over a period of time at a time step of 10s (dashed blue lines). Second, we obtain a precipitation map to represent the monthly weather conditions by simulating weather for a number of days each month. These monthly average weather conditions are used as input for the ecosystem simulation which uses a time step of one month (green line). After a step of ecosystem simulation we compute a vapor map as input for the subsequent month of weather simulation.

weather multiple times allows us to obtain an average temperature and precipitation profile for a given ecosystem (Fig. 30) that we store as a precipitation map (Fig. 32). The partitioning of monthly weather simulation into batches of individual days allows us to use plausible precipitation profiles for a given ecosystem. The coupling of weather and ecosystem simulation based on maps of precipitation and vapor defines the ecoclimate feedback loop in our model.

4.5.5 Vegetation Model

We use the method introduced in Makowski et al. [13] to model vegetation development. This method allows modeling the growth of a large number of interacting plant instances while maintaining an individual, geometric representation at branch scale. Furthermore, this method also describes climatic adaptation, shade tolerance, and seed dispersal strategies to place plant models realistically into an environment.

A plant model in our simulation is represented as an ordered tree graph of connected modules $u \in U$ (plant graph) embedded in a continuous 3D space representing the environment and a set of plant type parameters χ – altogether this defines a plant P. A module represents the skeletal graph (defined by nodes $c \in C_b$) of a branch cluster. During simulation time we express plant development by modifying the plant graph through adding, removing or adjusting modules. At each simulation step we calculate plant development based on light exposure values obtained for each module to express constraints of space and to avoid module collisions. When new modules are added to the plant graph they are interpolated from an axiomatic developmental stage (a single branch segment) to a maximally developed stage. The maximally developed stage is defined by one of nine pre-defined branch templates (as illustrated in Fig. 33).

To express the invasion of foreign species that did not start in the initial scene we place, with uniform distribution, seeds of other plant types at fixed time intervals (global seeding). We compute

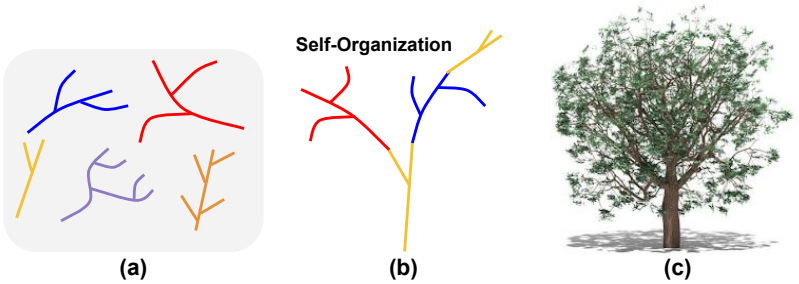

Figure 33: Module-based plant representation: plants are composed from a set of modules (a). Modules adapted through self-organization and are reused across the same plant and the entire ecosystem (b). Once the branch graph has been defined we generate the final plant geometry as illustrated in (c).

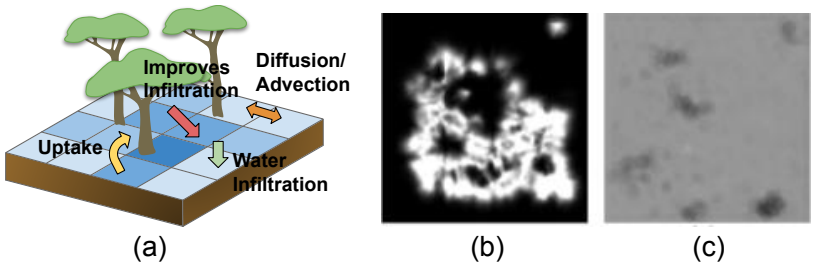

Figure 34: Our model describes the interaction between the available water and the vegeation (a). We define maps to store the average monthly vapor (b) and precipitation (c) of a terrain. Based on these maps we define the exchange of water quantities between the *Weather Voxel Space* and the *Ecosystem Voxel Space*.

a climatic adaptation parameter o that scales the global seeding interval for all plant types defined for the scene:

$$o = \frac{\mathcal{N}_T(T) \cdot \mathcal{N}_P(q_w)}{\mathcal{N}_T(T_A) \cdot \mathcal{N}_P(P_A)}\,, \tag{38}$$

where $\mathcal{N}_T(\cdot)$ and $\mathcal{N}_P(\cdot)$ denote the normal distributions of local temperature (mean is T) and local soil water (mean is q_w) which are obtained by reading the values from the voxel cell where the plant is located (*Ecosystem Voxel Space*). In contrast to Makowski et al. [13] (Sec. 6.4), where global temperature and precipitation values are used to linearly interpolate the maximum value of vigor (v_r) by o, our local sampling enables simulating microclimates.

4.5.5.1 Calculating Vapor Maps In the final step of a cycle of the development of vegetation we calculate vapor maps which are used as input data for the weather model (Fig. 34, b). We project all modules into a 2D grid. Then each grid cell that contains the geometric center of a module is updated with its biomass, scaled by a transpiration coefficient τ to define a final vapor value E_p at this cell

$$d_b = \begin{cases} \sqrt{\sum_{c \in C_b} d_c^2}, & C_b \neq \emptyset\,, \\ \phi, & \text{otherwise}\,, \end{cases} \tag{39}$$

$$\ell_b = \mathsf{min}(\ell_{\mathsf{max}}, \beta \cdot a_b)\,, \tag{40}$$

$$M_m = \sum_{u \in U} \sum_{c \in C_b} \ell_b (2d_b)^2 \pi \rho\,, \tag{41}$$

$$E_p = \tau \sum_{u \in U} M_{m,u}\,. \tag{42}$$

where d_b denotes branch segment diameters, a_b the age of a branch segment, ℓ_b branch segment lengths, and M_m the total mass of a module u. β is a scaling coefficient. ℓ_{max} the maximum length a branch can attain and ρ the average wood density. This process describes the amount of evapotranspiration over the terrain during a period of growth in our method. Furthermore, we define the cooling of air induced by plants by linearly interpolating the weather temperature to a minimum temperature T_{sh} in complete shade by the light exposure value Q of the *Ecosystem Voxel Space*. This linear interpolation of Q values represents a coupling of the *Weather Voxel Space* with the *Ecosystem Voxel Space*. Both voxel spaces are embedded in the *Ecosystem Continuous Space* which allows us to coherently sample them.

4.5.6 Soil Model

Our soil model expresses the change of soil (∂q_w) and surface water (∂q_o) due to precipitation (R), and the plant density (B). The model describes the interaction between the available water and the vegetation (Fig. 34, a). This interaction occurs on different time scales between the spreading of water and of vegetation growth which leads to spatial vegetation patterns. The soil model is defined by a set of partial differential equations which are coupled to the dynamics of the discrete vegetation growth model. It is therefore neither continuous nor discrete but instead represents a hybrid modelling approach. The differential equations are:

$$\begin{aligned} \frac{\partial q_w}{\partial t} = \alpha \cdot q_o \cdot \frac{B + k_2 \cdot W_0}{q_w + k_2} - g_{\mathsf{max}} \cdot \frac{q_w}{q_w + k_1} B \\ -r_w \cdot q_w + D_w \cdot \mathbf{\Delta} q_w + v_w \nabla q_w\,, \end{aligned} \tag{43}$$

$$\frac{\partial q_o}{\partial t} = R - \alpha \cdot q_o \cdot \frac{B + k_2 \cdot W_0}{q_w + k_2} + D_O \cdot \mathbf{\Delta} q_o + v_o \nabla q_o\,, \tag{44}$$

where g_{max} is the maximum water uptake, k_1 is a half-saturation constant of water uptake, α is the maximum infiltration rate, k_2 is the saturation constant of water infiltration, W_0 is the water infiltration rate in the absence of plants, r_w is the specific soil water loss due to evaporation and drainage, D_w is the diffusion coefficient for soil water, R is precipitation (Sec. 4.5.7.2), and D_O is the diffusion coefficient for surface water. Plausible parameters were obtained from the literature [67], [68] A Laplacian operator is used to express water diffusion. We account for the slope of the terrain to model water runoff by adding advection terms $v_w \nabla q_w$ and $v_o \nabla q_o$, in which v_w and v_o represent the downhill flow. The two-dimensional numerical simulations are solved using the forward Euler integration scheme resulting from the spatial discretization (precipitation map) of the diffusion operator.

In each simulation step, the plant density B (Eq. 43–44) of each grid cell is calculated by summing the biomass values of all the plant models P_i located in this cell. The plant models P_i are defined

by the vegetation model in Section 4.5.5:

$$B = \sum_{P_i \in P} \frac{P_{m,i}}{A}\,, \tag{45}$$

$$P_{m,i} = \sum_{u \in U} M_{m,u}\,, \tag{46}$$

where $M_{m,u}$ is the mass of module u of a plant model P_i, and $P_{m,i}$ the total biomass of the plant, and A the area of a side of a voxel cell. This coupled continuous and discrete model exhibits a Turing-like mechanism similar to the continuous model proposed by HilleRisLambers et al [68]. It is characterized by a short-range negative feedback and a long-range positive feedback of vegetation on itself (Eq. 43). Please note that these type of reaction-diffusion models are used to describe a variety of pattern formation, e.g. pigmentation patterning in flowers [69].

4.5.7 Atmosphere Model

Our weather model is based on the method described in Hädrich et al. [60] which includes additional derivation steps of the equations introduced here. This method enables a realistic simulation of the exchange of water, vapor, and heat between parcels of air and the terrain. Furthermore, it captures turbulent air flows enabling the simulation of a range of phenomena such as stormscapes and dynamic transitions between different cloud types.

Our weather model can be divided into an atmospheric model that describes temperature and pressure changes as a function of altitude and time, a 0D thermodynamics model that defines local forces and the formation of clouds, and the fluid dynamics model defining the motion of air in the atmosphere. The complex terrain-cloud feedback in the original method is expressed by noise functions defining ground vapor and heat values introduced at the bottom domain boundary of the fluid field. These functions are scaled by vapor V and heat emission E. Here, we extend the notion of ground vapor and heat by assuming that vapor and heat can be added from any boundary to the fluid domain to represent influx from the macroclimate. We refer to this vapor and heat as macroclimatic vapor E_M and heat E. Unlike Hädrich et al. [60] the cloud-terrain feedback is expressed in our model by the *Ecosystem Voxel Space* and the vapor maps generated by the soil and vegetation model. We add macroclimatic vapor E_M and evapotranspiration E_p stored in the vapor maps to the boundary of the *Weather Voxel Space*.

4.5.7.1 Fluid dynamics To account for phase transitions of water in the air, i.e. from water vapor q_v to condensed cloud q_c, and rain q_r, we extend Kessler's methodology [66]. Using the material derivative $\mathsf{D}_t\varphi = \partial\varphi/\partial t + \boldsymbol{v} \cdot \nabla\varphi$ [70], the transport equations are

$$\mathsf{D}_t q_v = -C_c + E_c + E_r + E_p + E_M\,, \tag{47}$$

$$\mathsf{D}_t q_c = C_c - E_c - A_c - K_c\,, \tag{48}$$

$$\mathsf{D}_t q_r = A_c + K_c - E_r\,, \tag{49}$$

where the source term C_c denotes condensation, E_c the evaporation of clouds, E_r the evaporation of rain from the ground, A_c autoconversion of raindrops from clouds, K_c the accretion of cloud water due to falling water drops, E_M the macroclimatic vapor, and E_p the evapotranspiration of plants. E_M is calculated from the macroclimatic vapor function and E_p is obtained from the vapor maps. E_p and E_M are non-zero only at the domain boundary (representing the terrain). Fig. 35 illustrates the phase transitions of water encapsulated by this model. Please refer to the derivation of the

source term C_c, the remaining variables, as well as the numerical implementation to Hädrich et al. [60].

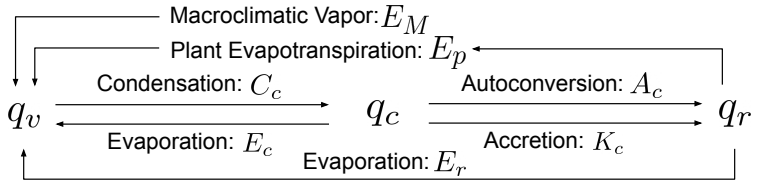

Figure 35: Illustration of our extended Kessler's scheme [66] for modeling the transport between surface water, soil water, vapor, cloud water, and rain.

4.5.7.2 Calculating Precipitation Maps To simulate the yearly variation of weather over a terrain we rely on our weather model to generate precipitation maps (Fig. 34c). These maps contain the input for the soil model describing the hydrological cycle on the ground. This provides us a detailed enough description to express a variety of microclimatic phenomena (e.g. forest edge effects). The macroclimatic parameters for the corresponding time in the year are obtained using the climate interpolation functions p_0 and T_0. Next, we simulate cloud formation for a fixed number of time steps, e.g. 10-100 steps. We then project the rain values q_r of each cell from top to bottom (a column in voxel space) of the grid as rain R into the precipitation map:

$$R = \sum_{q_r \in Q_r} q_r \,. \tag{50}$$

The variable R is used to compute the surface water q_o (Eq. 44). This process is repeated a number of times for each month to express a daily variation of weather conditions. To express this idea formally we sample a normal distribution of E_M and θ once for each day to finally obtain an average precipitation map for the given month. We compute 12 average precipitation maps representing the monthly rainfall over a year by using 12 sets of macroclimatic parameters (T_0, p_0) based on a climate graph (Fig. 30).

4.6 Implementation Details

We have implemented our interactive framework using C++, DirectX and CUDA. To generate the results shown in this chapter we used an Intel(R) Core i5, 4 x 2.5GHz with 8GB RAM, and a NVIDIA Geforce GTX 1050 GPU (4 GB RAM). We used the L3DT Terrain Editor to generate terrain meshes. The figures shown throughout the chapter are rendered with our interactive framework. Details about the plant types are provided in Tab. 2.

Joining models expressed with different formalisms, namely the continuous formulation of soil and weather with the discrete representation of vegetation is a non-trivial implementation task. At the beginning of each update step, we compute a set of parameter values for the weather simulation runs that will serve to represent annual weather conditions (Alg. 1, Lines 2-4). We then simulate for each instance of climatic conditions ψ a weather scene (Alg. 1, Lines 5-10). For the implementation of the fluid solver we rely on the integration scheme described in Hädrich et al. [60], which includes diffusion, advection and pressure projection (Alg. 1, Lines 5-10).

The WVS is used to store all relevant quantities representing the state of the weather simulation. For the advection process, we employ no-slip conditions at the bottom and free-slip conditions at

the ceiling. The vertical velocity is set identically to zero at the side boundaries and if an external wind field is specified, the horizontal velocities are computed as the corresponding wind speeds.

We provide the input for the soil simulation in the form of 2D precipitation maps obtained from the WVS (Alg. 1, Line 10). The soil is represented by two 2D grids representing the surface and soil water. We use Eulerian solvers to compute the diffusion and advection of water [71] based on the input of rain R obtained from the precipitation map (Alg. 1, Lines 11-14). We use free-slip conditions at the boundaries.

Next, we compute the light exposure values for the EVS. After computing local light and soil water values we initiate the growth simulation of vegetation for all plants P of a scene $\mathcal{S}$ (Alg. 1, Lines 11-14). First, we compute v_r based on the climatic adaptation parameter o which is obtained from the local temperature T and soil water q_w as described in Eq. 38. Then, we traverse all modules (M) of a plant P to compute their state changes, as well as orienting and positioning plant modules using stochastic gradient descent (Alg. 1, Lines 18-22) as outlined in Makowski et al. [13]. Finally, we update vapor and temperature values in the WVS based on the new state of the vegetation simulation and seed new plants in the scene (Alg. 1, Lines 24-27).

ALGORITHM 1: Overview of our numerical procedure.

Input: Current system state.
Output: Updated system state.
1 **Procedure:**
2 **for each** $\gamma \in \Gamma$ **do**
3 | Compute normally distributed pair of E and E_M as vector ν
4 based on annual climate profile as described in Sec. 4.5.4.
5 **for each** $\psi \in \Psi$ **do**
6 | Update atmospheric temperature $T(\boldsymbol{x})$. Diffuse, advect and
7 pressure project temperature θ, field $\boldsymbol{u}$ and atmospheric
8 water content q_j following the Eulerian solver
9 of Hädrich et al. [60].
10 | Update precipitation map as described by Eq. (50).
11 Compute water transfer between soil surface
12 and atmosphere as explained in Eq. (42).
13 Compute water exchange between surface, soil and plants
14 as explained in Eqs. (43), (44).
15 **for each** $\boldsymbol{P} \in \mathcal{S}$ **do**
16 | Update Light exposure values in EVS according to shadow
17 propagation algorithm as described in Makowski et al. [13].
18 **for each** $\boldsymbol{P}, \boldsymbol{M} \in \mathcal{S}$ **do**
19 | Compute v_r as explained in Eq. (38).
20 | Compute vigor values for all modules, shed branches and remove
21 plants, update module positions and orientations using SGD, as
22 described in Makowski et al. [13].
23 **for each** $\boldsymbol{P} \in \mathcal{S}$ **do**
24 | Update vapor values E_p in WVS as described in Sec. 4.5.5.1.
25 | Update temperature values T in WVS as described in Sec. 4.5.5.1.
26 | Seed new plants as described in Makowski et al. [13].
27 **end**

4.7 Results and Evaluation

In this section we describe how our ecoclimate framework can be used to model highly complex and realistic landscapes. As we are proposing a large parameter space our main goal is to carefully validate our results based on a range of different experiments that assess the impact and usefulness of each of the introduced models – atmosphere, soil, vegetation. The main advantage of our model, compared to other approaches that consider modeling the macroclimate (e.g. Makowski et al. [13]), is the simulation of a microclimate. Consequently, we can generate more realistic landscapes with a larger variety of ecoclimate phenomena. We consider our method to be interactive, meaning we generate all results with frame rates high enough to allow for a fast response of the simulation to user interaction. Finally, we compare our simulation results to recent theoretical studies of climatic changes and real world examples.

4.7.1 Ecoclimate Dynamics

Jointly simulating the soil, vegetation, and atmosphere models generates feedback loops that allow us to capture effects of climatic changes mediated by the water cycle. Specifically, we show that our atmospheric model is able to represent different climatic conditions by providing examples of a variety of cloud formations. We also establish that the dynamics of the atmosphere affect the development of the vegetation model. Conversely, we show that the development of vegetation influences the atmospheric conditions which – in turn – may lead to changing cloud formations.

4.7.1.1 Atmosphere Similar to previous results on cloud formation [60] we also simulate cloud dynamics. Unlike the previous work we couple our vegetation and atmosphere models through a dynamically computed vapor map, which allows us to establish the necessary feedback loop between vegetation and atmosphere. In Fig. 36 we vary parameter values for vapor and heat emission of the macroclimate over the same boreal forest patch. This parameter space exploration results in the formation of different cloud types ranging from foggy clouds to stratocumulus and cumulus clouds. For this experiment we extended the model of Häedrich et al. [60] by using a vapor map obtained from the vegetation simulation, described in Section 4.5.5.1, instead of a vapor map defined by a noise function.

4.7.1.2 Atmosphere-Vegetation Our framework allows us to simulate the impact of the atmosphere on the vegetation. The interaction between atmosphere and vegetation models is defined by a precipitation map, which is used to provide soil water necessary for vegetation growth. This means, that changing atmospheric conditions of macroscopic vapor will impact vegetation development. In Figure 37 we demonstrate the atmosphere-vegetation feedback by simulating an ecoclimate in the Yosemite Valley around Half Dome (a) resulting in a dense population of pine trees (a, inset). Reducing the macroscopic vapor leads to a reduced availability in soil water resulting in forest dieback (b). In this case, ribbon-like structures of pine trees emerge as result of this climatic change (b, inset). Further decreasing the vapor eventually causes more trees to die (c), which leads to an arid landscape with fewer and feebler trees (c, inset).

The visual forest patterns emerging due to changing climatic conditions are very complex. In Fig. 40 we show the transition of a tropical forest to an arid landscape by reducing the macroscopic vapor gradually with simulation time. The tropical forest is characterized by 6 species which are organized in a mixed stand (a). As precipitation decreases to 3700mm the less well-adapted tree species die back forming large forest gaps (b). This allows fast growing and more climate-adapted species to proliferate, changing the forest composition in the process (c, 2500mm). As the climate

Figure 36: We varied macroclimatic parameters of vapor and temperature to approximate different cloud types for the same ecosystem scene. This includes clouds types such as stratocumulus, stratus, and cumulus.

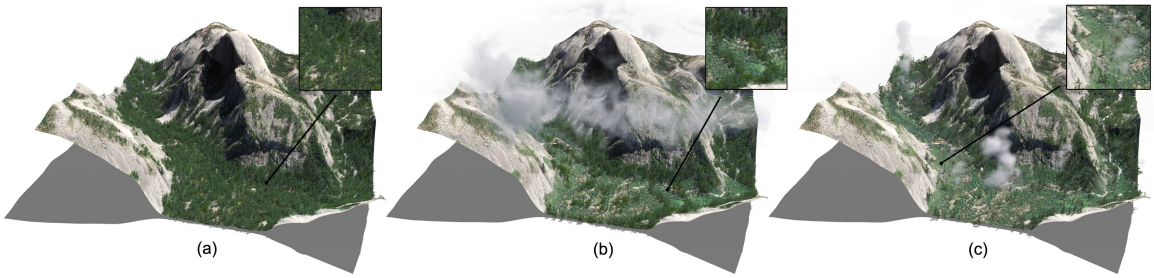

Figure 37: Forest growth in the terrain around Half Dome in the Yosemite National Park: We simulate an ecoclimate with a dense population of pine trees (a). We then modify vapor values and continue growing the forest to simulate a change of climate. Typical ribbon-like structures emerge due to spatial patterning of plants (b). Finally, severe forest dieback occurs resulting in an arid landscape with fewer an feebler trees (c).

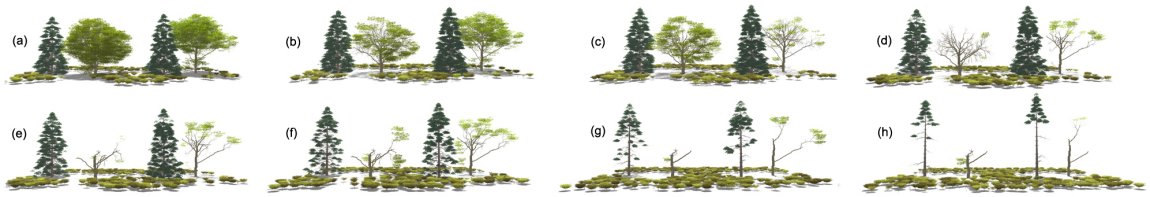

Figure 38: Illustration of a climatic change for a small vegetation patch: our approach represents trees with individual branch geometry, which allows trees to individually adapt to changing conditions. From initially beneficial conditions (a), we gradually decrease average precipitation from 1200 mm to 100 mm (b-h). The more precipitation-adapted oak trees exhibit changes to its architecture before the less precipitation-adapted pine trees. After shedding most of its branches the oak trees continue to adapt to the drier conditions growing even under severe water stress (e, f). Shrubs continue to grow throughout the drought conditions as they are highly adapted to either climate.

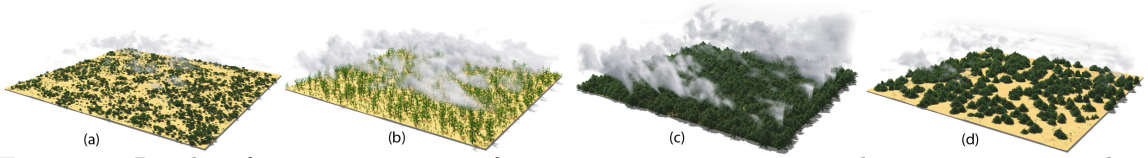

Figure 39: Results of evapotranspiration from vegetation: we set microclimatic parameter values constant in four different biomes. The plant species determines the evapotranspiration rate of a plant leading to different cloud formations in a shrubland (a) and a patchy oak forest (b). In (c) we show denser cloud formations over a pine forest; by reducing the density of pines less vapor is available for cloud formation (d). Please note that clouds in the images are rendered at low altitudes for visualization purposes.

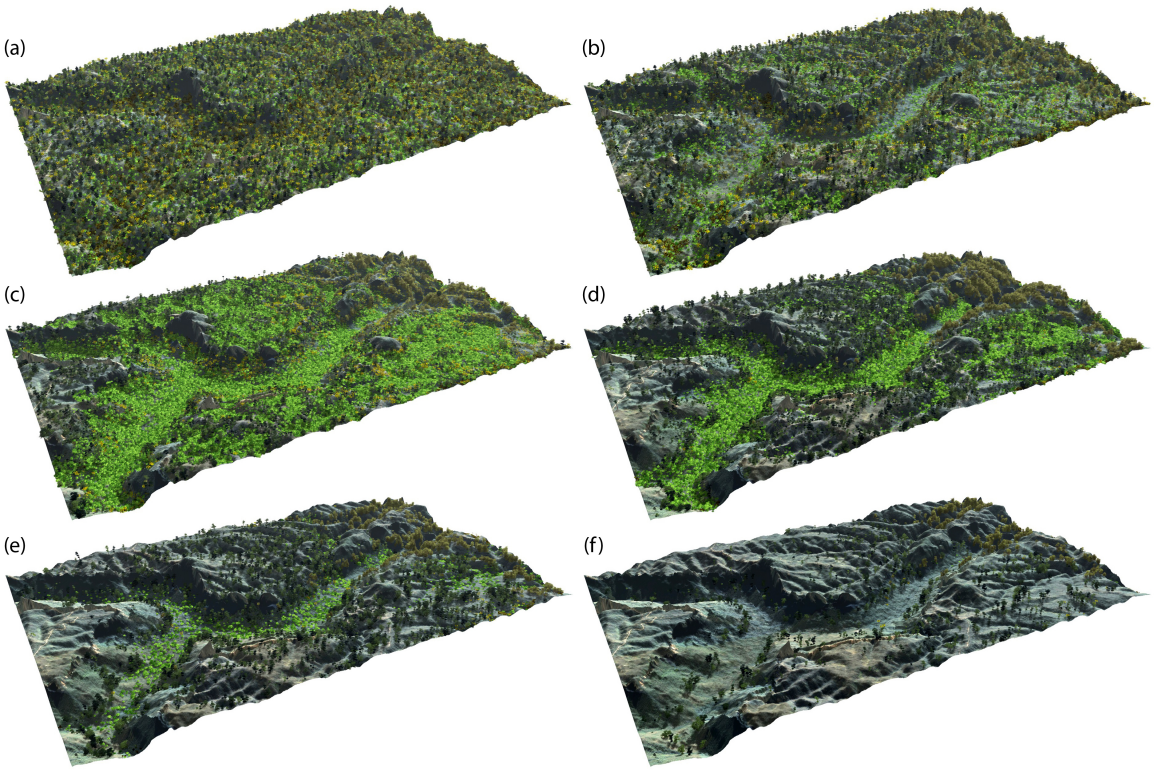

Figure 40: In this result we demonstrate the visual complexity of ecosystems in relation to climate dynamics. A tropical forest scene with 4300mm average annual precipitation contains six mixed species uniformly distributed across the terrain (a). As precipitation decreases to 3700mm the less well-adapted tree species die back forming large forest gaps (b). This allows fast growing and more climate-adapted species to proliferate, changing the forest composition in the process (c, 2500mm). As the climate further changes plant species segregate to exploit climatic niches on the terrain (d, 1260mm). Finally, continued precipitation decrease results in arid vegetation pattern (e-f, 900-400mm).

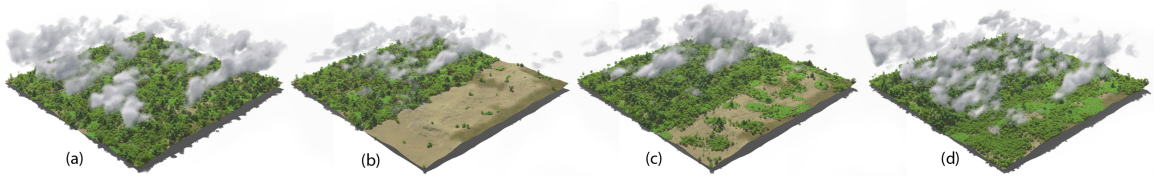

Figure 41: Our method models the feedback between vegetation, soil, and weather. To illustrate this, we conduct a deforestation experiment while keeping the macroclimate in our weather model constant. In (a) we show a tropical rainforest with cumulus clouds. In (b) we remove a large portion of the rainforest thereby modifying the vapor emission from the terrain. Consequently, fewer cumulus clouds form, especially over the deforested area. After continuing ecosystem growth cloud formation increases slightly (c). Only after significant portions of the rainforest have regrown, cumulus cloud formation is restored (d). Please note that clouds in the images are rendered at low altitudes for visualization purposes.

further changes plant species segregate to exploit climatic niches on the terrain (d, 1260mm). Finally, continued decrease of precipitation results in arid vegetation pattern.

In Fig. 38 we show a close-up simulation of a changing climate on a smaller patch of vegetation consisting of oaks, pines and shrubs. Our framework specifically models both the above-ground as well as below-ground interactions between different plants. This allows us to generate vegetation structures with unique geometries adapted to their local environment. For example, in (a) - (d) the right oak tree sheds its left facing branches first due to the shade of the nearby pine tree. Furthermore, after the oak trees lose most of their branches and their shade impact vanishes, shrubs grow into the space with the now better light conditions (g) - (h). These detailed above-ground vegetation interactions could not be simulated by soil-mediated interactions due to the coarseness of the precipitation and evaporation maps.

4.7.1.3 Vegetation-Atmosphere To validate the impact of vegetation on the atmosphere we conducted the following experiment: we selected four different ecosystems with the same atmospheric conditions – parameter values are identical across all scenes. Then, we simulated the atmospheric model for the exact same amount of steps of weather simulation. Figure 39a shows an arid shrubland comprised by a species with a low evaporation rate. In this case, only a small, faint patch of clouds is forming over the terrain. In contrast, a young oak forest with a high evaporation rate generates more visible clouds as depicted in Figure 39b. In Figure 39c, d we created two different pine forests with the same evaporation rate. The overall higher biomass of the denser pine forest (Figure 39c) results in higher vapor values in the vapor map and consequently in the formation of cumulonimbus clouds. In contrast, the sparser pine forest with overall lower vapor values generates only faint cloud formation (Figure 39d). These results showcase the feedback of vegetation on the atmosphere via plant evaporation rates and biomass.

4.7.2 Microclimate

The main motivation behind our ecoclimate model is to describe the feedback loops between soil, atmosphere and vegetation locally. Therefore, all spaces used to represent the soil, atmosphere and vegetation components of our ecoclimate model are described by grids. This local representation allows us to express spatial gradients of temperature, light availability and water representing the microclimate. In contrast to a global definition of climatic parameters such as used in [13], this enables simulating various important phenomena controlled by the microclimate. We demonstrate the usefulness of a local, bidirectional vegetation-soil feedback by simulating the effects of topography of vegetation growth and the plausible vegetation growth dynamics at forest edges. Furthermore, we present the Foehn effect as an example of how a local description of the atmosphere allows modeling realistic vegetation distribution along mountain sides. Finally, we show how deforestation can locally affect the atmosphere by changing cloud formation dynamics.

4.7.2.1 Geomorphic Effects and Plant Cooperation Our method emergently expresses the effects of the topography on vegetation growth via the hydrological cycle. In Eq. 44 of the soil model we describe the diffusion and run-off of surface water based on ground slopes. Water infiltration is diminishing with the steepness of slopes. Consequently, this means that plant development is affected by the geomorphology of the terrain – more water is available in terrain crevasses. Therefore, soil water can establish elevational gradients of species distributions. Additionally, we model that the presence of vegetation improves soil permeability based on Eq. 44. This allows us to simulate plant species cooperation: less precipitation-adapted species serve as pioneers for improving soil permeability, which consequently becomes a preferential habitat for a more precipitation-adapted

species. Geomorphic controls on vegetation composition and plant species cooperation are well documented in scientific literature [65], [72].

In Fig. 42 we show the results of an ablation study of the impact of the soil model with enabled and disabled microclimate. We compare two identical developing ecosystems that are comprised of two plant species. The yellow plant species is more precipitation-adapted than the green species. After a few iterations, in both microclimate-enabled (top) and microclimate-disabled (bottom) simulations the distribution of yellow and green species is similar (a, e). However, after further development an elevational gradient for the green species is emerging in the microclimate-enabled case (b, c), whereas the microclimate-disabled simulation exhibits uniform growth (f, g). After soil permeability has been increased by the green species, the more precipitation-adapted yellow species appears in the crevasses of the terrain for the microclimate-enabled case (d) – an example of species cooperation. The microclimate-disabled simulation does not capture this succession of species (h). This result demonstrates that our model effectively captures emergently plant species successions by simulating competition as well as cooperation.

4.7.2.2 Edge Effects It has been recognized that human-caused forest fragmentation leads to increased edge effects, e.g. in the South American rainforest [73]. Edges of forests are known to exhibit steep climatic gradients which lead to different vegetation distribution, species richness, and vegetation growth attributes.

Our microlimate models allows us to emergently simulate edge effects. In Fig.43 we show the results of an developing ecosystem composed of four different plant species. Three smaller species are more drought-adapted compared to a taller climax species. Initially, we start with a mixed stand of plants (a). Over time, the locally varying microclimate leads to drier regions at the forest edge and a wetter region inside the forest. This causes the drought-adapted species to preferentially grow at the edges of the forest, while the climax species favors the wetter interior (b). To show the emergence of edge effects we removed all tree models near the center line of the forest patch (c). The regrowing forest patch exhibits similar edge effects as before, where drought-adapted species develop near the center line (d). This phenomenon is completely dependent on a local specification of the climate and cannot be obtained by non-local ecoclimate models.

4.7.2.3 Deforestation Effects Simulating vegetation in a detailed and individual-based way also allows us to express a local vegetation-atmosphere feedback. We demonstrate this in Fig. 41 where we show an extreme case of this feedback to cloud formation. By keeping the macroclimatic parameter values constant during the simulation we ensure consistent cloud formation patterning over a dense rainforest landscape (a). Then, we remove a large patch of the rainforest, which results in drastic changes to the values stored in the vapor map. As a result, vapor values in the *Weather Voxel Space* above the deforested area drop below the cloud formation threshold (b). Finally, we continue vegetation growth for several years until clouds are again observable above the previously deforested region (c, d). In our simulation, each plant of the vegetation model contributes through evaporation to the hydrological cycle leading to local variations of the atmosphere. This local feedback is a novel topic of climate research and referred to as surface heterogeneity control of cloud formation [63].

4.7.2.4 Foehn Effects As another example for the importance of the microclimate we simulate the Foehn effect – a phenomenon that requires a local atmosphere-vegetation feedback instead of a purely global one. The Foehn effect is characterized by a temperature gradient resulting from a laminar wind flow over a steep mountain ridge. This atmospheric change may impact vegetation

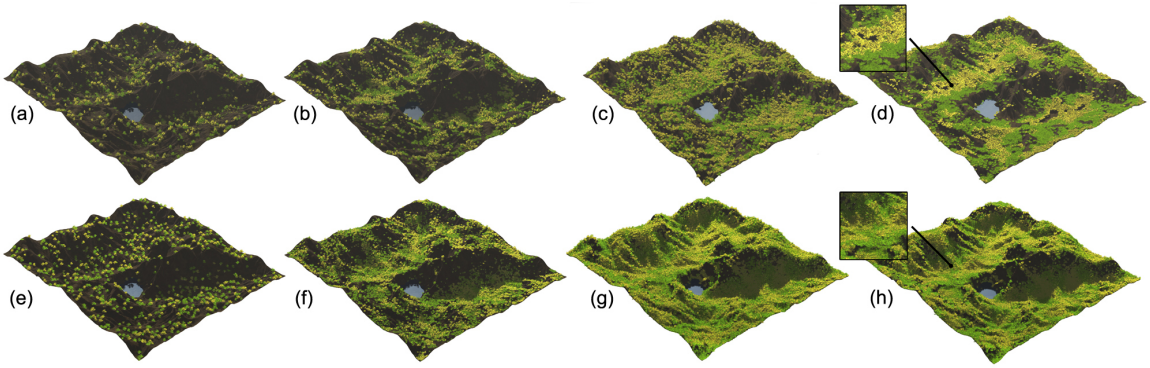

Figure 42: Comparison to [13]: Temporal progression of a developing ecosystem composed of a drought-adapted green-leaved and a yellow-leaved species generated with microclimates (a-d) and without microclimates (e-h). The inclusion of microclimates allows for more realistic patterning of vegetation at the slopes of the terrain capturing geomorphic effects. Additionally, patterns of self-organization emerge as the yellow-leaved species establishes itself primarily in the valleys of the terrain after water infiltration is sufficiently improved through the presence of the green-leaved species (top row): a case of plant cooperation (d and h, inset).

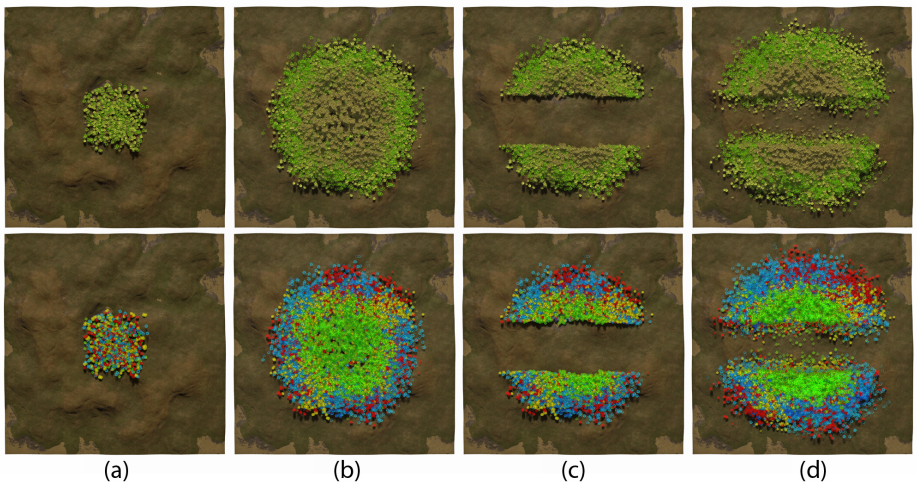

Figure 43: A mixed stand forest patch emerging from centrally distributed seeds of four different species (a). After further simulation a climax species establishes itself in the center of the forest patch with the remaining species at the forest edges due to microclimates (b). We interactively cut back trees to fragment the forest into two patches (c). After several years plants grow back into the gap with similar species distributions at the edges as before the disturbance (d). Our microclimate model realistically captures increasing edge effects due to forest fragmentation. In the bottom row we visualize plant species with colors red, blue and yellow for edge species and green for the climax species.

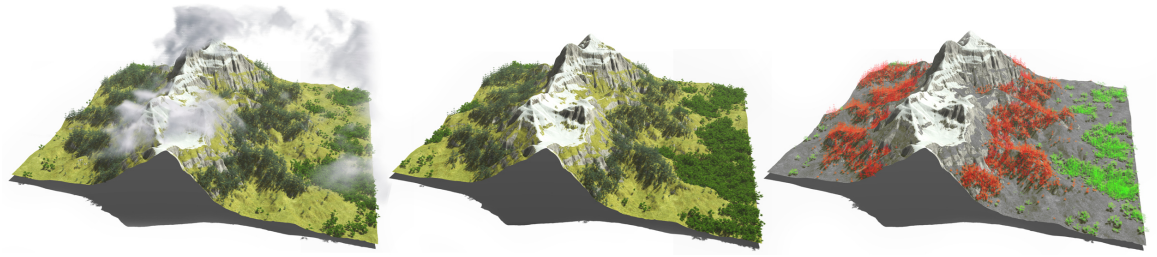

Figure 44: Our method is able to capture complex wind-vegetation interactions (left). One example is the Foehn effect which causes a temperature gradient over a mountain slope. The change of temperatures in the microclimate leads to different compositions of vegetation on the leeward and windward side of the mountain (center). Different species are highlighted with different color (right).

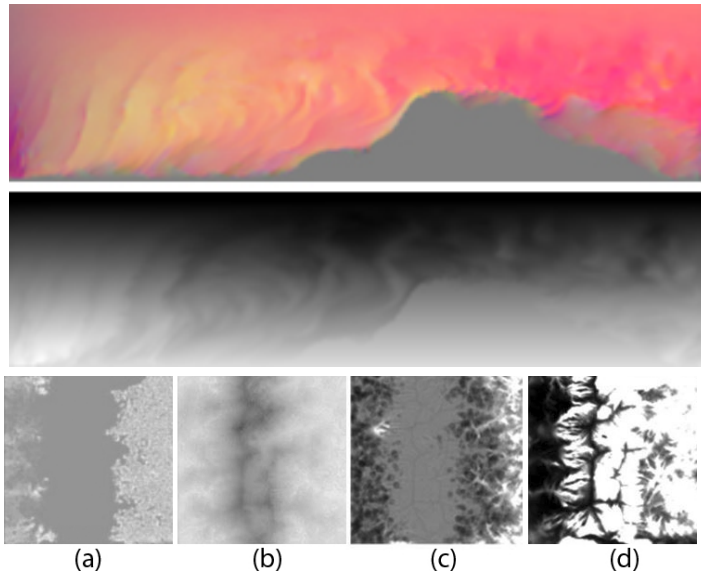

Figure 45: Top and middle row: side view of velocity (top) and temperature (middle) profiles illustrating the Foehn effect discussed in Fig. 44. Due to the interaction of the wind field with the mountain side a differential temperature gradient results. The left side of the mountain is cooler than the right side (velocity field rendered as RGB colors). The color image indicating velocities shows turbulence on the right side of the mountain. Bottom row: top-down views of the vapor, temperature, soil and precipitation maps, respectively. The vapor map indicates the less pronounced vegetation presence on the left side of the mountain (a), cooler temperatures at higher elevation (b), wetter soil on the right side (c) and the regions of high precipitation (d). For all maps brighter colors indicate higher values.

development resulting in differential ecosystem compositions on either side of the mountain. This complex effect is captured in an emergent way by our method (Fig. 44, left). Due to the non-uniform boundary conditions imposed by a mountainous height map the uniform, unidirectional wind field is oriented upwards in our simulation grid, which results in a cooling of air. Fig. 45 shows the resulting velocity (top) and temperature (bottom) profiles. On the other side of the mountain the down-flowing air heats up again and exhibits turbulent air motion. This results in a warmer leeward mountain side (center), which is indicated by the lighter colors in the temperature profile. In this scene, we placed two species with varying temperature adaptation and simulated their growth for 200 years. For the resulting ecosystem we can observe that the forest on the windward side is composed of only the cold-adapted conifers. Whereas, on the other side both plant species establish themselves. The species distribution is illustrated in Fig. 44 (right) by color-coding the two plant species of the ecosystem (red denotes the cold-adapted conifers, green the warm-adapted deciduous trees). Please note that for this experiment we do not consider the geographic orientation of the scene, e.g. the light exposure differences between north and south facing slopes.

4.7.3 Comparative Analysis

To evaluate the plausibility of our simulations we conduct a series of comparative analyses to theoretical studies in climatology and ecology research, as well as to real world examples.

In Fig. 46 we show a comparison of our simulated results to Meron [74], an analytical study of the formation of spot and stripe patterns. Meron [74] describes the response of vegetation to various precipitation regimes. Specifically, they propose a vegetation growth model which only depends on the impact of precipitation. Further, their method expresses vegetation abstractly as concentrations of biomass. In contrast, our method considers also light, temperature and represents vegetation geometrically. This way our method allows us to express non-trivial feedback loops for competition for water and light, as well as cooperation for improving water infiltration (Eqs. 43 and 44). This allows us to express Turing-like patterns via short-distance inhibition due to plants competing for the same space and long-distance promotion of plant development due to improving soil permeability. We explore the capability of our method and compare to the results reported by Meron [74] describing a variety of spot, gap, and stripe patterns, as well as their morphological transitions (Fig. 46, top). Analogously, to their method we can express all these spatial vegetation patterns as a function of the vapor parameter E_M (Fig. 46, bottom). These patterns can be simulated in a steady state over longer periods of simulation time, i.e. we simulated an ecosystem for 500 years and observed no qualitative change for specific patterns. Additionally, our soil model considers the topography and therefore also captures the feedback between terrain slopes and spatial vegetation patterning (Fig. 40). These results indicate that our method is realistically modeling the precipitation response of vegetation.

Time scales of forest growth make experimental research studies on ecoclimates inherently difficult to conduct. Therefore, ecologists commonly employ analytical approaches. Recent theoretical results indicate that vegetation response to climatic changes can vary according to the rate of such changes. For example, [1], [67] conducted theoretical experiments to study the differential response of vegetation to climate changing at varying speeds by reducing the rate of precipitation by a factor of 10. In their slow climatic change experiment they observe that spatial patterning of vegetation corresponds to a more uniform distribution compared to the fast climatic change experiment. This discrepancy is explained by the additional time that plants have to redistribute across space and more efficiently take up soil water. Furthermore, the interconnection between climate and vegetation has been described as a tipping point phenomenon [75]. According to these findings response of vegetation to climatic change may be unnoticeable for long periods of time and then unexpectedly

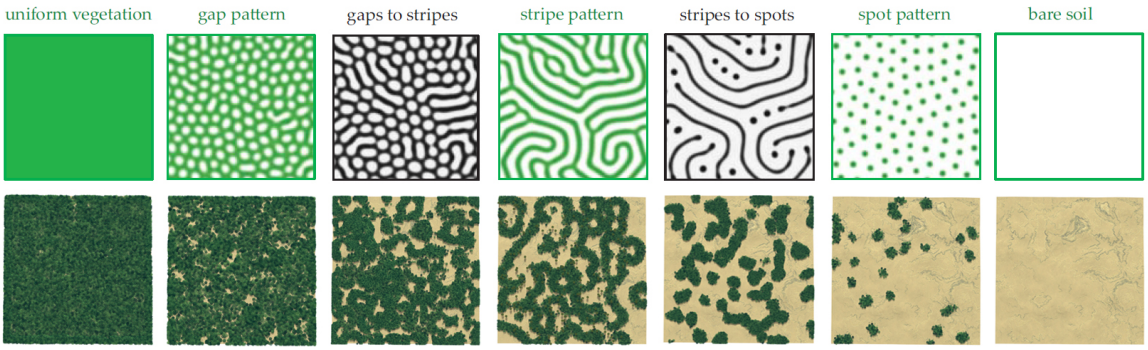

Figure 46: Our results correspond to the recent analytical study performed in ecology research (top row, adapted from [74], Fig. 5) which highlights morphological transitions (black and white panels) between gap, stripe and spot patterns (green panels). Our method simulates similar spatial vegetation patterns obtained by different the macroscopic vapor E_M (values decreasing from left to right).

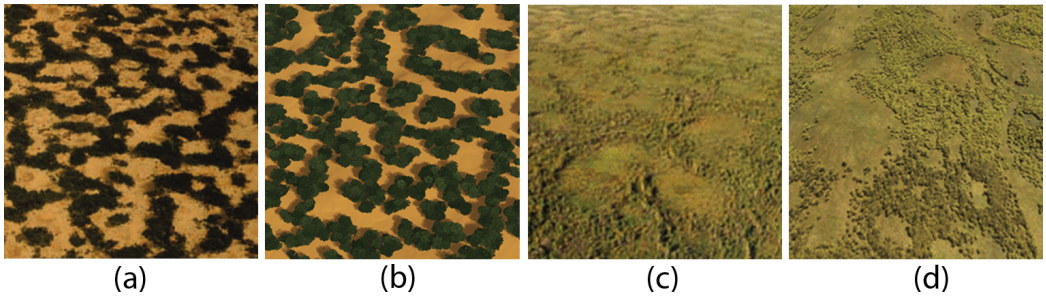

Figure 47: Comparison of a photograph of an arid ecosystem in Niger (a) and our simulation result (b), as well as a photograph of peatlands in Western Siberia (c) and our corresponding simulation (d). Our method is able to generate realistic spatial vegetation patterns for different environments. Photographs are taken from Rietkerk et al. [75].

shift catastrophically.

Similar to these studies, we conducted experiments to evaluate whether our method also captures (1) varying response of vegetation to slow and fast changes of climate; and (2) the occurrence of tipping points and catastrophic shifts. The results are shown in Fig. 48. Our goal is to compare a slow (a-f) and a fast (m-r) climatic change scenario by changing vapor E_M with different rates (10 times difference) over time. Additionally, we compare both scenarios with a baseline that does not use microclimates (h-l). The initial ecosystem used for all scenarios is shown in (g). Plant distributions are shown as scatter plots with blue points. To quantitatively assess the progression of the three ecosystems we use persistent homology to measure the topological features of plant distributions, such as spots, gaps, and stripes. To illustrate the changes of vegetation patterning over time we assess the persistence of topological features as H_1 barcodes for each plant distribution. Long barcodes indicate persisting topological features whereas short barcodes indicate noise.

Starting with an initial ecosystem the result of a climatic change scenario without microclimates is shown in (g-l). As shown in the scatter plots (g, i, k), the plant distributions for this simulation remain randomly distributed, while the overall number of plants diminishes. The barcodes (h, j, l)

do not contain persistent topological features indicating a lack of catastrophic shifts of vegetation patterning.

The fast climatic change scenario is shown in the plots (m-r). Starting from the initial plant distribution (g) we simulate climatic change over a period of 10 years. In contrast to the baseline without microclimates, the scatter plots illustrate clustered distributions of plants (m, o, q). Moreover, the corresponding barcodes (n, p, r) expose the presence of persisting topological features indicating the presence of gaps in the plant distributions. These features appear over a short period of time (p, r) thereby indicating a tipping point phenomenon.

Finally, the slow climatic change scenario is shown in the plots (a-f). For this scenario the change of climate takes place over a period of 80 years. The distribution of plants initially changes less significantly, but then also hits a tipping point after 64 years (c) that consequently results in a severely reduced plant distribution (f). The changes of plant distributions and topological features for this scenario can be observed in (b, d, f).

These climatic change scenarios illustrate that our method realistically captures the formation and expansion of forest gaps resulting from catastrophic shifts. In addition, our method produces more dispersed plant distributions for the slow climatic change scenario which corresponds to research results reported in ecology [1], [75]. The model without microclimates does not capture these phenomena and thus does not simulate climatic changes in a plausible way.

We further evaluate our model by quantitatively assessing canopy height distributions. We simulate two forest patches, one composed of a mixed stand of different plant species, and a forest composed only of pine trees. The results of this experiment are reported in Fig. 49. Canopy height gradients at the forest edge are steeper for the pine forest (right) compared to the mixed tree stand (left) as a result of differential microclimates. This qualitatively conforms to observations in the subtropical region reported by Delgado et al. [76].

Our method enables the exploration of a vast array of different ecoclimatic phenomena, which can be validated with comparisons to real world observations. In Fig. 47 we show qualitative comparisons of our simulation results to real photographs. In particular, we show a comparison of an arid ecosystem in Niger (a, b) and a comparison to peatlands in Western Siberia (c, d). As illustrated our method enables simulating ecoclimates with high visual similarity of spatial vegetation patterning compared to real ecosystems. Photographs were taken from [75].

4.8 Discussion and Limitations

We have presented a method for simulating ecoclimates capable of generating highly realistic images. At the core of our method lies the modeling of a detailed, bidirectional feedback between clouds and vegetation that captures phenomena such as spatial patterning in ecosystems, varied vegetation gradients on forest edges, realistic features in different climatic change scenarios, and plausible dynamics of cloud formation over different biomes. In contrast to methods that are based on authoring clouds or ecosystems our approach relies on a mechanistic description of the various biological and physical processes. This allows our method to generate not only momentary views of the cloud- and ecosystem-related phenomena but also to express their emergent dynamics over different time scales. However, these advantages are balanced by a generally slower run-time compared to a more descriptive, authoring approach.

Furthermore, we extend existing simulation work in graphics by demonstrating how stable patterning of vegetation can be obtained. In previous methods [13] spatial vegetation patterns are only modeled transiently and not to the same degree of realism. Our method improves cloud dynamics by incorporating heat transfer and vapor released by vegetation resulting in more realistic cloud distribution. Moreover, the joint simulation of ecosystem, soil and cloud models allows emergently

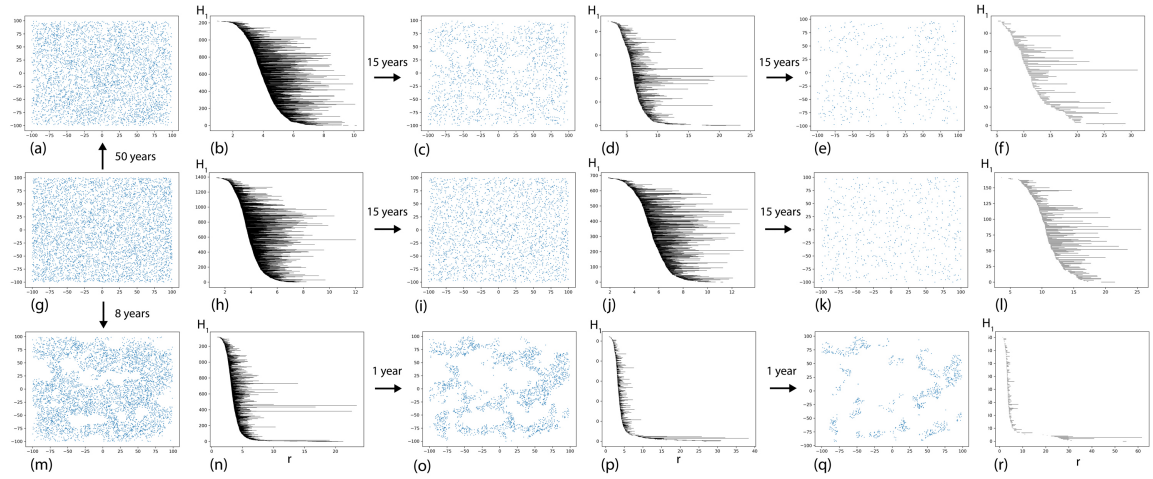

Figure 48: We evaluate the impact of three climatic change simulations on the same initial vegetation pattern composed of a single plant species. We show plant distributions as scatter plots with blue points indicating plant positions on the ground surface and the corresponding H_1 persistent homology barcodes obtained from the point clouds. The initial vegetation scene before decreasing vapor values is depicted in (g), and its barcode is shown in (h). The results of a naive ecoclimate model without microclimates is shown in (i-l) - no persistent topological features emerge. In the top row (a-f), we show plant distributions and barcodes for a slow climatic change scenario with microclimates. In this case, more persistent topological features emerge. In the bottom row (m-r), we show plant distributions and barcodes for a fast climatic change scenario (10 times faster vapor value decrease than the slow scenario) with microclimates. Here, the barcodes reveal that topological features are more persistent than in the other scenarios. The plant distribution appears less uniformly spread across space compared to both the naive, as well as the slow climatic change model.

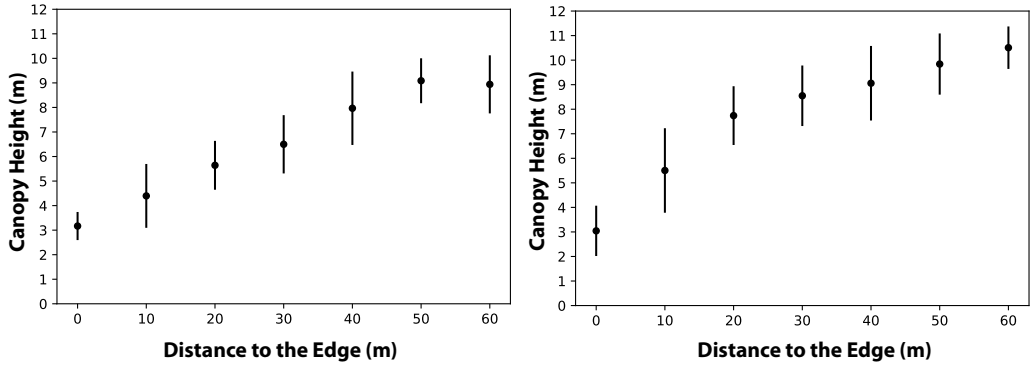

Figure 49: Canopy height depicted as a function of distance to the forest edge (canopy > 1 meter) for a mixed forest (left) and a pine forest (right). These canopy profiles conform with observations reported for forests in a subtropical climate [76]: the pine forest has a steeper gradient of canopy height compared to the mixed forest.

capturing phenomena, such as the Foehn effect. However, we do not take into account the complex hydrological dynamics between water bodies, soil and vegetation, which limits the scope of cloud formation phenomena that can be modeled.

Compared to analytical models studied in ecology research, our method expresses plant growth and their spatial interaction with considerably greater realism by describing detailed 3D geometry of plants and their microclimate. We aid research in ecology by demonstrating that realistic spatial patterning of vegetation can be explained by a model relying on plant competition for light as well as their cooperation for soil permeability, rather than competition for water uptake alone. Furthermore, we show that emerging microclimates due to weather and vegetation feedback are sufficient to qualitatively explain forest edge effects. These findings indicate that our model may serve as a theoretical framework for testing ecological research hypotheses in the future.

In climate research, large eddy simulations are used to study ecoclimates with similar spatial fidelity compared to our method. These approaches generally describe the water transfer between vegetation and atmosphere using some variation of the Penman-Monteith (PM) equation. These types of models rely on a spatially averaged description of vegetation and consequently do not allow for the realistic rendering of individual plant geometry. In our method, plants are treated in an individual-based way meaning that vegetation-atmosphere feedback is described at a lower scale of abstraction compared to PM models. This allows to formulate and test hypotheses which rely on such detailed representation. In general, state-of-the-art climate models describe and study feedbacks which we did not take into account, e.g. the diurnal cycle, variations of directional lighting caused by seasonal changes, or light-mediated feedback between terrain and the atmosphere (i.e. solar irradiance). Specifically, adding the geographic orientation and the resulting shading differences of sloped terrain would make a reconstruction of ecoclimates in mountainous scenes more realistic. On the other hand, our results indicate that for the phenomena simulated in this work a detailed model of irradiance is not required.

4.9 Conclusion

In this chapter, we have advanced 3D outdoor scene modeling by introducing a method that for the first time captures realistic vegetation development in response to climatic changes. Our method is based on the coupling of complex models of plant ecosystems, soil hydrology, and weather. This enables us to express important feedback loops between the different climate systems to simulate ecoclimates with an unprecedented degree of detail. We have presented a variety of patterns that can be explored with a coupled vegetation, soil and weather model. These patterns are controlled by mechanisms occurring at different time scales - from seconds to years. This poses considerable modelling challenges which we addressed here by leveraging state-of-the-art models for cloud formation, vegetation modeling and recent advances in climate research. Although complex in construction, by a lightweight interface our method allows for the interactive exploration of a parameter space containing phenomena which have never been described before in computer graphics. These include detailed descriptions of self-organized spatial patterning in arid ecosystems, varied vegetation gradients on forest edges, realistic features in different climatic change scenarios, and feedback of vegetation on cloud formation dynamics.

4.10 References

[1] R. Bastiaansen, A. Doelman, M. B. Eppinga, and M. Rietkerk, "The effect of climate change on the resilience of ecosystems with adaptive spatial pattern formation," *Ecology Letters*, vol. 23, no. 3, pp. 414–429, 2020.

[2] P. Liang, X. Wang, H. Sun, Y. Fan, Y. Wu, X. Lin, and J. Chang, "Forest type and height are important in shaping the altitudinal change of radial growth response to climate change," *Scientific Reports*, vol. 9, no. 1, p. 1336, 2019.

[3] R. P. Allan, M. Barlow, M. P. Byrne, A. Cherchi, H. Douville, H. J. Fowler, T. Y. Gan, A. G. Pendergrass, D. Rosenfeld, A. L. S. Swann, L. J. Wilcox, and O. Zolina, "Advances in understanding large-scale responses of the water cycle to climate change," *Ann. N.Y. Acad. Sci.*, 2020.

[4] M. Kovenock and A. L. S. Swann, "Leaf trait acclimation amplifies simulated climate warming in response to elevated carbon dioxide," *Global Biogeochemical Cycles*, vol. 32, no. 10, pp. 1437–1448, 2018.

[5] F. Zellweger, P. De Frenne, J. Lenoir, P. Vangansbeke, K. Verheyen, M. Bernhardt-Römermann, L. Baeten, R. Hédl, I. Berki, J. Brunet, H. Van Calster, M. Chudomelová, G. Decocq, T. Dirnböck, T. Durak, T. Heinken, B. Jaroszewicz, M. Kopecký, F. Máliš, M. Macek, M. Malicki, T. Naaf, T. A. Nagel, A. Ortmann-Ajkai, P. Petřık, R. Pielech, K. Reczyńska, W. Schmidt, T. Standovár, K. Świerkosz, B. Teleki, O. Vild, M. Wulf, and D. Coomes, "Forest microclimate dynamics drive plant responses to warming," *Science*, vol. 368, no. 6492, pp. 772–775, 2020.

[6] O. Deussen, C. Colditz, M. Stamminger, and G. Drettakis, "Interactive visualization of complex plant ecosystems," *VIS '02*, pp. 219–226, 2002.

[7] M. Jaeger and J. Teng, "Tree and plant volume imaging - an introductive study towards voxelized functional landscapes," *PMA*, 2003.

[8] B. Lane and P. Prusinkiewicz, "Generating spatial distributions for multilevel models of plant communities," *Graphics Interface*, pp. 69–80, 2002.

[9] O. Deussen, P. Hanrahan, B. Lintermann, R. Měch, M. Pharr, and P. Prusinkiewicz, "Realistic modeling and rendering of plant ecosystems," *ACM Trans. Graph.*, pp. 275–286, 1998.

[10] T. Hädrich, D. T. Banuti, W. Pałubicki, S. Pirk, and D. L. Michels, "Fire in paradise: Mesoscale simulation of wildfires," *ACM Transaction on Graphics*, vol. 40, no. 4, 2021.

[11] G. Cordonnier, E. Galin, J. Gain, B. Benes, E. Guérin, A. Peytavie, and M.-P. Cani, "Authoring landscapes by combining ecosystem and terrain erosion simulation," *ACM Trans. Graph.*, vol. 36, no. 4, 2017, ISSN: 0730-0301.

[12] P. Ecormier-Nocca, G. Cordonnier, P. Carrez, A.-M. Moigne, P. Memari, B. Benes, and M.-P. Cani, "Authoring consistent landscapes with flora and fauna," *ACM Trans. Graph.*, vol. 40, no. 4, Jul. 2021, ISSN: 0730-0301. DOI: 10.1145/3450626.3459952. [Online]. Available: https://doi.org/10.1145/3450626.3459952.

[13] M. Makowski, T. Hädrich, J. Scheffczyk, D. L. Michels, S. Pirk, and W. Pałubicki, "Synthetic silviculture: Multi-scale modeling of plant ecosystems," *ACM Trans. Graph.*, vol. 38, no. 4, 2019, ISSN: 0730-0301.

[14] M. Aono and T. Kunii, "Botanical tree image generation," *IEEE Comput. Graph. Appl.*, vol. 4(5), pp. 10–34, 1984.

[15] P. E. Oppenheimer, "Real time design and animation of fractal plants and trees," *Proc. of SIGGRAPH*, vol. 20, no. 4, pp. 55–64, 1986, ISSN: 0097-8930.

[16] P. Prusinkiewicz, "Graphical applications of l-systems," in *Proc. on Graph. Interf.*, 1986, pp. 247–253.

[17] B. Lintermann and O. Deussen, "Interactive modeling of plants," *IEEE Comput. Graph. Appl.*, vol. 19, no. 1, pp. 56–65, Jan. 1999, ISSN: 0272-1716. DOI: 10.1109/38.736469. [Online]. Available: https://doi.org/10.1109/38.736469.

[18] B. Li, J. Kałużny, J. Klein, D. L. Michels, W. Pałubicki, B. Benes, and S. Pirk, "Learning to reconstruct botanical trees from single images," *ACM Transaction on Graphics*, vol. 40, no. 6, Dec. 2021.

[19] B. Neubert, T. Franken, and O. Deussen, "Approximate image-based tree-modeling using particle flows," *ACM Trans. Graph.*, vol. 26, no. 3, 2007, ISSN: 0730-0301.

[20] D. Bradley, D. Nowrouzezahrai, and P. Beardsley, "Image-based reconstruction synthesis of dense foliage," *ACM Trans. Graph.*, vol. 32, no. 4, 74:1–74:10, 2013, ISSN: 0730-0301.

[21] P. Tan, T. Fang, J. Xiao, P. Zhao, and L. Quan, "Single image tree modeling," *ACM Trans. Graph.*, vol. 27, no. 5, 108:1–108:7, 2008, ISSN: 0730-0301.

[22] L. Quan, P. Tan, G. Zeng, L. Yuan, J. Wang, and S. B. Kang, "Image-based plant modeling," *ACM Trans. Graph.*, vol. 25, no. 3, pp. 599–604, 2006, ISSN: 0730-0301.

[23] C. Li, O. Deussen, Y.-Z. Song, P. Willis, and P. Hall, "Modeling and generating moving trees from video," *ACM Trans. Graph.*, vol. 30, no. 6, 127:1–127:12, 2011, ISSN: 0730-0301.

[24] Y. Livny, S. Pirk, Z. Cheng, F. Yan, O. Deussen, D. Cohen-Or, and B. Chen, "Texture-lobes for tree modelling," *ACM Trans. Graph.*, vol. 30, no. 4, 53:1–53:10, 2011, ISSN: 0730-0301.

[25] H. Xu, N. Gossett, and B. Chen, "Knowledge and heuristic-based modeling of laser-scanned trees," vol. 26, no. 4, Article 19, 13 pages, 2007.

[26] T. Ijiri, S. Owada, and T. Igarashi, "Seamless integration of initial sketching and subsequent detail editing in flower modeling," *Comp. Graph. Forum*, vol. 25, no. 3, pp. 617–624, 2006.

[27] M. Okabe, S. Owada, and T. Igarashi, "Interactive design of botanical trees using freehand sketches and example-based editing," in *ACM SIGGRAPH Courses*, San Diego, California: ACM, 2007, ISBN: 978-1-4503-1823-5.

[28] J. Wither, F. Boudon, M.-P. Cani, and C. Godin, "Structure from silhouettes: a new paradigm for fast sketch-based design of trees," *CGF*, vol. 28, no. 2, pp. 541–550, 2009.

[29] S. Pirk, B. Benes, T. Ijiri, Y. Li, O. Deussen, B. Chen, and R. Měch, "Modeling plant life in computer graphics," in *ACM SIGGRAPH 2016 Courses*, Anaheim, California: ACM, 2016, 18:1–18:180, ISBN: 978-1-4503-4289-6.

[30] R. Měch and P. Prusinkiewicz, "Visual models of plants interacting with their environment," in *Proc. of SIGGRAPH*, ACM, 1996, pp. 397–410.

[31] W. Palubicki, K. Horel, S. Longay, A. Runions, B. Lane, R. Měch, and P. Prusinkiewicz, "Self-organizing tree models for image synthesis," *ACM Trans. Graph.*, vol. 28, no. 3, 58:1–58:10, 2009, ISSN: 0730-0301.

[32] S. Pirk, O. Stava, J. Kratt, M. A. M. Said, B. Neubert, R. Měch, B. Benes, and O. Deussen, "Plastic trees: Interactive self-adapting botanical tree models," *ACM Trans. Graph.*, vol. 31, no. 4, 50:1–50:10, 2012, ISSN: 0730-0301.

[33] O. Stava, S. Pirk, J. Kratt, B. Chen, R. Měch, O. Deussen, and B. Benes, "Inverse procedural modelling of trees," *CGF*, vol. 33, no. 6, pp. 118–131, 2014, ISSN: 1467-8659.

[34] T. Hädrich, B. Benes, O. Deussen, and S. Pirk, "Interactive modeling and authoring of climbing plants," *CGF*, vol. 36, no. 2, pp. 49–61, 2017, ISSN: 0167-7055.

[35] S. Longay, A. Runions, F. Boudon, and P. Prusinkiewicz, "Treesketch: Interactive procedural modeling of trees on a tablet," in *Proc. of the Intl. Symp. on SBIM*, 2012, pp. 107–120.

[36] H. Y. Wang, M. Z. Kang, J. Hua, and X. J. Wang, "Modeling plant plasticity from a biophysical model: Biomechanics," in *Proceedings of the 12th ACM SIGGRAPH Intl. Conf. on VRCAI*, ACM, 2013, pp. 115–122, ISBN: 978-1-4503-2590-5.

[37] Y. Zhao and J. Barbič, "Interactive authoring of simulation-ready plants," *ACM Trans. Graph.*, vol. 32, no. 4, 84:1–84:12, 2013, ISSN: 0730-0301.

[38] H. Shao, T. Kugelstadt, T. Hädrich, W. Pałubicki, J. Bender, S. Pirk, and D. L. Michels, "Accurately solving rod dynamics with graph learning," in *NeurIPS*, 2021.

[39] S. Pirk, T. Niese, T. Hädrich, B. Benes, and O. Deussen, "Windy trees: Computing stress response for developmental tree models," *ACM Trans. Graph.*, vol. 33, no. 6, 204:1–204:11, 2014, ISSN: 0730-0301.

[40] S. Pirk, M. Jarząbek, T. Hädrich, D. L. Michels, and W. Palubicki, "Interactive wood combustion for botanical tree models," *ACM Trans. Graph.*, vol. 36, no. 6, 197:1–197:12, 2017, ISSN: 0730-0301.

[41] T. Niese, S. Pirk, M. Albrecht, B. Benes, and O. Deussen, "Procedural urban forestry," *ACM Transaction on Graphics*, vol. 41, no. 1, (in press) 2022.

[42] O. Argudo, C. Andújar, A. Chica, E. Guérin, J. Digne, A. Peytavie, and E. Galin, "Coherent multi-layer landscape synthesis," *The Visual Computer*, vol. 33, no. 6, pp. 1005–1015, 2017.

[43] E. Bruneton and F. Neyret, "Real–time realistic rendering and lighting of forests," *Comput. Graph. Forum*, vol. 31, no. 2pt1, pp. 373–382, 2012.

[44] B. Neubert, S. Pirk, O. Deussen, and C. Dachsbacher, "Improved model- and view-dependent pruning of large botanical scenes," *Comp. Graph. Forum*, vol. 30, no. 6, pp. 1708–1718, 2011.

[45] B. Beneš, N. Andrysco, and O. Št'ava, "Interactive modeling of virtual ecosystems," in *Proceedings of the Fifth Eurographics Conference on Natural Phenomena*, ser. NPH'09, Munich, Germany: Eurographics Association, 2009, pp. 9–16, ISBN: 9783905674118.

[46] J. Gain, H. Long, G. Cordonnier, and M.-P. Cani, "Ecobrush: Interactive control of visually consistent large-scale ecosystems," *Computer Graphics Forum*, vol. 36, no. 2, pp. 63–73, 2017.

[47] K. Kapp, J. Gain, E. Guérin, E. Galin, and A. Peytavie, "Data-driven authoring of large-scale ecosystems," *ACM Trans. Graph.*, 2020.

[48] H. Pretzsch, R. Grote, B. Reineking, T. Rötzer, and S. Seifert, "Models for forest ecosystem management: A european perspective," *Annals of botany*, vol. 101, pp. 1065–87, Jun. 2008.

[49] B. Zhang and D. L. DeAngelis, "An overview of agent-based models in plant biology and ecology," *Annals of Botany*, vol. 126, no. 4, pp. 539–557, Mar. 2020, ISSN: 0305-7364.

[50] E. Ch'ng, "Realistic placement of plants for virtual environments," *IEEE Comput. Graph. Appl.*, vol. 31, no. 4, pp. 66–77, 2011, ISSN: 0272-1716.

[51] M. J. Harris, W. V. Baxter, T. Scheuermann, and A. Lastra, "Simulation of cloud dynamics on graphics hardware," in *ACM SIGGRAPH/EUROGRAPHICS Conference on Graphics Hardware*, ser. HWWS '03, San Diego, California: Eurographics Association, 2003, pp. 92–101, ISBN: 1581137397.

[52] D. Overby, Z. Melek, and J. Keyser, "Interactive physically-based cloud simulation," in *10th Pacific Conference on Computer Graphics and Applications, 2002. Proceedings.*, 2002, pp. 469–470.

[53] R. Miyazaki, S. Yoshida, T. Nishita, and Y. Dobashi, "A method for modeling clouds based on atmospheric fluid dynamics," in *PG*, USA: IEEE Computer Society, 2001, p. 363, ISBN: 0769512275.

[54] A. Bouthors, F. Neyret, N. Max, E. Bruneton, and C. Crassin, "Interactive multiple anisotropic scattering in clouds," in *I3D*, ser. 2008, 2008, pp. 173–182, ISBN: 9781595939838.

[55] F. Neyret, "Qualitative simulation of convective cloud formation and evolution," in *Computer Animation and Simulation '97*, D. Thalmann and M. van de Panne, Eds., Vienna: Springer Vienna, 1997, pp. 113–124.

[56] P. Goswami and F. Neyret, "Real-time landscape-size convective clouds simulation and rendering," in *Proceedings of the 13th Workshop on Virtual Reality Interactions and Physical Simulations*, ser. VRIPHYS '17, Lyon, France: Eurographics Association, 2017, pp. 1–8, ISBN: 9783038680321.

[57] C. W. Ferreira Barbosa, Y. Dobashi, and T. Yamamoto, "Adaptive cloud simulation using position based fluids," *Comput. Animat. Virtual Worlds*, vol. 26, no. 3–4, pp. 367–375, 2015, ISSN: 1546-4261.

[58] U. Vimont, J. Gain, M. Lastic, G. Cordonnier, B. Abiodun, and M.-C. Cani, "Interactive meso-scale simulation of skyscapes," *Eurographics*, 2020.

[59] A. Webanck, Y. Cortial, E. Guérin, and E. Galin, "Procedural cloudscapes," *CGF*, vol. 37, no. 2, pp. 431–442, 2018.

[60] T. Hädrich, M. Makowski, W. Pałubicki, D. Banuti, S. Pirk, and D. L. Michels, "Stormscapes: Simulating cloud dynamics in the now," *ACM Transactions on Graphics (Proceedings of SIGGRAPH Asia)*, 2020.

[61] R. M. Pringle and C. E. Tarnita, "Spatial self-organization of ecosystems: Integrating multiple mechanisms of regular-pattern formation," *Annual Review of Entomology*, vol. 62, no. 1, pp. 359–377, 2017.

[62] N. Maréchal, E. Guérin, E. Galin, S. Mérillou, and N. Mérillou, "Heat transfer simulation for modeling realistic winter sceneries," *CGF*, vol. 29, pp. 449–458, May 2010.

[63] H. Xiao, L. K. Berg, and M. Huang, "The impact of surface heterogeneities and land-atmosphere interactions on shallow clouds over arm sgp site," *Journal of Advances in Modeling Earth Systems*, vol. 10, no. 6, pp. 1220–1244, 2018.

[64] G. L. Horn, H. G. Ouwersloot, J. Vilà-Guerau de Arellano, and M. Sikma, "Cloud shading effects on characteristic boundary-layer length scales," *Boundary-Layer Meteorology*, vol. 157, no. 2, pp. 237–263, Nov. 2015, ISSN: 1573-1472.

[65] G. Bonan, *Ecological Climatology: Concepts and Applications*, 3rd ed. Cambridge University Press, 2015.

[66] E. Kessler, "On the distribution and continuity of water substance in atmospheric circulations," in *On the Distribution and Continuity of Water Substance in Atmospheric Circulations*. Boston, MA: American Meteorological Society, 1969, pp. 1–84, ISBN: 978-1-935704-36-2.

[67] M. Rietkerk, F. van den Bosch, and J. van de Koppel, "Site-specific properties and irreversible vegetation changes in semi-arid grazing systems," *Oikos*, vol. 80, no. 2, pp. 241–252, 1997.

[68] R. HilleRisLambers, M. Rietkerk, F. van den Bosch, H. H. T. Prins, and H. de Kroon, "Vegetation pattern formation in semi-arid grazing systems," *Ecology*, vol. 82, no. 1, pp. 50–61, 2001.

[69] L. Ringham, A. Owens, M. Cieslak, L. D. Harder, and P. Prusinkiewicz, "Modeling flower pigmentation patterns," *ACM Trans. Graph.*, vol. 40, no. 6, Dec. 2021, ISSN: 0730-0301. DOI: 10.1145/3478513.3480548.

[70] P. K. Kundu, I. M. Cohen, and D. R. Dowling, *Fluid Mechanics*, ser. Science Direct e-books. Elsevier Science, 2012, ISBN: 9780123821003.

[71] J. Stam, "Stable fluids," *Proc. of ACM SIGGRAPH*, SIGGRAPH '99, pp. 121–128, 1999.

[72] E. Bertuzzo, F. Carrara, L. Mari, F. Altermatt, I. Rodriguez-Iturbe, and A. Rinaldo, "Geomorphic controls on elevational gradients of species richness," vol. 113, no. 7, pp. 1737–1742, 2016, ISSN: 0027-8424.

[73] E. N. Broadbent, G. P. Asner, M. Keller, D. E. Knapp, P. J. C. Oliveira, and J. N. Silva, "Forest fragmentation and edge effects from deforestation and selective logging in the brazilian amazon," *Biological Conservation*, vol. 141, no. 7, pp. 1745–1757, 2008, ISSN: 0006-3207.

[74] E. Meron, "Vegetation pattern formation: The mechanisms behind the forms," *Physics Today*, vol. 72, no. 11, pp. 30–36, 2019.

[75] M. Rietkerk, S. C. Dekker, P. C. de Ruiter, and J. van de Koppel, "Self-organized patchiness and catastrophic shifts in ecosystems," *Science*, vol. 305, no. 5692, pp. 1926–1929, 2004, ISSN: 0036-8075.

[76] J. Delgado, N. Arroyo, J. R. Arevalo, and J. Fernández-Palacios, "Edge effects of roads on temperature, light, canopy cover, and canopy height in laurel and pine forests (tenerife, canary islands)," *Landscape and Urban Planning*, pp. 328–340, Jul. 2007.

5 Future work

There are several areas for future work that can be pursued based on the current state of our framework. One potential direction is to further explore the utility of our method in validating and improving hypotheses in forestry and botany research that rely on detailed structural descriptions of plants. Examples of such research include the study of the effects of timber harvesting on the health and productivity of a forest ecosystem and the examination of plant responses to stressors such as drought, wildfires, or disease. Our method may also be useful in forest restoration projects by helping to select the appropriate species for local climate and soil conditions, improving the chances of successful restoration efforts.

Another promising area for future development is the adaptation of vegetation to climatic changes, as recent ecology research suggests that microclimates may have a significant impact on ecosystem development. Our detailed geometric plant representation could aid research in this area, as current models for climatic changes do not focus on modeling microclimates.

Integrating our method with models of the biosphere and anthroposphere is another possibility for future work. This could allow for the simulation of more complex ecological systems and provide valuable insights into the mutual relations between ecosystems, humans, and animals. For example, interactions between plants and animals, such as pollination, seed dispersal, and herbivory, as well as human activities like agriculture and urbanization, can alter the availability of resources and introduce new species. Understanding all of these interactions is important for conserving biodiversity and improving agricultural productivity.

Finally, we want to further improve the realism and performance of our model. Specifically, we plan to incorporate a diurnal cycle that captures temperature variations during the day and night, simulate solar irradiance, model seasonal changes in directional lighting, and consider the impact of wind on plants. We also hope to investigate how our modeling approach can be combined with other level of detail techniques to improve the efficiency of modeling larger ecosystems. All of these research directions have the potential to advance our method towards a more universal simulation of ecoclimate dynamics.

6 Publications by Miłosz Makowski

[1] M. Makowski, T. Hädrich, J. Scheffczyk, D. L. Michels, S. Pirk, and W. Pałubicki, "Synthetic silviculture: Multi-scale modeling of plant ecosystems," *ACM Trans. Graph.*, vol. 38, no. 4, 2019, ISSN: 0730-0301.

[2] T. Hädrich, M. Makowski, W. Pałubicki, D. Banuti, S. Pirk, and D. L. Michels, "Stormscapes: Simulating cloud dynamics in the now," *ACM Transactions on Graphics (Proceedings of SIGGRAPH Asia)*, 2020.

[3] W. Pałubicki, M. Makowski, W. Gajda, T. Hädrich, D. L. Michels, and S. Pirk, "Ecoclimates: Climate-response modeling of vegetation," *ACM Trans. Graph.*, 2022.